



**KTH Industrial Engineering
and Management**

Adhesion in the wheel–rail contact under contaminated conditions

Yi Zhu

Licentiate thesis
Department of Machine Design
Royal Institute of Technology
SE-100 44 Stockholm

TRITA – MMK 2011: 15
ISSN 1400-1179
ISRN/KTH/MMK/R-11/15-SE
ISBN 978-91-7501-181-3

TRITA – MMK 2011:15

ISSN 1400-1179

ISRN/KTH/MMK/R-11/15-SE

ISBN 978-91-7501-181-3

Adhesion in the wheel–rail contact under contaminated conditions

Yi Zhu, yiz@kth.se

Licentiate thesis

Academic thesis, which with the approval of Kungliga Tekniska Högskolan, will be presented for public review in fulfillment of the requirements for a Licentiate of Engineering in Machine Design. Public review: Kungliga Tekniska Högskolan, Room B 242, Brivellvägen 85, Stockholm, on December 1, 2011, at 10:00

Printed in Sweden

Universitetsservice US-AB

Abstract

Railway vehicles require a certain level of adhesion between wheel and rail to operate efficiently, reliably, and economically. Different levels of adhesion are needed depending on the vehicle running conditions. In the wheel tread–railhead contact, the dominant problem is low adhesion, as low adhesion on the railhead negatively affects railway operation: on one hand, the vehicle will lose traction resulting in delay when driving on low-adhesion tracks; on the other hand, low adhesion during deceleration will extend the braking distance, which is a safety issue.

This thesis examines the influence of several contaminants, i.e., water, oil, and leaves, on the adhesion in the wheel tread–railhead contact. This study will improve our knowledge of the low-adhesion mechanism and of how various contaminants influence adhesion. The thesis consists of a summary overview of the topic and three appended papers (**A–C**).

Papers **A** and **B** focus mainly on water and oil contamination examined using two methods, numerical simulation and lab testing. In paper **A**, real measured wheel and rail surfaces, low- and high-roughness surfaces, along with generated smooth surfaces are used as input to the numerical model for predicting the adhesion coefficient. Water-lubricated, oil-lubricated, and dry contacts are simulated in the model. In the research reported in paper **B**, scaled testing using a mini traction machine (MTM) was carried out to simulate the wheel–rail contact under lubricated conditions. Two types of disc surfaces of different roughnesses were run at different contact pressures and temperatures. A stylus machine and atomic force microscopy (AFM) were used to measure the surface topography. A study of leaf contamination on the railhead surface, based on field testing, is presented in paper **C**. Railhead surface samples were cut and the friction coefficient was measured on five occasions over the course of a year. Electron spectroscopy for chemical analysis (ESCA) and glow discharge optical emission spectrometry (GD-OES) were used to detect the chemical composition of the leaf-contamination layer on the railhead surface.

The main conclusion of the thesis is that different contaminants reduce the adhesion coefficient in different ways. Oil reduces the adhesion coefficient by carrying the normal force due to its high viscosity. Water can reduce the adhesion coefficient to different degrees depending on the surface topography and water temperature. The mixture of an oxide layer and water contamination may have an essential impact. A leaf-formed blackish layer causes low adhesion by means of a chemical reaction between the leaves and bulk material. The thickness of the friction-reducing oxide layer predicts the friction coefficient and the extent of leaf contamination.

Keywords: Adhesion; Wheel–rail contact; Contaminants; Rough surfaces.

Preface

The work in this thesis was carried out between September 2009 and October 2011 at the Department of Machine Design at Royal Institute of Technology (KTH), Stockholm, Sweden.

I would like to thank the SAMBA Swedish research programme and especially Trafikverket, SL and Railway Group at KTH for funding this project. My main supervisor Ulf Olofsson deserves particular thanks for giving me the chance to do this work, guiding me into the field of tribology and for his excellent guidances and encouragements. Special thanks also to Anders Söderberg as my co-supervisor for discussions and many good comments, Stefan Björklund for the discussion of contact mechanics, Saeed Abbassi for teaching me lots of railway technology, Ellen Bergseth for teaching me to use stylus machine and AFM, Peter Carlsson for helping me during the field test, Karin Persson and Rickard Nilsson as my papers' co-authors, Johan Andersson for your help during MTM testing, and all of my colleagues.

In addition, I want to gratefully acknowledge all my friends for being with me chatting and playing together.

Finally, I want to show my most heartfelt gratitude to my family, especially my dad and mum, for your supports and encouragements during my overseas study. Your efforts are beyond any words to be expressed!

Stockholm, October 2011

Yi Zhu

List of appended papers

This thesis consists of a summary and the following appended papers:

Paper A

Y. Zhu, U. Olofsson, A. Söderberg: “Adhesion modeling in the wheel–rail contact under dry and lubricated conditions using measured 3D surfaces”.

This paper was submitted to *Journal of tribology*. This paper is an extended version of : Y. Zhu, U. Olofsson, A. Söderberg , “Adhesion modeling in the wheel–rail contact under wet conditions using measured 3D surfaces”, *Proceedings of LAVSD 2011: International Symposium on Dynamic of Vehicles on road and tracks*, Aug 14-19, 2011, Manchester, UK.

The main part of the writing and adhesion modelling were performed by Zhu.

Paper B

Y. Zhu, U. Olofsson, K. Persson: “Investigation of factors influencing wheel–rail adhesion using a mini traction machine”.

This paper was submitted to *Wear*.

The experimental works and the main part of the writing were performed by Zhu.

Paper C

Y. Zhu, U. Olofsson, R. Nilsson: “A field test study of leaf contamination on the rail head surfaces”.

This paper was submitted to *The first International conference on Railway Technology: Research, Development and Maintenance*, Apr 18-20, 2012, Las Palmas de Gran Canaria, Spain

The main part of the writing and evaluation were performed by Zhu.

List of published papers not included in this thesis

R. Lewis, S. Lewis, Y. Zhu, S. Abbasi, U. Olofsson: “The modification of a slip resistance meter for measurement of railhead adhesion”, *IHHA 2011: International Heavy Haul Association Conference*, Jun 19-22, 2011, Calgary, Canada.

Contents

1	Introduction.....	1
2	Adhesion in the wheel–rail contact.....	3
2.1	Wheel–rail contact conditions	3
2.2	Friction and adhesion.....	5
2.3	Surface topography.....	6
3	Low adhesion under contaminated conditions	9
4	Computer simulation: adhesion modelling under dry and lubricated conditions	12
5	Scaled lab test: an MTM study of adhesion under dry and lubricated conditions	15
6	Field test: a study of leaf contamination on the railhead	18
7	Concluding remarks.....	21
8	References.....	24

Appended papers

- A. Adhesion modelling in the wheel–rail contact under dry and lubricated conditions using measured 3D surfaces
- B. Investigation of factors influencing wheel–rail adhesion using a mini traction machine
- C. A field test study of leaf contamination on railhead surfaces

1 Introduction

Railway vehicle operation depends on the adhesion between the wheel and rail. To run such vehicles efficiently and economically, the wheel–rail adhesion should be maintained at a certain level. According to the vehicle running conditions, wheel–rail contact is generally divided into two types, wheel tread–railhead contact on straight track and wheel flange–rail gauge contact on curved track. In most cases, flange contact requires a low adhesion coefficient to reduce wear and noise, while tread contact requires a comparatively high adhesion coefficient to obtain good accelerating and decelerating ability.

This thesis examines poor adhesion in the wheel tread–railhead contact, since this causes problems [1]. First, it affects vehicle performance because the vehicle will lose traction when driving on low-adhesion track. Moreover, low adhesion is also a safety issue, since poor adhesion when decelerating will extend braking distances. Since the wheel–rail contact is an open system, many environmental factors can contribute to low adhesion on the railhead. Common contaminants resulting in low adhesion are water, oil or grease and a leaf-formed blackish layer.

The overall goal of this thesis is to investigate the influence of contaminants (i.e., water, oil, and leaves) on the adhesion coefficient in the wheel tread–railhead contact, bearing in mind that different contaminants affect the adhesion differently. An enhanced understanding of the mechanism of low adhesion could help in predicting the adhesion coefficient in the wheel–rail contact and in finding a way to alleviate the poor adhesion problem.

The work addresses the following research questions:

- How does surface topography affect wheel–rail adhesion under water-lubricated conditions?
- How does surface topography affect wheel–rail adhesion under oil-lubricated conditions?
- Do other factors affect wheel–rail adhesion?
- What is the chemical composition of the leaf-contaminated blackish layer, and how does it differ from those of uncontaminated layers?
- Why does the presence of a leaf-formed blackish layer on the railhead surface give a low friction coefficient?

The methodology used here is briefly summarized in Fig. 1. This thesis deals with the low adhesion problems caused by contamination with water, oil, and the leaf-formed blackish layer. The influence of water and oil on the adhesion coefficient is studied based on computer simulation with a numerical model (paper **A**) and lab testing using a mini traction machine (paper **B**). In both papers **A** and **B**, the wheel–rail contact is also examined under dry conditions for purposes of comparison. Leaf contamination on the railhead surface is discussed in paper **C** with reference to a field test.

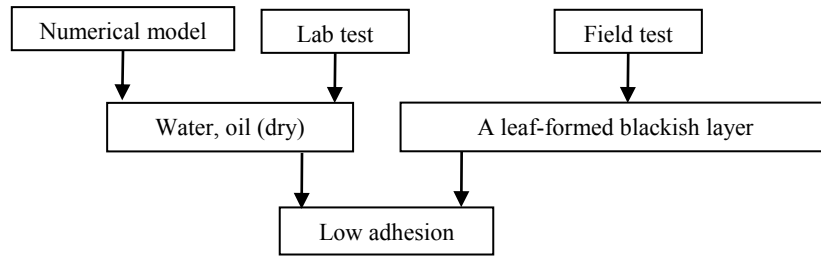


Figure 1. Schematic of the methodology of the thesis.

The thesis is structured as follows:

Chapter 2 presents the fundamentals of the wheel–rail contact. Chapter 3 discusses the fundamentals of various contaminants and their influence on the adhesion coefficient. Chapters 4–6 present the methodology used to investigate low adhesion under contaminated conditions based on numerical modelling, laboratory testing, and field testing. Summaries and the results of papers **A–C** are also briefly presented in these chapters. Chapter 7 presents the concluding remarks, which answer the research questions. Papers **A–C** are appended at the end of the thesis.

2 Adhesion in the wheel–rail contact

2.1 Wheel–rail contact conditions

Unlike road vehicles, such as the automobile, railway vehicles have some unique behaviours and properties, such as hunting motion, self-steering capability, and lateral dynamics. These unique features originate from the wheel–rail guidance system depending on wheel and rail geometry. First, the rail has a specific profile [2], governed by rules, and is mounted at a small inwards inclination (1:30 in Sweden) (indicated by no. 3 in Fig. 2) for better fit to the wheel profile and better load transfer to the sleepers and ballast. Second, the wheel is of a special design, including a wheel tread (where contact point 1 is located on the wheel in Fig. 2) and wheel flange (where contact point 2 is located on the wheel in Fig. 2). Moreover, the wheel profiles are usually conical (indicated by no. 4 in Fig. 2), leading to the difference in rolling radius in a curve for the two wheels in the same wheelset. Compared with tire–road interaction, the wheel–rail contact is very small at approximately 1 cm^2 [1]. As a result, the heavy axle load is transferred through a small patch generating high contact pressure.

Due to the above-mentioned factors, the wheel–rail contact area changes when running under different conditions. Generally, when the vehicle is running on a straight track, the contact area is usually between the wheel tread and railhead, as shown by contact point 1 in Fig. 2. When the vehicle is running on a curve, the contact area moves to between the wheel flange and rail gauge, as shown by contact point 2 in Fig. 2, or both of contact point 1 and 2. However, in real operation, the wheel rail contact varies constantly in terms of area and type, even starting from the same profile. In railway maintenance, wheels need to be changed and rails need to be re-ground after a certain time, depending on the contact conditions and wear.

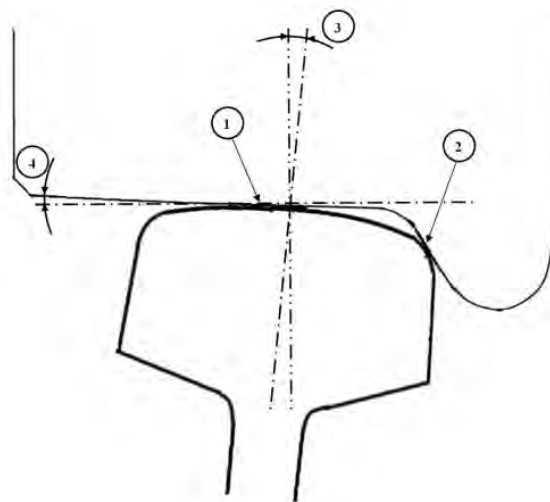


Figure 2. Schematic of two types of wheel–rail contact: 1. wheel tread–railhead contact and 2. wheel flange–rail gauge contact; 3. rail inclination; 4. conical wheel profile.

The two basic types of wheel–rail contact differ in many respects. Lewis and Olofsson [3] presented the operating conditions in a wheel tread–railhead contact and a wheel flange–

rail gauge contact, as shown in Fig. 3. As the contact area changes from wheel tread with railhead to wheel flange with rail gauge, both contact pressure and sliding velocity increase significantly. According to Olofsson and Telliskivi [4], rail hardness also has clear dependence on the contact type. In addition, the wear rate at the rail gauge is 10 times greater than the wear rate at the railhead [3]. In the present work, we will discuss only the wheel tread–railhead contact, which assumes that the vehicle is running on a straight track, and only longitudinal creep is considered. In the following sections, all discussions are based on this assumption.

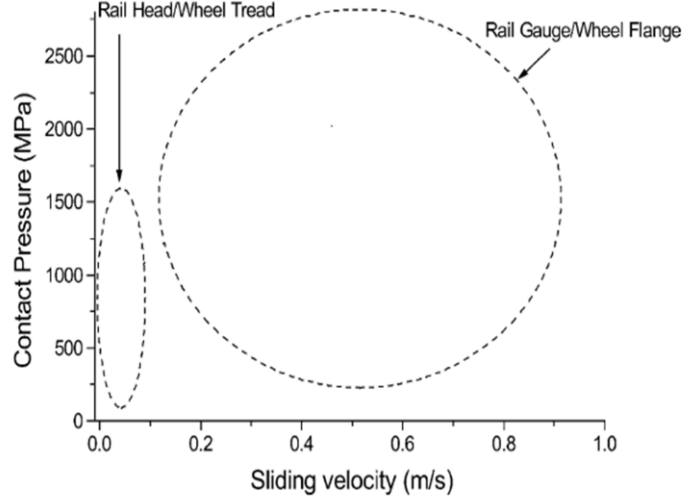


Figure 3. Contact conditions in a wheel rail contact [3].

The wheel–rail contact is a rolling–sliding contact. It is easy to imagine wheels rolling on tracks. On the other hand, wheels will also spin if the tracks are very slippery, for example, if there is ice on the track, in what is known as sliding motion. The combination of the two motions is called rolling–sliding contact. The difference between the circumferential velocity of a driven wheel and the translational velocity of the wheel over the track is usually a non-zero value, which is known as sliding velocity u_s . The ratio of sliding velocity to rolling velocity is called creep or creepage [5], which is the main source of creep force. In this thesis, we relate creep to a positive value assuming the vehicle is braking.

$$\xi = u_s / u_r = (u_v - u_w) / u_r \quad (1)$$

where u_v is the vehicle running speed or translational velocity of a wheel over a rail, u_w is the circumferential velocity of a wheel, and u_r is the rolling speed, defined as follows [5][6]:

$$u_r = (u_v + u_w) / 2 \quad (2)$$

Note that many sources treating railway dynamics define creep as the ratio of sliding velocity to vehicle speed, assuming very small creep. In wheel flange–rail gauge contact, creep is high, resulting in high sliding velocity, while in wheel tread–railhead contact, creep is usually relatively small.

When creep is zero (here we only consider longitudinal creep), which is a pure rolling case, no tangential force is transmitted and the contact area sticks. As soon as tangential force starts to be transmitted, a slip region appears in the trailing edge of the contact patch, while the rest of the contact patch remains stick. This stick–slip region results in rolling–sliding contact. The slip region increases and the stick region decreases in size with increasing creep. When the creep is high enough, the stick region disappears leading to gross slip. The relationship between tangential force and creep is presented in Fig. 4.

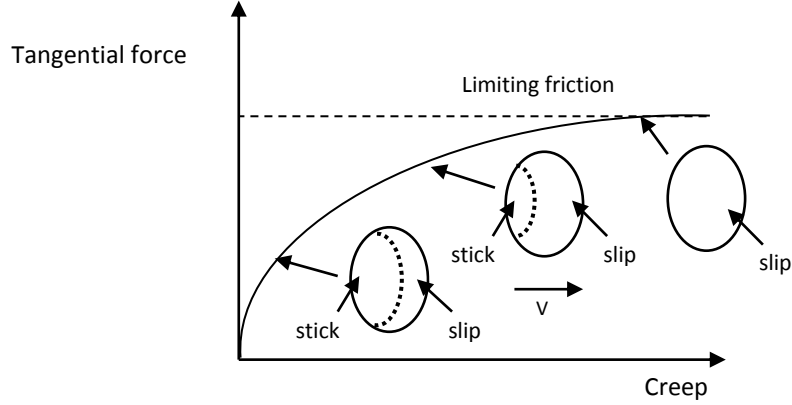


Figure 4. Relationship between tangential force and creep.

2.2 Friction and adhesion

In the late sixteenth century, Leonardo Da Vinci started systematically studying friction. Friction is defined as “the resisting force tangential to the common boundary between two bodies when, under the action of an external force, one body moves or tends to move relative to the surface of the other” [7]. Friction is usually represented by the friction coefficient, which is defined as the ratio of the friction force (F_f) and the normal force (F_N) in the contact between two surfaces, as given in Eq. 3:

$$\mu = \frac{F_f}{F_N} \quad (3)$$

In a railway context, ‘adhesion’ is the friction available to transmit tangential force between railway wheel and rail [1]. Therefore, the vertical axis in Fig. 4 could also be labelled ‘adhesion’. The term ‘adhesion’ is used by both braking and driving wheels. Note that some studies use the term ‘traction coefficient’ instead of ‘adhesion coefficient’, presumably because the research examined traction conditions, i.e., the wheels accelerating over the rail. The adhesion coefficient ($\mu_{adhesion}$) is limited by the friction coefficient ($\mu_{friction}$), which is defined as follows:

$$\mu_{adhesion} = \frac{F_T}{F_N} \leq \mu_{friction} \quad (4)$$

where F_T is the tangential force or adhesion.

The two types of wheel–rail contact require different adhesion levels, which are limited by the friction coefficient. Ideal friction coefficients in the wheel–rail contact [1] for

heavy haul traffic are shown in Fig. 5. When the vehicle is running on a straight track, high adhesion is desirable: during acceleration, low adhesion causes performance problems resulting in delays, while during deceleration, low adhesion dangerously extends the braking distance [1]. Adhesion coefficient requirements for braking and traction [8–10] are listed in Table 1. On the other hand, when the vehicle is travelling around curves, high adhesion in, for example, sharp curves, will also generate problems. In the worst case, excessive adhesion in curves causes wheel climb derailment, as in the 8 March 2000 train accident on a Tokyo metro line [11]. Since low adhesion is desirable in the wheel flange–rail gauge contact, lubricant is usually applied to curved rails. Adhesion in the wheel tread–railhead contact is expected to be comparatively high, so lubrication should be avoided. In some cases, a friction modifier is applied to keep the friction coefficient within a desirable range. According to field measurements [4], the coefficient of friction is higher on the railhead than on the rail edge. However, since the rail is open to the environment, many factors can affect railway adhesion, which will be discussed in the next chapter.

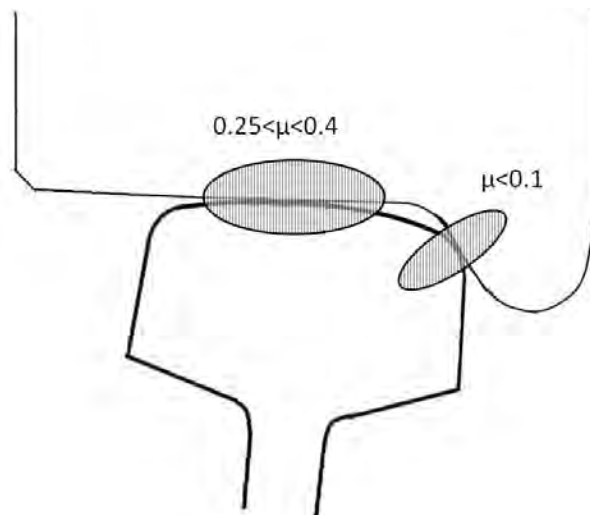


Figure 5. Ideal friction coefficients in the wheel–rail contact for heavy haul traffic [1].

Table 1. Required adhesion coefficients.

	Adhesion coefficient for braking	Adhesion coefficient for traction
Stockholm public transport	approximately 0.15	0.18
U.K.	0.09	0.2
Netherlands	0.07	0.17

2.3 Surface topography

All engineered surfaces are rough to some degree, even when the most advanced surface finishing techniques are used. In most machine elements, surface topography affects friction, wear, and longevity. Moreover, surface topography affects the size of the real contact area [12]. As shown in Fig. 6, surface roughness reduces the nominal contact area to a number of small asperity contact areas (‘contacting asperities’) that must support the entire normal load. The local pressure in some of these asperities will be greater than that

predicted by Herzian theory. According to Marshall et al. [13], maximum pressure between real surfaces is much greater than that predicted by Herzian theory which assumes smooth surfaces. As a result, the high-pressure concentrated area will experience plastic deformation and may work harden, both of which will affect the friction and wear.

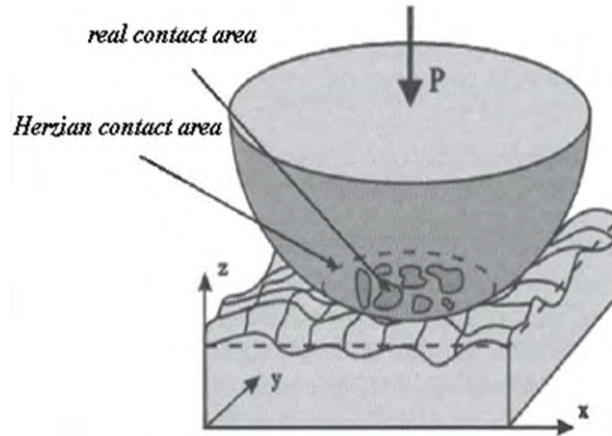


Figure 6. Schematic of contact between rough and smooth surfaces [12].

The surface topography of real wheels and rails is quite variable due to rail grinding and regular use [14][15]. According to Lundmark et al. [14], wheel and rail surfaces can change markedly after just one passing train. Measuring wheel and rail surface topography is difficult. In the field, a quick and repeatable method is to use the MINIPROF system [16]. This system has a small magnetic wheel, approximately 12 mm in diameter, attached to the extremities of two joint extensions. When the magnetic wheel is manually rolled over a surface, the angles of the two extensions are measured and recorded; then the computer can calculate the surface profile. Another way to measure surface topography is to use two-component acrylate plastic to create a negative replica of the original rail surface [4], which is then subjected to 3D surface measurements. However, the accuracy of these techniques are poor [4][17][18]. Some devices [14], such as stylus machines and atomic force microscopes (AFM), can measure the surface topography with high accuracy. Using these devices, both 2D and 3D surface measurements can be made and evaluated in terms of various roughness parameters [19][20]. The two most commonly used 2D parameters are root mean square (RMS) roughness, R_q , and centre-line average (CLA) roughness, R_a , which are defined as follows:

$$R_q = \sqrt{\frac{1}{L} \int_0^L z^2(x) dx} \quad (5)$$

$$R_a = \frac{1}{L} \int_0^L |z(x)| dx \quad (6)$$

where L is the evaluating length and $z(x)$ is the length of the asperity measured from the mean line. However, these measuring devices are heavy, sensitive, and usually time consuming to operate, making them impossible to use in the field. The wheel and rail

surface topographies shown in Fig. 7 (the computer illustration with very coarse grids) are of real wheel and rail samples cut in the field in Stockholm [13] and then measured using a stylus instrument. The left image is of an unused or new wheel–rail pair with R_a values of 4.11 and 2.65 μm , respectively. The right image shows two rough surfaces damaged by sand with R_a values of 12.45 and 20.38 μm for the wheel and rail, respectively. Comparing these two surface topographies shows that wheel and rail surfaces differ considerably.

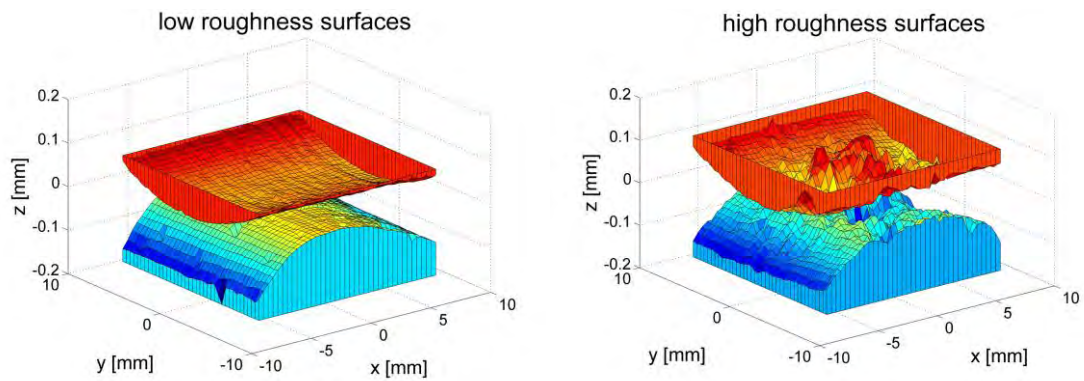


Figure 7. Wheel and rail surfaces of low roughness (left) and high roughness (right).

3 Low adhesion under contaminated conditions

As a rolling–sliding contact, a wheel–rail contact is similar to a rolling ball bearing or gears [1], though these are mostly closed systems with comparatively good lubricating conditions. The wheel–rail contact is an open system, which makes it extremely difficult to transfer knowledge from other well-studied but closed systems. For example, the friction coefficient on the railhead is high on a sunny day but decreases on a rainy day. Even on a sunny day, the friction coefficient can differ depending on the humidity and temperature. In addition, foreign substances, such as sand, dust, leaves, oil or grease, can also be present on the rail. All these factors will influence the friction coefficient, resulting in excessive or insufficient wheel–rail adhesion. Table 2 shows the friction coefficient measured using a hand-push tribometer [1]. The friction coefficient varies depending on the conditions, and is generally reduced by water, oil/grease, and wet leaves. Moreover, temperature and humidity can also change the friction coefficient [21]. Moore [22] presented the typical available friction, i.e., adhesion coefficient, under various conditions as shown in Table 3. Note that sand can increase the adhesion coefficient and moisture can reduce it, compared with outright wet conditions.

Table 2. Friction coefficients measured using a hand-push tribometer [1].

Conditions	Temperature (°C)	Friction coefficient
Sunshine dry rail	19	0.6–0.7
Recent rain	5	0.2–0.3
Substantial grease on rail	8	0.05–0.1
Damp leaf film on rail	8	0.05–0.1

Table 3. Examples of wheel–rail adhesion coefficients [22].

Rail conditions	Adhesion coefficient	Rail conditions	Adhesion coefficient
Dry and clean	0.25–0.3	Moisture	0.09–0.15
Dry with sand	0.25–0.33	Light snow	0.10
Wet and clean	0.18–0.20	Light snow with sand	0.15
Wet with sand	0.22–0.25	Wet leaves	0.07
Greasy	0.15–0.18		

In the context of the railway track, contamination refers to any material that is present on the rail and becomes entrained in the wheel–rail contact. The contamination can be divided into solid contamination, such as sand, dust, leaves, and debris, and liquid contamination, such as water, oil or grease. Of these contaminants, sand is usually used to increase adhesion and remove surface layer contamination, since modern power cars and locomotives require a higher friction coefficient on the railhead [1]. Liquid contaminants and leaves can reduce adhesion, especially when the rolling speed is increasing. Dust or debris could reduce the adhesion by mixing with liquids [23]–[26]. As a result, the dominant problem is too low adhesion in the wheel tread–railhead contact. This thesis focuses mainly on low adhesion in the wheel–rail contact caused by water, oil, and the leaf-formed blackish layer.

Water, which can be in the form of rain, drizzle, or even high humidity, is the most common rail surface contaminant causing low adhesion. Experimental investigation of water as a contaminant that reduces adhesion in the wheel–rail contact started in the UK in the 1970s [23]–[26]. Beagley et al. [23] reported that the adhesion coefficient declined considerably with increased rolling speed under wet conditions. He also pointed out that it was water mixed with wear debris that significantly reduced the adhesion, though the mechanism by which this occurred was still unclear. Oil, which could drip from leaking trains or be deposited at level crossings by vehicle tires or from spilt goods [1], is another typical railhead surface contaminant. Beagley et al. [23] also investigated the influence of oil on the adhesion coefficient, finding that adhesion did not decrease much with increased speed. Zhang et al. [27] used a full-scale roller rig to simulate the wheel–rail contact under oil-contaminated conditions, finding that adhesion dropped to a very low level, though essentially independently of speed.

Liquid contaminants, such as water and oil, are often used as lubricants in certain industrial applications. Lubricants significantly affect wear and friction and will usually improve the lifetime performance and reliability of a machine. Stribeck [28] studied the effects of lubricants in various lubrication regimes as a function of relative surface velocity (see Fig. 8). In the boundary lubrication regime (BL), the velocity is relatively low. The film build-up is negligible and the load is borne mainly by asperities. The main function of the lubricant is to reduce the adhesion component (i.e., atomic forces) of friction. In the full film lubrication regime (FL), the velocity is high and the two surfaces are fully separated by lubricant; the friction depends mainly on the shear stress in the lubricant. The region between BL and FL is known as the mixed lubrication regime (ML), in which part of the load is borne by asperities and part by lubricant. The friction of ML ranges between those of BL and FL. Elastohydrodynamic lubrication occurs when the surface deformation helps to form a film. The application of the lubrication regime concept to wheel–rail adhesion under water- and oil-lubricated conditions could yield a better understanding of the adhesion-reduction mechanism. Furthermore, since field tests or full-scale tests are usually expensive to run, it is crucial to find a connection between scaled lab tests and the real situation. The Stribeck curve and calculated film thickness parameters could be used to compare scaled tests and the real situation in terms of lubrication regimes, which is very important for selecting parameters and making comparisons in scaled tests.

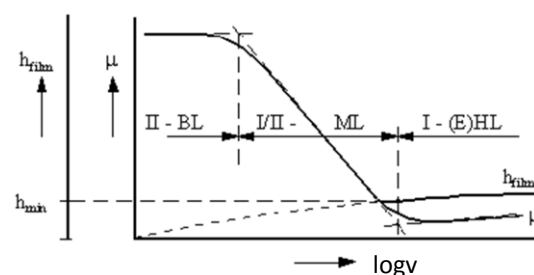


Figure 8. Stribeck curve.

In addition, rail services worldwide are disrupted by fallen leaves. In autumn, leaves fall on the rail lines, forming a blackish layer when they are crushed by passing wheels, resulting in serious adhesion loss. According to Fulford [29], these leaves do not have to fall precisely on the tracks. The turbulence of each passing train stirs up dead leaves that were previously on the track ballast by its slipstream swirling around the vehicle and getting crushed by passing wheels. The crushed leaves eventually form a hard, slippery, blackish layer that strongly adheres to the rail surface and is very difficult and expensive to remove [9][29][31]. This layer gives a friction coefficient of 0.1, or of 0.05 or even less when combined with a small amount of precipitation. Some lab tests [31]–[35] simulating the ‘leaves on the line’ problem have been conducted, indicating that a chemical reaction occurs on the rail surface resulting in low adhesion. However, the exact mechanism of the layer formation remains unknown, since it is very difficult to run tests that exactly reproduce the real situation. Furthermore, leaves cannot be treated as lubricants, so classical tribology theory cannot be applied. In examining various contaminants, the term ‘lubricant’ refers to water and oil in the following section.

4 Computer simulation: adhesion modelling under dry and lubricated conditions

A computer simulation is an attempt to model a real-life or hypothetical system on a computer so that it can be studied to see how it works. It is a useful approach for gaining insight into the operation of a system in an economical way. In the wheel–rail contact, computer simulation could be an efficient and repeatable way to study the influence of each parameter based on certain assumptions, since lab or field tests are usually expensive to run and difficult to control.

The complete contact model becomes extremely complicated if all factors are considered, factors such as deformation (e.g., of sleepers, ballast, and even substructures), track characteristics (e.g., irregularity, flexibility, surface roughness, and material properties), and contaminants. Therefore, the wheel–rail contact models developed are more or less based on certain assumptions, such as a rigid wheel and rail, smooth contact surfaces without contamination, and contact as a point contact. Most contact models aim at computing creep force (considering longitudinal, lateral, and spin creep) for vehicle dynamics calculations, which requires short computational time since vehicle running conditions vary greatly. These models [5][36] are based on Hertz's theory of elliptical contact.

However, under conditions of contamination with, for example, water and oil, the contact conditions change. It is well known that in a lubricated contact in which water or oil, for example, is present between the surfaces, a film will form in the interface between the two bodies. The formed film will share part of the normal load and lower the friction coefficient. The formation and effect of the film depend on factors such as surface topography and lubricant properties [37][38]. Therefore, the above-mentioned contact models are not suitable for computing creep force in lubricated contacts, since they assume smooth, uncontaminated surfaces. A new wheel–rail contact model should be developed at the micro level to accommodate contaminated conditions. The new model, as one part of a complete wheel–rail contact model, should investigate adhesion in terms of surface topography and the influence of various contaminants. Some assumptions are made to simplify the problem: the contact is treated as in a static state regardless of dynamic influence (i.e., fixed creep is used as an input to the model) and only longitudinal creep is considered.

The new adhesion model for lubricated conditions needs to include at least three phenomena in order to predict adhesion. The first is normally loaded asperity-to-asperity contact. The second is the pressure build-up in the fluid that interacts with the asperity-to-asperity contact and helps support the normal load. The last is the tangential stress in the rolling and sliding contact due to the tangential loading of the contact. A precursor to this work was conducted by Chen, who presented both 2D [39] and 3D [40] numerical solutions. Both these solutions consider wheel–rail adhesion as an elastohydrodynamic lubrication (EHL) problem, and water viscosity was included in both models. The author applied simple line contact theory in the 2D solution [39], and flow factors developed by

Patir and Cheng [41] in the 3D solution. However, in both solutions, only normally loaded contact and fluid interaction problems were considered. A tangentially loaded contact model was developed based on pure sliding motion. Tomberger et al. [42] proposed a complete contact model that considered all three phenomena mentioned above, and included contact temperature effects as well. According to the effects of the interfacial fluids, the contact range was divided into the dry contact, boundary lubrication, and mixed lubrication regimes. Normally loaded contact and fluid interaction problems were calculated at the micro scale, but viscosity effects were not included in the model. Tangential stress was computed at the macro scale on the basis of Kalker [36]. Popovici [43] developed a wheel–rail friction model considering all three problems at the macro scale. The mixed lubrication problem was divided into two components: the asperity and EHL components. Asperity contact was simplified as the sum of the individual Hertzian contacts of each micro contact. The EHL component was implemented based on film thickness calculations. The contact conditions were treated as a combination of pure rolling and pure sliding contact.

The adhesion models mentioned above are all based on statistical methods, which means that the wheel rail surfaces are described using mathematical methods. According to Björklund [12], there are two ways to model contacts between rough surfaces, i.e., statistical and numerical methods. Statistical methods make use of the stochastic nature of rough surfaces and are not concerned with the exact surface topography. The most-cited statistical model is the Greenwood and Williamson model [44]. On the other hand, numerical methods can be applied to known surface topography, and can model real pressure distribution in the contact patch. Using actual measured 3D surface topographies of wheels and rails as input, the real pressure distribution can be modelled. Numerical methods can also yield information on how real surfaces influence the adhesion coefficient and the fluid film formation.

A numerical model presented in paper **A** for predicting wheel–rail adhesion under dry and lubricated conditions can solve the problem at the micro level. The purpose of that work is to determine how real wheel and rail surfaces influence the adhesion coefficient under dry, water-lubricated, and oil-lubricated conditions. The assumptions are based on elastic contact bodies as infinite half-space with homogeneous and isotropic material. The model presented in paper **A** can be summarized in the framework shown in Fig. 9.

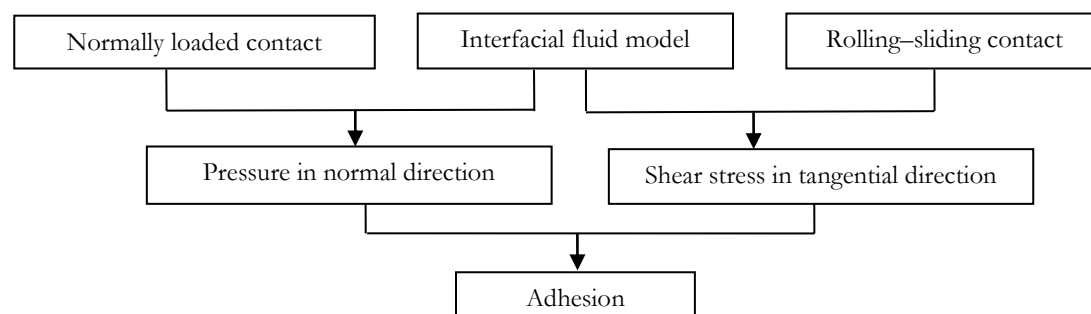


Figure 9. Framework of the numerical model.

- Normal contact model

The surfaces are discretized into a set of elements, each of which corresponds to a uniform pressure. The continuous pressure distribution is then replaced by a discrete set of pressure elements [45]. Given a certain global deformation, which can be regarded as the distance the two contact surfaces would have overlapped without any interaction, each contacting element will deform correspondingly. The real contact area is first estimated as the region the two contact surfaces penetrate without any deformation. The pressure of each element can be found based on the Boussinesq solution. Negative pressure, which indicates that the element is outside the real contact area, should be removed.

- Interfacial fluid model

Since real measured surfaces are used in the model, the gap between the two interacting rough surfaces in which fluid flows can be either convergent or divergent. In the convergent gap, the pressure in the fluid can build up. In the divergent gap, the pressure in the fluid drops, which may generate cavitation when the pressure drops to the ambient level. The solution of the numerical interfacial fluid model differs from those of other models based on statistical methods. The Reynolds equation is then solved in a modified form including cavitation [46]. To balance the load carried by asperities and fluids, an iterative algorithm is used to calculate the actual pressure.

- Rolling–sliding contact model

In modelling a rolling–sliding contact, the contact starts with a stick area and slip occurs when elastic deformation cannot support the relative motion of the two bodies. Based on a particular creep (static situation), the solution starts with the assumption that the whole contact area sticks, and then the shear stress near the trailing edge does not satisfy the boundary condition of limiting friction. These areas are actually slip areas and are removed from the previous stick areas.

As the input to the model, two pairs of measured wheel and rail surfaces (one with high roughness and one with low roughness) along with generated smooth surfaces are used. Simulations are performed under unlubricated and lubricated conditions using the numerical model. Good correlation is found when comparing the results for generated smooth surfaces with widely used approximate nonlinear creep force theory [47][48] under dry conditions. Results also indicate that under dry conditions, the adhesion coefficient peaks at a higher creep with increasing roughness. Under water and oil-lubricated conditions, the maximum adhesion coefficient for low-roughness surfaces is lower than that for high-roughness surfaces, with that for generated smooth surfaces lying between them. Effects of water and oil on the adhesion coefficient are also examined using fluid load capacity. The results indicate that the oil load capacity is greater than the water load capacity. With increased vehicle running speed, the fluid load capacity increases; however, the rate of increase differs between water and oil.

5 Scaled lab test: an MTM study of adhesion under dry and lubricated conditions

In science and technology, a scaled test entails either amplification or reduction of test conditions. A scaled test is of interest when a full-scale test is difficult to perform. Some scaled tests can be conducted in the lab under well-controlled test conditions and are suitable for parameter study.

In research into railway adhesion, some work is done by means of field tests or full-scale tests. Polach [49] studied wheel–rail adhesion under dry and wet conditions using Bombardier and Siemens locomotives in the field at speeds of 30–60 km h⁻¹. Chen et. al [50] and Ohyama [51] used a full-scale twin-disc rolling contact machine to investigate several factors influencing the wheel–rail adhesion coefficient at rolling speeds up to 120 km h⁻¹. Zhang et al. [27] also analyzed wheel–rail adhesion using a full-scale test rig under dry, water-lubricated, and oil-lubricated conditions at speeds up to 280 km h⁻¹. These tests based on locomotives and full-scale test rigs could be run under conditions very close to real ones in terms of axle load, contact geometry, and rolling speed. However, these tests are usually difficult to arrange and/or expensive to run. As a result, many experimental studies [23]–[26] have been performed in the laboratory using scaled test rigs, such as disc–disc, disc-on-cylinder, or disc-on-flat machines. The most common equipment for investigating wheel–rail adhesion under various conditions is the twin-disc machine [9][35]. Because the twin-disc machine can generate rolling–sliding contact, it can simulate the motion of the wheel on the rail. The discs are usually made of real wheel and rail material and the contact pressure is set to be close to the real wheel–rail contact pressure. The maximum rolling speed can range from 1 to 5 m s⁻¹ depending on the test set-up. In addition, the pin-on-disc test rig has also been used to simulate the sliding motion in the wheel–rail contact [52]. The above-mentioned scaled test rigs offer the advantages of repeatable, comparatively cheap, and well-controlled testing. However, twin-disc tests are usually conducted based on fixed creep and speed. It is difficult to change the creep and the speed during testing, so full adhesion and Stribeck curves are difficult to obtain. Pin-on-disc testing provides a pure sliding contact that can simulate only the sliding motion of the wheel–rail contact. Recently, Cann [34] used a mini traction machine (MTM) to investigate adhesion in the wheel–rail contact. The MTM is a ball-on-flat test rig that can generate a rolling–sliding contact under a wide range of contact pressures. Moreover, the rolling speed and creep (i.e., the slide–roll ratio in MTM testing) can be changed during testing, so both the adhesion and Stribeck curves can be obtained. It is also possible to specify the temperature of the lubricants in the contact.

A schematic of the MTM is shown in Fig. 10. The test rig consists of a steel ball and a steel disc. The ball is loaded against the face of the disc in what is known as a ball-on-flat contact. The ball and disc can be rotated independently by two motors to generate a rolling–sliding contact. This results in a slide-to-roll ratio (*SRR*), defined as:

$$SRR = \frac{|U_{disc} - U_{ball}|}{(U_{disc} + U_{ball})/2} \quad (7)$$

where U_{disc} and U_{ball} are the velocities of the disc and ball, respectively. The denominator of Eq. 7 is known as the MTM entraining speed.

The ball-on-disc set-up is tested in a closed environment to keep the temperature at the required level. The lateral force exerted on the ball is measured using a force transducer, which further yields the coefficient of friction.

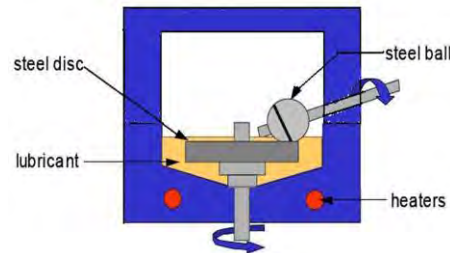


Figure 10. Schematic of the MTM.

The testing can be run in two ways. One way is to keep the entrainment speed constant, increasing (or decreasing) the SRR value to obtain an adhesion curve. The other way is to keep the SRR value constant, increasing (or decreasing) the entrainment speed to obtain a Stribeck curve. Note that for each entrainment speed, measurements are made with $U_{disc} > U_{ball}$ and $U_{disc} < U_{ball}$, keeping SRR constant. The average is taken of the two measurements to remove any offset errors in lateral force measurements. In MTM testing, the SRR and entrainment speed can be considered equivalent to creep and rolling speed in railway applications.

Paper **B** presents an experimental study, using an MTM, of adhesion in the wheel–rail contact. This work seeks to determine the influence of several factors, for example, lubricants, rolling speed, and surface roughness, on the adhesion coefficient under dry and lubricated conditions. Testing specimens are discs of two roughnesses (i.e., smooth and rough) and balls; all specimens are made of AISI 52100 steel. The hardness of the disc is approximately 300 HV (close to that of rail material) while that of the ball is 800 HV. Tests are performed to determine both adhesion curves and Stribeck curves. The SRR value ranges from 0 to 100% while the entraining speed ranges from 10 to 1500 mm s^{-1} . Tests are performed at two lubricant temperatures (i.e., 5 and 20°C) and contact pressures (i.e., 700 and 900 MPa). The film thickness parameter (λ) is computed in both scaled tests and real wheel–rail contacts to compare the scale and field tests and determine the relationship between them. The surface topography of the specimens before and after testing is measured and analyzed using the stylus machine. The stylus instrument is a Taylor Hobson Form Talysurf PGI800, which has a stylus tip radius of 2 μm and is traceable to national standards. Atomic force microscopy (AFM) and scanning force microscopy (SFM) are also used for imaging tiny surface scratches found on the disc. AFM is an ultra-high-resolution type of scanning probe microscopy operating at nanometre scale; the instrument consists of a cantilever with a sharp tip (20-nm probe)

used to scan the specimen surface. Both 2D and 3D topography are obtained using the above instruments for surface analysis.

In the dry testing, surface roughness did not exert a significant influence on the adhesion coefficient, which ranged from 0.6 to 0.7. In the oil-lubricated testing, surface roughness, contact pressure, and lubricant temperature were found to exert a slight influence on the adhesion coefficient. In the water-lubricated testing, the adhesion coefficient for smooth discs was extremely low at 0.02 compared to 0.2 for rough discs. The value is even lower than those obtained under oil-lubricated conditions. Higher water temperatures (i.e., 5–20°C) were able to increase the adhesion coefficient from 0.15 to 0.2 on rough discs. Surface topography measurements indicated only small scratches on the water-lubricated smooth discs. The number of scratches is fewer and their depth less than those on oil-lubricated discs. Rough discs tested under water-lubricated conditions display a clear wear track. Comparison of the experiments using the MTM with those using the real wheel–rail contact is presented in terms of lubrication regime based on lambda value calculations.

6 Field test: a study of leaf contamination on the railhead

A field test is a test conducted under actual operating conditions instead of under controlled conditions in a laboratory. Compared with a lab test, a field test can reflect the real situation but usually under very complex conditions.

With regard to adhesion in the wheel–rail contact, the low adhesion caused by leaf contamination is more complicated than wheel–rail adhesion under lubricated conditions. In the cases of water and oil, we already have some data on the lubricants and it is also possible to measure their unknown properties. However, we know little about leaves and the associated low adhesion problem, though low adhesion caused by leaf contamination is severe and widespread. Fulford [8] reports that the leaf-formed blackish layer gives a very low friction coefficient, which becomes even lower with the presence of a small amount of precipitation. These blackish layers are extremely difficult to remove [31]. According to the Swedish national railroad administration, the cost associated with ‘leaves on the line’ in Sweden was estimated to be SEK 100 million annually as of 1996 [29], and the annual cost was reportedly GBP 50 million in the United Kingdom as of 2001 [30]. In the Netherlands, extremely low adhesion one day in autumn 2002 increased wheel defects by 20%, forcing the rail operator to halt service on most of the network that day [9]. In this decade, some tests have been conducted to simulate the ‘leaves on the line’ problem. Poole [53] used a full-scale test rig to produce leaf film in the laboratory, in order to compare the results with those from the field. Olofsson and Sundvall [31] carried out pioneering work to simulate leaf contamination using a pin-on-disc machine in the laboratory, while Olofsson himself presented a multi-layer model [32] of the contaminated rail surface. In devising this model, he measured the friction coefficient on the leaf-contaminated surface and other related factors [32]. The chemical composition of these contaminated surfaces was analyzed using glow discharge optical emission spectrometry (GD-OES). In addition, Gallardo-Hernandez and Lewis [35] and Arias-Cuevas [33] simulated leaf contamination using a twin-disc machine. Cann [34] used an MTM to study the ‘leaves on the line’ problem, and found that the pectin and cellulose in the film resulted in the low friction coefficient. The blackish layer was formed by chemical reactions between leaves and the bulk material. However, all these results were obtained from lab testing. Since we still do not understand the actual mechanism by which leaves cause low adhesion, it is necessary to investigate the real situation, as it includes all potential factors. Therefore, field testing is best suited for studying leaf contamination on the railhead and can provide complementary results for comparison to lab testing results.

Paper **C** presents a field test study of leaf contamination on the railhead surface. The work seeks to determine the characteristics of the leaf-contaminated layer and their connection to the low friction coefficient. The test track is part of the Stockholm Underground track system operated and maintained by Stockholm Public Transport AB (SL). The test track, a parallel straight section near the Brommaplan underground station, has a long history of adhesion problems. Over the course of one year, the friction

coefficients of rail sections were measured in five periods (i.e., June 2008, September 2008, October 2008, November 2008, and March 2009) using a hand-push tribometer; rail samples were cut in each period for surface analysis. The surface analysis techniques used in this study are described below.

- Electron spectroscopy for chemical analysis (ESCA)

ESCA, also known as X-ray photoelectron spectroscopy (XPS), is a quantitative spectroscopic technique that measures the elemental composition and chemical state of elements in the analysed material. The spectra are obtained by irradiating a material with a beam of X-rays while simultaneously measuring the kinetic energy and number of electrons that escape from the top 1 to 10 nm of the material. The raw ESCA spectrum results comprise a plot of detected electrons versus their binding energy. Each element produces characteristic peaks at characteristic binding energies, which can be directly identified as each element present in the surface of a material. The number of detected electrons in each characteristic peak is directly related to the amount of the element in the irradiated area. Some examples of ESCA spectra are shown and discussed in Olefjord et al. [54].

- Glow discharge optical emission spectrometry (GD-OES)

GD-OES is an analytical technique widely used for the elemental and depth profiling analysis of materials. The depths amenable to such analysis range from a few nanometres to approximately 100 μm . In GD-OES, the test specimen forms the cathode in a glow discharge lamp. The discharge support gas is usually argon. A low-power argon plasma is initiated by the applied high potential between two electrodes (known as the d.c. glow discharge source) [55]. The applied high potential causes the discharge gas to break down electrically to form electrons and positively charged ions. The positive ions are attracted towards the sample surface by the electric fields within the plasma, which may reach substantial kinetic energies. When an ion strikes the sample surface with sufficient energy, the transfer of momentum into the atomic lattice structure of the surface may cause the release of surface material into gas phase, in a process known as ‘sputtering’. The sputtered material then undergoes a larger number of collisional processes, such as electronic excitation, that make the sputtered material exist in the glow charge as excited state species. Photons, which are emitted by the excited state species in the plasma, can be measured and analyzed based on elements’ characteristics. The emission intensities as a function of sputtering time yield elemental depth profiles. To quantify the recorded depth profiles involving sputtering through layers of highly varying composition, special calculation algorithms for quantifying sputtered depth and elemental mass fractions are used. The method is capable of detecting all chemical elements. More details of GD-OES and a comparison with EXCA are discussed by Dizdar [56] and Bengtson [57].

Hand-push tribometer measurements indicate that the friction coefficient in the contaminated period is only 0.15, which is quite low compared with the results from other periods. Note that the maximum friction coefficient recorded in these tests is 0.7 for dry uncontaminated rail. Surface analysis results indicate that high amounts of

calcium, carbon, and nitrogen and a reduced amount of iron are found only in the blackish layer. The distributions of other elements, from the outermost surface and a depth of several microns below the surface, in the blackish layer also differ from other samples. Samples taken on other occasions and those taken on the same occasion but without the blackish layer do not display the same characteristics. The thickness of the friction-reducing oxide layer, D_0 (see Fig. 11) [58][59], is calculated based on the depth profiles of the iron and oxygen contents. Nano-indentation tests indicate that the blackish layer is softer than the uncontaminated layers.

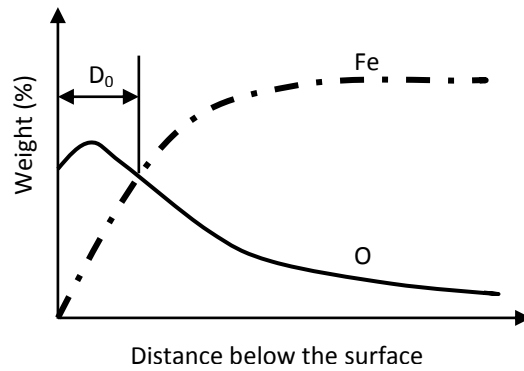


Figure 11. Schematic depth profile. The thickness of the friction-reducing oxide layer is D_0 .

7 Concluding remarks

The concluding remarks take the form of answers to the research questions. The research questions can be divided into two groups, one related to water- and oil-lubricated contacts and the other to leaf contamination. The former is discussed in papers **A** and **B**, while the latter is discussed in paper **C**.

- *How does surface topography affect wheel–rail adhesion under water-lubricated conditions?*

This question was addressed using both numerical simulation and lab testing. The numerical study found that the adhesion coefficient for low-roughness surfaces was lower than that for high-roughness surfaces, with that for generated smooth surfaces lying between them, though the difference among the three was fairly small. With increased speed, the reduction of the adhesion coefficient was also small. Water can reduce the limiting friction from 0.52 (dry) to 0.17, as measured on the rail section. According to fluid load capacity results, only a very small part of the load is borne by water, most of the load being carried by asperities. This indicates that a water-lubricated contact is boundary lubricated because of the low viscosity of water; this finding is in line with the minimum film thickness calculated by Hamrock [60]. However, experimental results indicate a significant difference between the adhesion coefficients for smooth and rough discs. The measured and numerically simulated adhesion coefficients are similar for rough discs, but the adhesion coefficient for smooth surfaces is extremely low. Full-scale lab testing and field testing also indicate that wheel–rail adhesion under wet conditions decreases significantly with increasing speed [51], a phenomenon not attributable to the hydrodynamic effect of fluids. As a result, chemical reaction or the particular water–contaminant mixture may have an essential impact on wheel–rail adhesion. Beagley and Pritchard [25] found that the presence of water in a stainless steel contact could reduce the friction coefficient only from 0.7 to 0.57, indicating that the effect of pure water was very limited. Beagley [26] also suggested that the presence of a small amount of oil in water substantially reduced the friction, the extent of the reduction depending on the amount of oil present. Furthermore, water mixed with wear debris could be reduce adhesion greatly because of the high viscosity of the mixture [26]. In boundary lubrication, chemical reactions are also important; for example, the presence of a thin oxide layer on the surface can give very low friction [56][61][62]. However, neither the water–contaminant mixture nor the chemical reaction could be simulated by the present model. The influence of surface topography under water-lubricated conditions was investigated by Chen et al. [50] using both a full-scale and a scaled test rig; the authors used three kinds of abrasive paper, i.e., #80, #320, and #800, to generate three levels of surface roughness with R_q values of 2.01, 0.78, and 0.53 μm , respectively. Results indicated that increasing roughness would increase the adhesion coefficient, in line with the results presented here.

- *How does surface topography affect wheel–rail adhesion under oil-lubricated conditions?*

This question was addressed using both numerical modelling and lab testing. The results of the numerical model correlated with those of the lab testing under oil-lubricated conditions. The adhesion coefficient for low-roughness surfaces is lower than that for high-roughness surfaces, because rough surfaces negatively affect film formation, reducing the fluid load capacity. However, the adhesion coefficient for the generated smooth surface is between those for the two measured surfaces. This can be explained by the ‘pocket’ effect found by Zhu and Hu [37]. Surface roughness is helpful in the boundary lubrication regime, as it can generate ‘pockets’ that retain lubricant in the contact. As a result, the fluid load capacity of low-roughness surfaces is higher than that of perfectly smooth surfaces, resulting in a lower adhesion coefficient for low-roughness surfaces. When the surface topography is very rough, for example, in the case of the high-roughness surfaces shown in Fig. 7, the ‘pocket’ effect disappears because the film pressure in the ‘pocket’ areas decreases. The conclusion that the adhesion coefficient increases with increasing surface roughness is true only for relatively rough surfaces, while the opposite is the case for relatively smooth surfaces. The lubrication regimes prevalent under oil-lubricated conditions are as follows: on extremely smooth surfaces, the effects of elastohydrodynamic lubrication are marked particularly with increasing speed; on medium-smooth surfaces, mixed lubrication prevails; while on rough surfaces, boundary lubrication dominates. This conclusion agrees well with lambda calculations for real wheel–rail contacts, indicating that the lubrication regime in oil-lubricated wheel–rail contacts varies from boundary to elastohydrodynamic depending on the speed and surface roughness. An early experimental investigation [51] classified wheel–rail adhesion under oil-lubricated conditions as boundary lubrication; this might not always be correct, since the lubrication regime depends on the surface roughness and speed. Beagley et al. [23] found that variation in wheel–rail adhesion was also associated with changes in the quantity of oil on the surface. Unfortunately, it is very difficult to change the amount of lubricant when using an MTM, since the contact is submerged in the lubricant. In numerical simulation, it is also very tricky to specify the viscous effect of the lubricant according to the amount.

- *Do other factors affect wheel–rail adhesion?*

Yes, many other factors do affect adhesion in the wheel–rail contact, as follows:

- 1) Speed and creep. Note that the speed investigated in paper **A** is vehicle running speed while in paper **B** it is rolling speed; creep in paper **B** is called *SRR*. The relationships between these parameters are explained in the two papers. In the low creep range, the adhesion coefficient increases with increased creep because the slip region increases in extent. When creep reaches a certain value, gross slip appears, at which point speed is the governing factor. With increased speed, the adhesion coefficient decreases, since increased speed will increase the fluid load capacity.
- 2) Lubricant temperature. This is discussed in paper **B**. Under water-lubricated conditions, increasing the water temperature from 5 to 20°C can increase the adhesion coefficient for rough discs. However, similar behaviour is not apparent for smooth discs or under oil-lubricated conditions.

3) Contact pressure. This is discussed in paper **B**. Higher contact pressure will increase the adhesion coefficient under water-lubricated conditions, but only for rough surfaces. Under oil-lubricated conditions, the influence of oil temperature is very slight.

- *What is the chemical composition of the leaf-contaminated blackish layer, and how does it differ from those of uncontaminated layers?*

The surface analysis indicates the chemical composition of the leaf-contaminated blackish layer differs greatly from that of the uncontaminated layers, when sampled both on the same and different occasions. Significantly large amounts of carbon, calcium, oxygen, and nitrogen and a reduced amount of iron were found in the blackish layer. In addition, the blackish layer also differs distinctly from that of other samples in the contents of other elements. These results indicate that the leaves chemically reacted with the bulk material to form the blackish layer. Hardness testing also indicates that the blackish layer is softer than the uncontaminated layers.

- *Why does the presence of a leaf-contaminated blackish layer on the railhead surface give a low friction coefficient?*

The thickness of the friction-reducing oxide layer is very closely correlated with the friction coefficient; however, the blackish layer is the thickest layer and gives the lowest friction coefficient. It is not the leaves themselves that cause the low friction coefficient but the blackish layer which is formed by leaves chemically reacted with the bulk material. The depth profiles of the iron and oxygen contents are useful to predict the friction coefficient. However, the possibility that other elements may also affect the friction coefficient merits further examination.

Based on the present results, the following further research would be productive:

- *The numerical model could be further improved by including the effects of contact temperature, plastic deformation, and the presence of an easily sheared surface layer.*
- *The experimental work could be further improved by studying the effects of surface texture and the oxide layer in combination with water or other contaminants.*

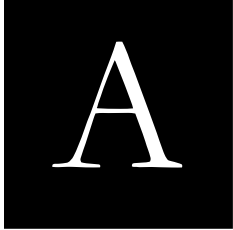
8 References

- [1] Lewis R., Olofsson U.: *Wheel-rail interface handbook*, Woodhead Publishing Limited, Cambridge, UKs, 2009, pp. 24, 284, 437, 510, 514.
- [2] Esveld C.: *Modern railway track*, 2nd edition, ISBN 90-800324-3-3, 2001
- [3] Lewis R., Olofsson U.: Mapping rail wear regimes and transitions, *Wear* 257 (2004), pp. 721–729
- [4] Olofsson U., Telliskivi T.: Plastic deformation and friction of two rail steels: a full-scale test and a laboratory study, *Wear* 254(2003), pp. 80–93
- [5] Carter F.W.: On the action of a locomotive driving wheel, *Proceedings of Royal Society of London* A112 1912, pp. 151–157.
- [6] Kalker J.J.: Wheel-rail rolling contact theory, *Wear* 144 (1991), pp. 243–261.
- [7] ASM handbook, Vol.18: friction, lubrication, and wear technology. *ASM international* 1992
- [8] Fulford C.R.: *Review of low adhesion research*, published by Rail Safety and Standards Board (May 2004)
- [9] Arias-Cuevas O.: *Low adhesion in the wheel-rail contact*, Doctoral thesis, TUD, Delft, 2010
- [10] Jacobsson M.: *Teknikforum Halt Spår*, Technical report (in Swedish), Stockholm Local Traffic, Mar. 2011.
- [11] Baek K., Kyogoku K., Nakahara T.: An experimental study of transient traction characteristic between rail and wheel under low slip and low speed conditions, *Wear* 265(2008), pp. 1417–1424.
- [12] Björklund S.: *Elastic contacts between rough surfaces*, Doctoral thesis, KTH, Stockholm, 1995
- [13] Marshall M.B., Lewis R., Dwyer-Joyce R.S., Olofson U., Björklund S.: Experimental characterization of wheel-rail contact patch evolution, *J. Tribol.* 128/3 (2006), pp. 493–504.
- [14] Lundmark J., Höglund E., Prakash B.: Running-in behaviour of rail and wheel contacting surfaces, AITC-AIT 2006, *International Conference on Tribology*, Parma, Italy, 20–22 Sept. 2006.
- [15] Chen H., Ishida M.: influence of rail surface roughness formed by rail grinding on rolling contact fatigue, *QR of RTRI*, Vol.47, No.4, 2006
- [16] Esveld C.: MINIPROF: wheel and rail measuring equipment, Esveld Consulting Services BV, The Netherlands
- [17] Sundh J.: *On the wear transitions in the wheel-rail contact*, Doctoral thesis, KTH, Stockholm, 2009
- [18] Ohlsson O., Rosen B.: On replication and 3D stylus profilometry techniques for measurement of plateau-honed cylinder liner surfaces, in: R. J. Hocken (Ed.), *Proceedings of the ASPE 1993 Annual Meetings*, Seattle, Washington, USA, 7–12 November 1993
- [19] Thomas T.R.: *Roughness surfaces*, 2nd edition, Imperial college press, 1999
- [20] Whitehouse D.J.: *Handbook of surface and nanometrology*, ISBN 0 7503 0583 5, Institute of physics publishing, 2003

- [21] Lewis R., Lewis S., Zhu Y., Abbasi S., Olofsson U.: The modification of a slip resistance meter for measurement of railhead adhesion, *Proceedings of International Heavy Haul Association Conference 2011*, Calgary, Canada.
- [22] Moore D.F. *Principles and Applications of Tribology*, Elsevier, Amsterdam (1998)
- [23] Beagley T.M., Mcewen I.J., Pritchard C.: Wheel/rail adhesion: boundary lubrication by oily fluids, *Wear* 31 (1975) 77–88.
- [24] Beagley T.M., Mcewen I.J., Pritchard C.: Wheel/rail adhesion: the influence of railhead debris, *Wear* 33 (1975) 141–152.
- [25] Beagley T.M., Pritchard C.: Wheel/rail adhesion: the overriding influence of water, *Wear* 35 (1975) 299–313.
- [26] Beagley T.M., The rheological properties of solid rail contaminants and their effect on wheel/rail adhesion, *Proc. Instn. Mech. Engrs.* 190 (39) (1976) 419–428.
- [27] Zhang W., Chen J., Wu X., Jin X.: Wheel/rail adhesion and analysis by using full scale roller rig, *Wear* 253 (2002) 82–88.
- [28] Stribeck R., Die wesentlichen eigenshaften der Gleit-und rollenlager, *Zeitschrift des vereins deutscher ingenieure*, 46 pp. 1341–1348, 1432–1438, and 1463–1470
- [29] Forslöv L., wheel slip due to leaf contamination, *Swedish National Rail Administration TM 1996 03 19*, Borlänge, Sweden, 1996
- [30] Managing low adhesion, Report published by the Adhesion Working Group, UK, (September 2001)
- [31] Olofsson U., Sundvall K.: Influence of leaf, humidity and applied lubrication on friction in the wheel–rail contact: pin-on-disc experiments, *Proc. Instn Mech. Engrs Vol. 218 Part F: J. Rail and Rapid Transit*, 2004
- [32] Olofsson U.: A multi-layer model of low adhesion between railway wheel and rail, *Proc. Instn Mech. Engrs Vol. 221 Part F: J. Rail and Rapid Transit*, 2007
- [33] Arias-Cuevas O.: Investigation some sanding parameters to improve the adhesion in leaf contaminated wheel–rail contacts. *Proc. Instn Mech. Engrs Vol. 224 Part F: J. Rail and Rapid Transit*, 2010, pp. 139–157
- [34] Cann P.M.: The ‘leaves on the line’ problem: a study of leaf residue film formation and lubricity under laboratory test conditions, *Tribology letters*, Vol. 24, No. 2, 2006, pp. 151–158
- [35] Gallardo-Hernandez E.A., Lewis R.: Twin disc assessment of wheel/rail adhesion, *Wear* 265 (2008) 1309–1316.
- [36] Kalker J. J., A fast algorithm for the simplified theory of rolling contact, *Vehicle System Dynamics* 11 1982, pp. 1–13
- [37] Zhu D., Hu Y.: A computer program package for the prediction of EHL and mixed lubrication characteristics, friction, subsurface stresses and flash temperatures based on measured 3-D surface roughness, *Tribology Trans.* Vol. 44(2001), 3, pp. 383–390
- [38] Bergseth E.: *Influence of surface topography and lubricant design in gear contacts*, Licentiate thesis, Royal Institute of Technology, Department of machine Design, Stockholm, Sweden, 2009

- [39] Chen H., Ban T., Ishida M., Nakahara T.: Adhesion between rail/wheel under water lubricated contact, *Wear* 253(2002), pp. 75–81.
- [40] Chen H., Ishida M., Nakahara T.: Analysis of adhesion under wet conditions for three dimensional contact considering surface roughness, *Wear* 258 (2005), pp. 1209–1216.
- [41] Patir N., Chen H.S., Effects of surface roughness orientation on the central film thickness in EHD contact, *Proceedings of the 5th Leeds–Lyon Symposium on Tribology*, 1978, pp. 15–21
- [42] Tomberger C., Dietmaier P., Sextro W., Six K.: Friction in wheel–rail contact: a model comprising interfacial fluids, surface roughness and temperature, *8th International Conference on Contact Mechanics and Wear of Rail/Wheel System (CM2009)*, Firenze, Italy, 15–18 September 2009, pp. 121–132.
- [43] Popovici R.I.: *Friction in wheel–rail contact*, Doctoral thesis, University of Twente, Department of Engineering Technology, Enschede, Netherlands (2010).
- [44] Greenwood J.A., Williamson J.B.P.: Contact of nominally flat surfaces, *Proc. R. Soc. Lond. A* 6, 295/1442 (1966), pp. 300–319.
- [45] Björklund S., Andersson S.: A numerical method for real elastic contacts subjected to normal and tangential loading, *Wear* 179 (1994), pp. 117–122.
- [46] Ausas R.F., Jai M., Buscaglia G.G.: A mass-conserving algorithm for dynamical lubrication problems with cavitation, *J. Tribol.* 131/3 (2009), pp. 1–7.
- [47] R.C. White, D.A. Limbert, J.K. Hederick, N.K. Cooperrider: *Guideway–Suspension Tradeoffs in Rail Vehicle Systems*, report DOT-OS-50107, Washington DC (1978).
- [48] Z.Y. Shen, L. Hedrick, and J.A. Elkins: A comparison of alternative creep-force models for rail vehicle dynamic analysis, *Proc. of 8th LAVSD Symposium on Dynamics of Vehicles on Roads and on Tracks*, Boston, MA (1983), pp. 591–605.
- [49] Polach O.: Creep forces in simulations of traction vehicles running on adhesion limit, *Wear* 258 (2005), 992–1000.
- [50] Chen H., Ban T., Ishida M., Nakahara T.: Experimental investigation of influential factors on adhesion between wheel and rail under wet condition, *Wear* 265 (2008) 1504–1511.
- [51] Ohya T.: Tribological studies on adhesion phenomena between wheel and rail at high speeds, *Wear* 144 (1991) 263–275.
- [52] Sundh J., Olofsson U., Sundvall K.: Seizure and wear rate testing of wheel–rail contacts under unlubricated conditions using pin-on-disc methodology, *Wear* 265 (2008) 1425–1430.
- [53] Poole W.: Characteristics of railhead leaf contamination, summary report published by Rail Safety and Standards Board (May 2007)
- [54] Olefjord I., Brox B. and Jelvestam J.: Surface composition of stainless steels during anodic dissolution and passivation studied by ESCA, *J. Electrochem. Soc.* Vol 132(1985) 2854–2861.
- [55] Winchester M.R., Payling R.: Radio-frequency glow discharge spectrometry: A critical review, *Spectrochimica Acta Part B* 59 (2004) pp. 607–666

- [56] Dizdar S.: *Formation and failure of chemireacted boundary layers in lubricated steel contacts*, Doctoral thesis, KTH, Stockholm, 1999
- [57] Bengtson A.: Summary of ISO/TC 201 Standard: III ISO 14707:2000 – Surface chemical analysis – Glow discharge spectrometry – Glow discharge optical emission spectrometry – Introduction for use Surf. *Interface Anal.* 2002; 33: pp. 363–364
- [58] Zhao Y.W., Liu J.J., Zheng L.Q.: The oxide film and oxide coating on steels under boundary lubrication. *Proceedings of 16th Leeds–Lyon Symposium on Tribology* (1989), pp. 305–311.
- [59] Zhao Y.W., Liu J.J.: The nature of the friction transition as a function of load and speed for the steel/steel system, *ASME/STLE Tribol. Trans.* 33(1990), pp. 648–652.
- [60] Hamrock B.J.: *Fundamental of fluid film lubrication*, NASA, 1991
- [61] Baek K-S., Kyogoku K., Nakahara T.: An experimental investigation of transient traction characteristics in rolling–sliding wheel/rail contacts under dry–wet conditions, *Wear* 263 (2007), pp. 169–179
- [62] Nakahara T., Baek K-S., Chen H., Ishida M.: Relationship between surface oxide layer and transient traction characteristics for two steel rollers under unlubricated and water lubricated conditions, *Wear* 271 (2011), pp. 25–31



Adhesion modeling in the wheel–rail contact under dry
and lubricated conditions using measured 3D surfaces

Y. Zhu, U. Olofsson, A. Söderberg

An extended version of “Adhesion modeling in the wheel–rail contact under wet
conditions using measured 3D surfaces”

Proceedings of LAVSD 2011

International Symposium on Dynamic of Vehicles on road and tracks,

Aug 14-19, Manchester

Submitted to *Journal of Tribology*

ADHESION MODELING IN THE WHEEL–RAIL CONTACT UNDER DRY AND LUBRICATED CONDITIONS USING MEASURED 3D SURFACES

Yi Zhu, Ulf Olofsson, Anders Söderberg

Department of Machine Design, Royal Institute of Technology

Brinellvägen 83, 100 44 Stockholm, Sweden

E-mail: yiz@kth.se, phone: 46 8 790 6861, fax: 46 8 202287

Abstract: Adhesion between wheels and rails plays an essential role in the safe, efficient, and reliable operation of a railway network. Particularly under lubricated conditions, trains can experience adhesion loss. This paper presents an adhesion model constructed using measured 3D wheel–rail surfaces. The numerical model comprises three parts: a normally loaded contact model, an interfacial fluid model, and a rolling–sliding contact model. Simulation examples use the numerical model to investigate how dry conditions and wet contamination (i.e., water and oil) might affect wheel–rail adhesion in contacts with different surface roughness levels. Simulation indicates that with increased roughness, adhesion peaks at a higher creep value under dry conditions. Under both water- and oil-lubricated conditions, the adhesion coefficient of low-roughness surfaces is lower than that of high-roughness surfaces, though the adhesion coefficient of generated smooth surfaces is a slightly higher than that of low-roughness surfaces. Furthermore, the fluid load capacity is inversely proportional to the adhesion coefficient, both of which are clearly dependent on vehicle speed. It is theoretically clear that under oil-lubricated conditions, the lubrication regime is boundary to mixed lubrication depending on surface topography and speed. However, boundary lubrication prevails in a wheel–rail contact under pure water-lubricated conditions.

Keywords: wheel–rail contact; adhesion; numerical model; measured 3D surfaces

Nomenclature

A_c, A_f	Contact areas occupied by asperities and fluids	C_p, C_q	Matrix of influential coefficients
C_0	Constant generated from the integration	d	Deformation of contact asperities
F_{Ntotal}	Computed total normal force in the iteration	F_N, F_T	Normal force, tangential force
g	The gap between two surfaces before loading	F_{Tc}, F_{Tf}	Tangential force from the asperity contact and fluids
n	Number of strips	h	Film thickness
q	Shear stress in the asperities	p_c, p_f	Pressure in the asperities and fluids
u_r, u_s	Rolling speed and sliding speed	s	Sliding distance
u_w	Wheel speed or the circumferential velocity of a wheel	u_v	Vehicle running speed or the translational velocity of a wheel over a rail
α	Dimensionless velocity: $\alpha = 12u_r\eta$	x	Distance between the concerned element and the leading edge of the strip
δ_z	Global deformation	β	Coefficient of normal force ($\beta \leq 1$)
η	Viscosity of the fluid	ε	Error
μ	Adhesion coefficient	θ	Cavitation-governing parameter
ζ	Creep in %	μ_{lim}	Coefficient of limiting friction
τ	Shear stress in the fluid		

1 Introduction

Since the beginning of railway transport, wheel–rail adhesion has been a crucial factor. Early on, locomotive designers changed the wheel arrangement according to the optimal weight distribution to obtain maximum adhesion [1]. Worldwide, adhesion problems nowadays affect both railway operations and safety. In accelerating, low adhesion causes performance problems resulting in delays, while in decelerating, low adhesion extends the braking distance leading to danger [2]. On the other hand, high adhesion in certain areas, such as sharp curves, can also generate problems; in the worst case, it can cause wheel climb derailment (e.g., the 8 March 2000 train accident on the Tokyo Metro line [3]). Wheel–rail adhesion is influenced not only by railway operation factors such as running speed, creep, and surface roughness, but also by environmental factors such as water, oil, wear particles, and leaves.

Several models are available with which to predict wheel–rail adhesion under dry conditions; most of these are based on the work of Carter [4] and Kalker [5–7]. More recently, efforts have been made to model wheel–rail adhesion under wet conditions. This modeling work must take account of at least three phenomena in order to predict adhesion. The first is normally loaded asperity–asperity contact. The second is the pressure build-up in the fluid that interacts with the asperity–asperity contact and helps support the normal load. The third is the tangential stress in the rolling–sliding contact due to the tangential loading of the contact.

Chen pioneered this effort by presenting both 2D [8] and 3D [9] numerical solutions. Both methods treat wheel–rail adhesion as an elastohydrodynamic lubrication (EHL) problem, and both models include water viscosity. In the 2D solution, the author applied line contact theory, while in 3D solution, flow factors developed by Patir and Cheng [10] were utilized. However, both methods treat only normally loaded contact and fluid interaction problems; tangentially loaded contacts were not considered, so the contact condition was limited to sliding contact rather than rolling–sliding contact. Tomberger [11] proposed a complete contact model including all three mentioned phenomena and the contact temperature effect as well. According to the interfacial fluid effects, the contact range can be divided into dry contact, boundary, and mixed lubrication regimes. Normally loaded contact and fluid interaction problems were calculated at a micro-scale level, but the viscosity effect was not included in the model. Tangential stress was computed at a macro-scale level using Kalker theory [8]. Popovici [12] developed a wheel–rail friction model considering all three phenomena at a macro-scale level. The mixed lubrication problem was divided into two components: an asperity and an EHL component. The asperity contact was simplified as the sum of the Hertzian contact of all micro-contacts. The EHL component was implemented based on film thickness calculations. The contact condition was regarded as a combination of pure rolling and pure sliding contact. All above models could predict adhesion under wet-lubricated conditions. As these models were based on surfaces described using statistical methods and the asperity heights used followed a Gaussian distribution, these models provide no information about the contact state at a micro-scale level.

In the present work, the authors present a wheel–rail adhesion model using real measured 3D surfaces. The surfaces were cut from actual wheel and rail sections and measured using a stylus machine [13]. The model consists of three parts: normally loaded asperity–asperity contact, interfacial fluid pressure build-up, and tangential stress in the rolling–sliding contact. Furthermore, simulation examples are presented in which the contact condition applies from unlubricated contact to lubricated contact. Both water and oil are used as lubricants, while the effects of speed, roughness, fluid load capacity, real contact area, and creep are investigated.

2 Modeling

2.1 Summary of the model

The adhesion coefficient, μ , is used to evaluate the available adhesion and is calculated using the available tangential force, F_T , divided by the normal force, F_N . Note that some studies use the term traction coefficient instead of adhesion coefficient, presumably because the research was examining traction conditions, i.e., wheels accelerating along the rail. In this paper, the term adhesion coefficient is used assuming braking conditions. Under wet conditions, water or oil will form an interfacial layer. We assume that the tangential force can be divided into a tangential force in the fluids, F_{Tf} , and a tangential force relating to the asperity contacts, F_{Tc} . The adhesion coefficient can be calculated as:

$$\mu = \frac{F_T}{F_N} = \frac{F_{Tf} + F_{Tc}}{F_N} \quad (1)$$

Three problems need to be solved here. First, a normally loaded contact model is used to solve the asperity–asperity contact problem. Second, an interfacial fluid model is used to solve the fluid pressure problem. These two models work together to generate a pressure distribution in the normal direction, as the applied normal load is shared by both asperities and fluids. Furthermore, the friction force in the fluids can be calculated in the interfacial fluid model. Third, a rolling–sliding contact model is used to calculate the adhesion force in the tangential direction from the known pressure distribution. The framework of the model is presented in Fig. 1.

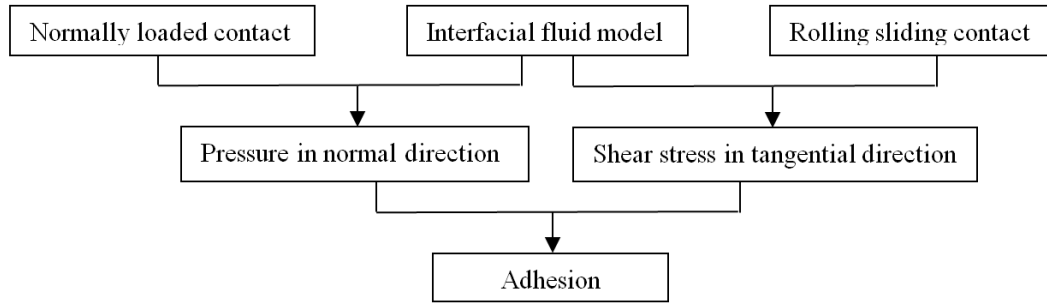


Fig. 1 Framework of the model

2.2 Normally loaded contact model

A normally loaded contact comprises the interaction of two contact bodies loaded with a normal force. A simple approach to solving this problem is Hertz theory, assuming smooth surfaces of non-conformal contact in the case of elastic solids. If surface roughness is considered, the methods can be divided into two approaches. The first approach is based on surfaces described using statistical methods [14], while the second uses actual measured surfaces to calculate pressure. In this work, since measured 3D surfaces are used, the numerical method proposed by Björklund and Andersson [15] is employed. The method assumes frictionless contact and treats the elastic contact bodies as infinite half-space. It works by replacing the continuous pressure distribution with a discrete set of pressure elements. This method is briefly outlined below.

First, the contact area is divided into a set of rectangular elements, each related to a unique pressure. Knowing the gap, g , between the two contact bodies and the global deformation, δ_z , which can be regarded as the distance the two contact surfaces would have overlapped without any interaction, the contact pressure, p_c , can be obtained by:

$$C_p p_c = \delta_z - g \quad (2)$$

where C_p is a matrix of influence coefficients for uniform pressure on a rectangular element as found by Love [16]. Note that in this model, the deformation at one element will be influenced by the deformation and pressure at other elements. As the real contact area is unknown in advance, it is first estimated as the region where the two contacting surfaces interpenetrate without any deformation (Fig. 2). Solving Eq. (2) will result in some pressures having negative values, indicating that these elements are outside the contact region. These elements are removed until all pressures become positive.

When the pressure distribution is known, the total deformation in each element is computed as:

$$d = C_p p_c \quad (3)$$

and the gap between the two deformed surfaces, which is used as the initial film thickness, can be found as:

$$h = g - \delta_z + d \quad (4)$$

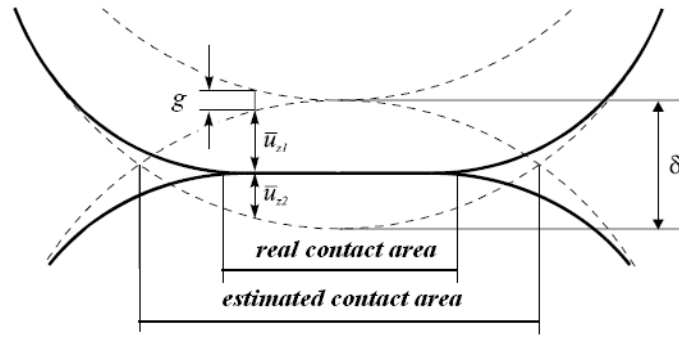


Fig. 2. Real and estimated contact area [15]; broken and solid lines refer to the geometry of the contact bodies before and after deformation, respectively

2.3 Interfacial fluid model including cavitation

The interfacial fluid model aims to calculate the pressure distribution in the fluid that supports the normal load together with the asperity–asperity contacts. Since real measured surfaces are used in the model, the gap between the two interacting rough surfaces in which fluid flows can be either convergent or divergent. In a convergent gap, pressure can build up in the fluid, while in a divergent gap, the pressure drops in the fluid, possibly generating cavitation when the pressure drops to the ambient level. Pioneers in this field were Jakobsson and Floberg [17] and Olsson [18]; then Elrod and Adams (1974) [19] and Elrod (1981) [20] extended their work to form a universal cavitation algorithm. They introduced a cavitation-governing parameter, usually denoted by θ . This model satisfies both a null pressure gradient in the cavitation region and mass conservation under boundary conditions. The method used in the present model is based on a cavitation solver proposed by Ausas et al. [21]. The modified Reynolds equation describing the cavitation problem can then be written as:

$$\frac{\partial}{\partial x}(\alpha\theta h - h^3 \frac{\partial p_f}{\partial x}) + \frac{\partial}{\partial y}(-h^3 \frac{\partial p_f}{\partial y}) = 0 \quad (5)$$

$$\alpha = 12u_r\eta \quad (6)$$

$$u_r = \frac{(u_w + u_v)}{2} \quad (7)$$

where u_r is the rolling speed, and u_v and u_w are the speeds of the vehicle and wheel, respectively [5, 22]. Here, the water viscosity is obtained from the experimental work of Dorsey [23] and the oil viscosity is based on the Barus equation. In the full-film lubrication region, $p > 0$, $\theta = 1$; furthermore, in the cavitated region, $p = 0$, $\theta <$

1. As an initial condition, the whole contact area is assumed to be in the full-film lubrication region ($\theta = 1$). The pressure distribution in fluid can be calculated using a finite difference method.

In the normal direction, applied load is shared by both asperities and fluids. Then an iteration algorithm is needed to combine both the normally loaded contact model and the interfacial fluid model to determine the actual pressure distribution over the concerned area. The algorithm is summarized in the following flow chart (Fig. 3).

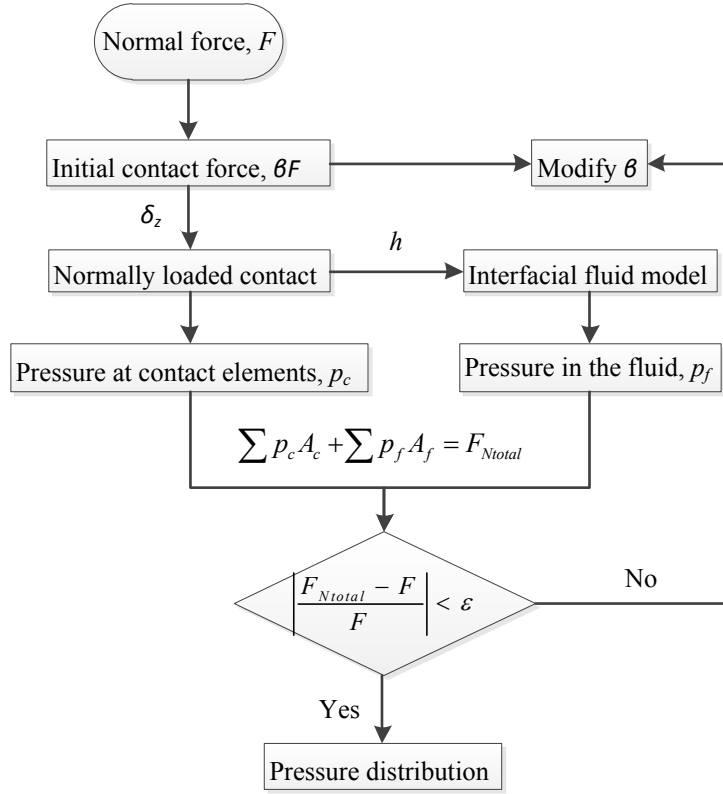


Fig. 3. Flow chart of iteration algorithm for interfacial fluid model

The normal force is known in advance. First, we assume that part of the normal force, βF , is carried by asperity–asperity contacts. The normally loaded contact model solves the pressure distribution, p_c , in the asperities as well as the initial film thickness. Then the interfacial fluid model computes the pressure distribution, p_f , in the fluid. At the same time, areas occupied by asperity–asperity contacts and fluid, A_c and A_f , respectively, can be obtained. The total normal force, F_{Ntotal} , can be computed and compared with the known applied normal force. If the result satisfies the convergence, we can obtain the pressure distribution over all elements; if it does not, coefficient β needs to be modified and the whole iteration has to be done again.

2.4 Tangential rolling–sliding contact

For a classical sliding contact, Coulumb’s law of friction can be employed to calculate the tangential force given known normal force. In a pure rolling contact, adhesion is zero and no tangential force is transmitted. However, the wheel–rail contact is a combination of sliding and rolling contact, since there is usually a velocity difference between wheel rolling speed and vehicle running speed. The ratio between the velocity difference and the rolling speed is defined as creep, ζ (as shown in Eq. 8). Note that creep is positive for the braking condition and negative for the driving condition.

$$\xi = \frac{u_v - u_w}{u_r} \quad (8)$$

Due to creep, the contact areas are divided into stick and slip regions at the micro-scale level (Fig. 4). When creep is zero, the motion is pure rolling motion and the stick region covers the whole contact area. When a tangential force starts to be transmitted, a slip region appears in the contact patch. With increasing creep, the slip region increases and the stick region decreases in size, resulting in a rolling–sliding contact. When creep is great enough, the stick region disappears leading to gross slip. The maximum tangential force is limited by the friction force available between two surfaces.

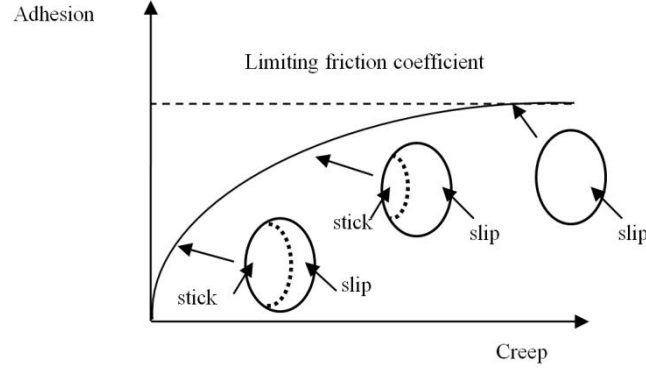


Fig. 4. Relationship between adhesion and creep

Several methods [5, 22] can solve the tangential stress in rolling–sliding contact. The approach used here is strip theory, which was established by Haines and Ollerton [24] and further developed by Kalker [25]. In this approach, the contact area is divided into strips based on the meshed elements according to the rolling direction. Each strip starts with a stick region, and slip appears when elastic deformation cannot support displacement. Given known pressure distribution and creep, the shear stress, q , can be obtained using:

$$\sum_{i=1}^n \mathbf{C}_q \mathbf{q}_i = -\xi \mathbf{x}_i + \mathbf{s}_i + (\mathbf{c}_0)_i \quad (9)$$

where the local tangential traction is limited by the condition

$$q \leq \mu_{\text{lim}} P_c \quad (10)$$

Here, the contact area is divided into n strips. \mathbf{C}_q is a matrix of influences that govern the relationship between shear stress and deformation. Tangential stress, q , is solved for each strip; \mathbf{c}_0 is a constant generated from the integration [22], to make tangential stresses start from zero at the leading edge, and \mathbf{s} is the sliding distance, which is not really calculated in the solution. The solution starts with the assumption that there is no slip in the contact area. If Eq. (9) is solved, the tangential stresses near the trailing edge will violate the limiting friction condition, i.e., Eq. (10) [15]. These violating elements are then moved out of the unknown part of the equation, though they still affect the remaining elements. Eq. (10) will be solved repeatedly until all remaining elements are sticking or sliding (no stick elements).

The other component in a tangentially loading contact is the tangential stress in the fluid. Given known local film thickness, h , and viscosity, η , the shear stress in the fluid can simply be computed as:

$$\tau = \eta \frac{u}{h} \quad (11)$$

The temperature effect is not considered in the model, so η is limited by a set maximum value. The shear stress has a limiting value, according to Dyson's empirical formulae [26]. Compared with the tangential stress in the asperities, the fluid shear stress is very small. Then the adhesion coefficient can be obtained using:

$$\mu = \frac{F_T}{F_N} = \frac{F_{Tf} + F_{Tc}}{F_N} \approx \frac{\sum qA_c + \sum \tau A_f}{F_N} \quad (12)$$

3 Simulation set-up

Two types of real measured surfaces, unused (i.e., low roughness) and sand-damaged (i.e., high roughness) pairs, along with generated perfectly smooth surfaces were analyzed (Fig. 5). Surface topography was measured using a stylus machine (Taylor Hobson PGI800) system; for details regarding the surfaces, see Marshall et al. [13]. The measurement resolution is 0.01 mm in the x and y directions. The mesh grids used in the simulation are 38×38 elements, each $0.4 \text{ mm} \times 0.4 \text{ mm}$ in size. For the generated smooth surfaces and low-roughness surfaces, the mesh grids can represent the surface topography: since the waviness is great, the numerical error is comparatively small. However, for the high-roughness surfaces, the mesh grids supply inadequate resolution, since the surface waviness is fairly small. As a result, the mesh grids cannot reflect the whole surface topography in detail. The results obtained for the high-roughness surfaces may contain comparatively large error and can only be used for purposes of comparison with smooth and low-roughness surfaces.

The inputs to the model, unless otherwise stated, are summarized in Table 1. Vehicle speeds of $1\text{--}21 \text{ m s}^{-1}$ are chosen because this is the typical speed range of a commuter train in the Stockholm local network. The coefficient of limiting friction in Eq. (10) was measured along a rail section using a pendulum rig in the lab. The rail section, which was cut from track in Brommaplan, Stockholm, in March 2009 during a period of good adhesion, had a clean railhead appearance. The experiments were conducted under dry, water-lubricated, and oil-lubricated conditions at a temperature of $20 \pm 2^\circ\text{C}$ and humidity of $30 \pm 5\%$. Details of the experiment are presented in Lewis et al. [27]. Simulation is performed using this numerical model under dry and lubricated conditions to investigate adhesion and other influential factors; water and oil are used as lubricants in the simulation.

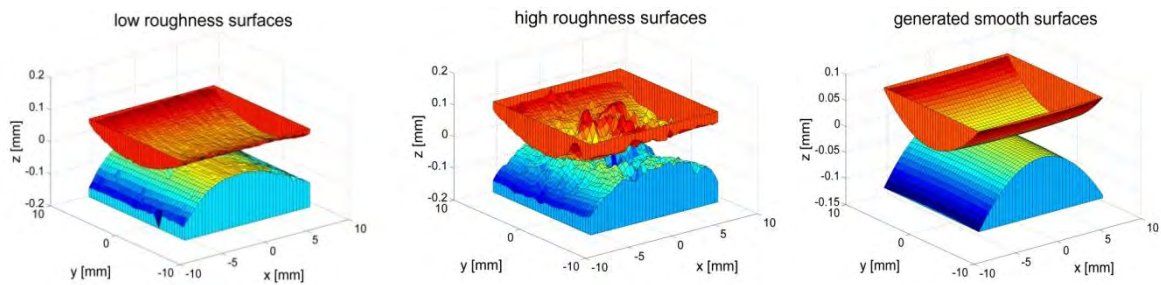


Fig. 5 Measured 3D wheel and rail surfaces: low-roughness (left), high-roughness (middle), and generated smooth (right) surfaces

Table 1 Simulation conditions

Fluid	Water, oil*
Water temperature	20°C^{**}
Normal load	80 kN
Vehicle running velocity	$1\text{--}21 \text{ m s}^{-1}$
Coefficient of limiting friction	0.52 (dry), 0.17 (water-lubricated), and 0.08 (oil-lubricated)

* Absolute viscosity at ambient pressure, $0.2 \text{ Pa} \cdot \text{s}$; viscosity coefficient, $2.2 \times 10^{-8} \text{ m}^2 \text{ N}^{-1}$

** Water viscosity was approximated by a polynomial of the 4th power of pressure according to Dorsey [23]

4 Results

4.1 Dry contacts

The results of simulations under dry conditions are shown in Fig. 6. Here, the results for generated smooth surfaces are compared with those obtained using the widely used approximate nonlinear creep force theory (ANCF theory) proposed by White [28] and Shen et al. [29]. The two curves are very close, the maximum error being approximately 6%. All the adhesion curves increase with increased creep before adhesion peaks due to the limiting friction coefficient. This is because with increased creep, the slip regions increase leading to increasing adhesion. However, the rate of increase differs: smooth surfaces reach maximum adhesion at lower creep levels (approximately 1%), while high-roughness surfaces peak at a creep of 6%. The maximum value of the adhesion coefficient is the same for the various surface topographies, so the adhesion coefficient remains constant after reaching the limiting friction coefficient. Temperature effects resulting from increasing sliding speed, which can change the conditions, are not included in the model [8, 11]. The actual pressure distributions on three different surfaces when creep is 0.5% are shown in Fig. 7. The pressure distribution on generated smooth surfaces coincides with other theoretical results quite well [5, 6]. The pressure distribution on low-roughness surfaces follows the surface topography, but we can still distinguish the slip area from the stick area. However, difference, in terms of pressure distributions and contact areas, could be found between high-roughness surfaces and the rest of the two pairs of surfaces. A comparison of real contact area and mean contact pressure is shown in Table 2. The contact area of generated smooth surfaces is close to that of low-roughness surfaces, while the contact area of high-roughness surfaces is much smaller. On the other hand, mean contact pressure is inversely proportional to the contact area. On high-roughness surfaces, the mean contact pressure is even higher than the ultimate strength of the wheel and rail material, which indicates that the high-roughness surfaces will experience considerable plastic deformation. Unfortunately, the model assumes elastic contact, so plastic deformation is not considered.

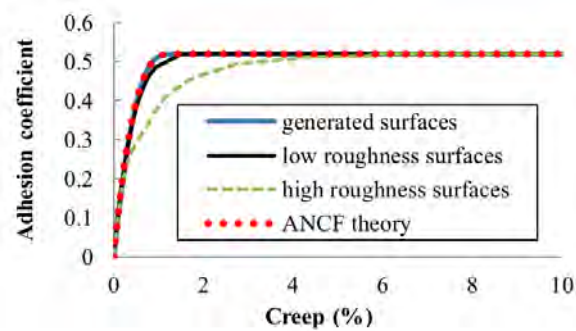


Fig. 6. Adhesion curves for three surfaces and according to ANCF theory

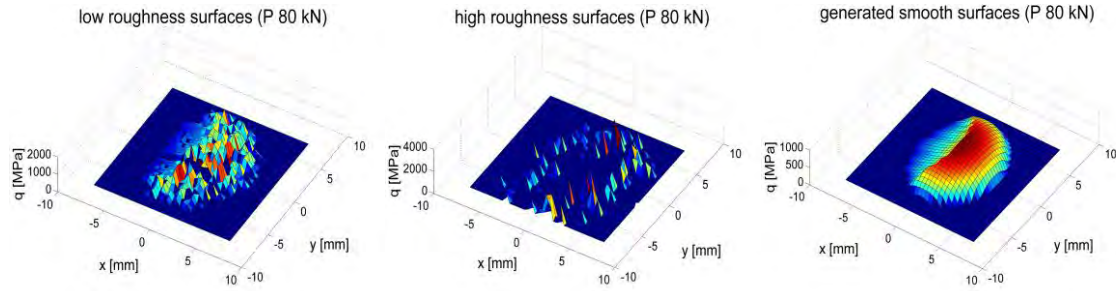


Fig. 7 Pressure distribution on low-roughness (left), high-roughness (middle), and generated smooth (right) surfaces with 0.5% creep

Table 2 Real contact area and mean contact pressure under dry conditions

Surface types	Analysis techniques	Contact area (mm ²)	Average pressure (MPa)
Smooth	Hertzian theory	89.9	890
	Numerical model	92.0	870
Low roughness	Numerical model	83.7	956
High roughness	Numerical model	37.6	2128

4.2 Lubricated contacts

Water and oil are used as lubricants to investigate the influence of fluids on the adhesion coefficients of low-roughness, high-roughness, and generated smooth surfaces (Fig. 8). The limiting coefficient of friction sets an upper limit on the maximum adhesion coefficient. Compared with a maximum adhesion coefficient of 0.52 in dry contacts, the maximum adhesion coefficient declines to 0.17 in water-lubricated contacts and 0.08 in oil-lubricated contacts. Under both water- and oil-lubricated conditions, the adhesion coefficient of low-roughness surfaces is lower than that of high-roughness surfaces, because increasing roughness weakens the formation of fluid films that can help carry the normal load. This is in agreement with the results of previous numerical [8, 9, 11] and experimental [30, 31] studies. However, the difference in adhesion coefficient between two measured surfaces under oil-lubricated conditions is greater than that under water-lubricated conditions, because water viscosity is low and the variation in water viscosity is also small compared with that of oil. On the other hand, the adhesion coefficient of the generated smooth surfaces lies between that of the two measured surfaces under both water- and oil-lubricated conditions.

To clarify the dependence of adhesion decrease on surface roughness and lubricant, the fluid load capacity is also presented in Fig. 8. The fluid load capacity is defined as the load carried by the fluid divided by the applied load. In the high-roughness surface case, the load capacity is approximately 0.7% and 5% versus approximately 2% and 19% for generated smooth surfaces and 2.5% and 22% for the low-roughness surfaces under water- and oil-lubricated conditions, respectively. In addition, reduced fluid load capacity can be found with increasing creep, because creep is always positive in this work, indicating that the vehicle is braking. In this situation, the rolling speed decreases, as shown in Eq. 13, since the creep increases while the vehicle running speed is kept constant in the simulation. Therefore, reducing the rolling speed would weaken the effect of lubricants on adhesion. Another interesting phenomenon is that the adhesion coefficient peaks at a lower creep value under oil-lubricated than water-lubricated conditions, which is also reported by Gallardo-Hernandez and Lewis [32].

$$u_r = \frac{(u_v + u_w)}{2} = \frac{2u_v}{(2 + \xi)} \quad (13)$$

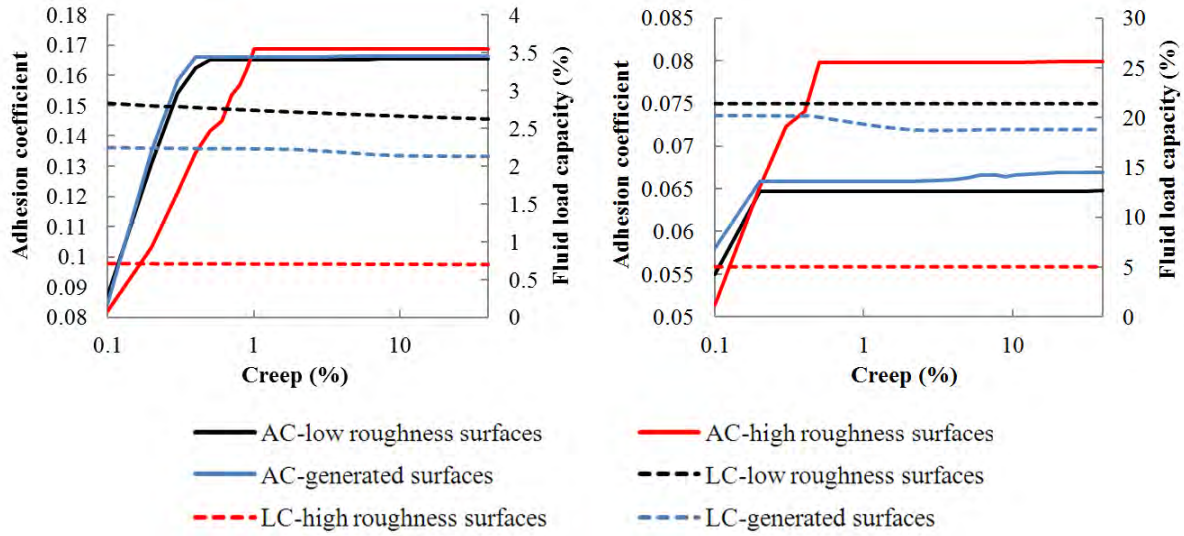


Fig. 8 Adhesion curve and fluid load capacity under water-lubricated conditions (left) and oil-lubricated conditions (right) (AC = adhesion coefficient, LC = fluid load capacity)

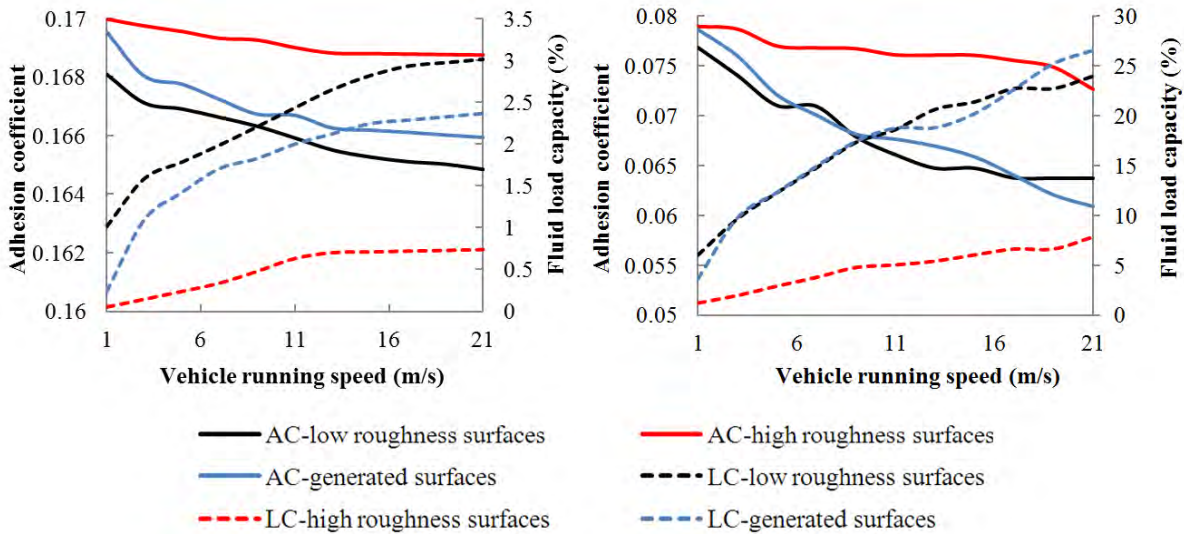


Fig. 9 Adhesion vs. vehicle running speed and fluid load capacity under water-lubricated conditions (left) and oil-lubricated conditions (right) (AC = adhesion coefficient, LC = fluid load capacity)

In Fig. 9, the influence of vehicle running speed on adhesion coefficient under water- and oil-lubricated conditions is analyzed at 2% creep, which ensures that gross slip appears in all cases. All adhesion coefficients decrease with increased vehicle running speed, which coincides with other findings obtained using both numerical simulation [8, 9, 11] and testing [30–32]. The explanation is straightforward: Increasing the speed increases the fluid’s capacity to share more load, lowering the adhesion coefficient. However, the adhesion coefficient under oil-lubricated conditions decreases from approximately 0.079 to 0.073 on high-roughness surfaces, from approximately 0.077 to 0.065 on low-roughness surfaces, and from approximately 0.079 to 0.06 on perfectly smooth surfaces, compared with a small reduction under water-lubricated conditions. The oil load capacity is greater than the water load capacity, because the oil is much more viscous than the water. From these two figures, a fairly good correlation can be found between adhesion coefficient and fluid load capacity. The

greater the proportion of the load carried by the fluid, the lower the adhesion coefficient. Furthermore, the adhesion coefficient decreases more on low-roughness than on high-roughness surfaces throughout the vehicle running speed range. It is also notable that when vehicle running speed exceeds 17 m s^{-1} , the oil load capacity on perfectly smooth surfaces is greater than on low-roughness surfaces, so the adhesion coefficient is lower on smooth surfaces.

5 Discussion

The accuracy of the simulation depends on the resolution or number of mesh grids. The use of fine-meshed surfaces can increase the numerical accuracy but is limited by computation speed and numerical stability. Model simulations of high-roughness surfaces may not reflect the actual surface topography, so results for such surfaces are useful only for comparison with results for the other two surface types.

In dry contacts, the adhesion peaks at a higher creep value with increased surface roughness, mainly due to the difference in shear stress distribution near the leading edge. This reason for the phenomenon is clarified in Fig. 10, which shows the difference in shear stress distribution between smooth and rough surfaces at 0.8% and 10% creep. The 10% creep level is chosen to ensure that the shear stress reaches its limiting value (gross slip), while the shear stress distribution at 0.8% creep can offer a good comparison. On the generated smooth surfaces, the shear stress is close to the saturated value (i.e., 10% creep in this figure) at 0.8% creep. However, on the high-roughness surfaces, the shear stress on the leading edge (i.e., the stick area) is still far from the saturated value (i.e., when gross slip appears), since the saturated shear stress in this region is very high due to the high roughness. Since high asperity pressure is more likely to appear on rough than smooth surfaces, the shear stress near the leading edge needs greater creep to reach saturation on rough surfaces, because the saturated area (i.e., slip region) increases from the trailing edge to the leading edge. Generally speaking, therefore, the adhesion peaks at a higher creep value with increasing roughness. However, the pressure distribution on a high-roughness surface is not continuous, in which case the tangential rolling–sliding contact model may not be applicable, calling for further study. Moreover, plastic deformation would affect the shear stress distribution by lowering the limiting pressure.

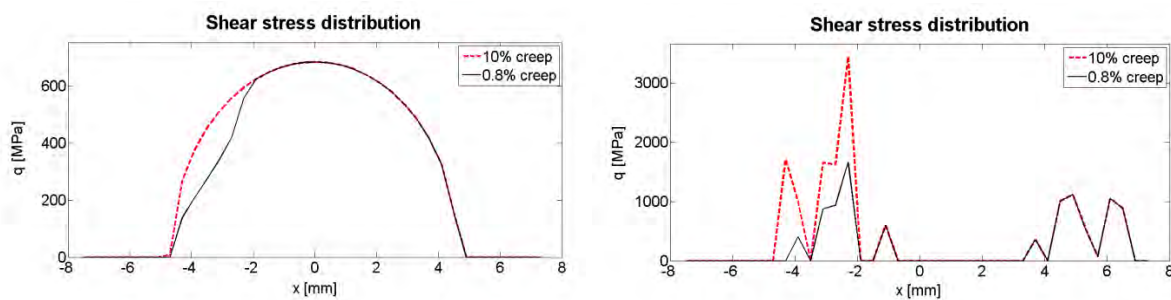


Fig. 10 Two-dimensional shear stress distribution on generated smooth surfaces (left) and high-roughness surfaces (right) at 0.8% and 10% creep

The adhesion curve results obtained under lubricated conditions indicate that the adhesion coefficient does not always increase linearly with increased roughness. It is clear that under water-lubricated conditions, the lubrication regime is complete boundary lubrication, while under oil-lubricated conditions, it ranges from boundary to mixed lubrication. As a result, most of the load is carried by asperities instead of fluids under water-lubricated conditions. According to Zhu and Hu [33], surface roughness is helpful in the boundary lubrication regime, as the “pockets” formed in the asperities help retain lubricant in the contact. This could explain why the fluid load capacity is higher on low-roughness than perfectly smooth surfaces, resulting in a lower adhesion

coefficient for low-roughness surfaces. When the surface topography is very rough, as on high-roughness surfaces, the “pocket” effect disappears because the film pressure in the “pocket” areas decreases. The conclusion that the adhesion coefficient increases with increasing surface roughness applies only to relatively rough surfaces, while on relatively smooth surfaces, the opposite is the case. Surface topography plays an essential role in wheel–rail contact under wet conditions when speed is low (boundary lubrication). In Fig. 9, the adhesion coefficient is shown to be lower for smooth than for low-roughness surfaces under oil-lubricated conditions when the speed exceeds 17 m s^{-1} . This could be explained by the fact that with increased speed, the effects of elasto-hydrodynamic lubrication start to exert an impact. In that case, the two contacting surfaces are lifted a little and the “pocket” effect is no longer significant. Under water-lubricated conditions, however, the situation remains the same as described previously, since boundary lubrication prevails.

These results indicate that the effect of water on the adhesion coefficient is limited by its low viscosity. The reduction in adhesion coefficient with increasing speed is small under water-lubricated conditions. Water lubrication in the wheel–rail contact constitutes boundary lubrication, which means that most of the tangential force is transmitted by the asperities instead of the fluid, so the influence of the water is slight while that of surface roughness is marked. The results of recent tests [34] indicate that surface topography exerts great influence on adhesion coefficient, and that a very smooth surface can have an extremely low adhesion coefficient under water-lubricated conditions. However, other studies [8, 9, 11, 30–32] have reported a significant decrease in adhesion coefficient with increasing speed under water-lubricated conditions. There are two possible explanations for this. First, the present work ignores the squeeze effect of rolling motion, which may affect adhesion. In modeling the squeeze effect, surface topography needs to be considered as a time-dependent term throughout the rolling process, making it difficult and time consuming to implement in the model. More importantly, in real situations, water may be mixed with other contaminants, such as leaves, oil, wear debris, and foreign particles, that, in combination with the metal or oxide layer, can create an easily sheared surface layer that can reduce the adhesion [35, 36].

The presented results indicate that creep makes a major contribution to the adhesion coefficient in the low-creep range, because when creep is low, increasing it will increase the slip area, resulting in increasing the adhesion coefficient. When the whole contact area slips, rolling speed is the factor governing the adhesion coefficient while the effect of creep is comparatively limited. Under these conditions, increased creep leads to increased sliding speed, u_s , as shown in Eq. 14, which increases the temperature of the metal and fluid. However, the effect of rolling speed outweighs that of temperature increase [37].

$$u_s = u_v - u_w = \frac{2\xi u_v}{(2 + \xi)} = \frac{2u_v}{\left(\frac{2}{\xi} + 1\right)} \quad (14)$$

6 Conclusions

The numerical model is used to predict adhesion based on two real measured 3D surfaces and a generated smooth surface under dry and lubricated conditions. Some conclusions can be drawn from this study:

- Surface topography affects the creep value when the adhesion coefficient peaks under dry conditions.
- Surface topography plays an essential role under both water- and oil-lubricated conditions. “Pockets” formed on rough surfaces help retain lubricants thus fluids carrying more load than on smooth surfaces. But the “pockets” effects depend on the surface roughness.

- Water and oil reduce the adhesion coefficient in different ways. In water-lubricated contacts, the lubrication regime is complete boundary lubrication due to its low viscosity. The significant reduction of the adhesion coefficient in the field might be due to the presence of a water–contaminant mixture or to squeeze effects. On the other hand, in oil-lubricated contacts, the lubrication regime is boundary to mixed lubrication. Elastohydrodynamic lubrication starts to exert an effect as speed increases in oil-lubricated contacts since oil has high viscosity.

Acknowledgements

This research was performed under the auspices of the KTH Railway Group, with the support of Stockholm Public Transport and Swedish Transport Administration.

References

- [1] Andrews, H. I., 1986, *Railway Traction: The Principles of Mechanical and Electrical Railway Traction*, Elsevier Science, Amsterdam.
- [2] Lewis, R., and Olofsson, U., 2009, *Wheel–Rail Interface Handbook*, Woodhead Publishing Limited, Cambridge, UK, pp. 510, 438–448.
- [3] Baek, K., Kyogoku, K., and Nakahara, T., 2008, “An Experimental Study of Transient Traction Characteristics between Rail and Wheel under Low Slip and Low Speed Conditions,” *Wear*, **265**(9–10), pp. 1417–1424.
- [4] Carter, F. W., 1912, “On the Action of a Locomotive Driving Wheel,” *P. R. Soc. Lond. A*, **A112**(760), pp. 151–157.
- [5] Kalker, J. J., 1991, “Wheel–Rail Rolling Contact Theory,” *Wear*, **144**(1–2), pp. 243–261.
- [6] Kalker, J. J., 1971, “Survey of the Theory of Local Slip in the Elastic Contact Region with Dry Friction,” *Int. Appl. Mech.*, **7**(5) 1971, pp. 472–483.
- [7] Kalker, J. J., 1982, “A Fast Algorithm for the Simplified Theory of Rolling Contact,” *Vehicle Syst. Dyn.*, **11**(1), pp. 1–13
- [8] Chen, H., Ban, T., Ishida, M., and Nakahara, T., 2002, “Adhesion between Rail/Wheel under Water Lubricated Contact,” *Wear*, **253**(1–2), pp. 75–81.
- [9] Chen, H., Ishida, M., and Nakahara, T., 2005, “Analysis of Adhesion under Wet Conditions for Three-dimensional Contact Considering Surface Roughness,” *Wear*, **258**(7–8), pp. 1209–1216.
- [10] Patir, N., Chen, H. S., 1978, “Effect of Surface Roughness Orientation on the Central Film Thickness in EHD Contacts,” *Proc. 5th Leeds–Lyon Symp. on Tribology, Elastohydrodynamics and Related Topics*, D. Dowson et al., eds., Inst. Mech. Engrs. Publ., London, pp. 15–21.
- [11] Tomberger, C., Dietmaier, P., Sextro, W., and Six, K., 2009, “Friction in Wheel–Rail Contact: A Model Comprising Interfacial Fluids, Surface Roughness and Temperature,” 8th International Conference on Contact Mechanics and Wear of Rail/Wheel System (CM2009), Firenze, Italy, 15–18 September 2009, pp. 121–132.
- [12] Popovici, R. I., 2010, “Friction in Wheel–Rail Contact,” Ph.D. thesis, University of Twente, Department of Engineering Technology, Enschede, Netherlands.
- [13] Marshall, M. B., Lewis, R., Dwyer-Joyce, R. S., Olofson, U., and Björklund, S., 2006, “Experimental Characterization of Wheel–Rail Contact Patch Evolution,” *J. Tribol.*, **128**(3), pp. 493–504.
- [14] Greenwood, J. A., and Williamson, J. B. P., 1966, “Contact of Nominally Flat Surfaces,” *P. R. Soc. Lond. A*, **295**(1442), pp. 300–319.

- [15] Björklund, S., and Andersson, S., 1994, “A Numerical Method for Real Elastic Contacts Subjected to Normal and Tangential Loading,” *Wear*, **179**(1–2), pp. 117–122.
- [16] Love, A. E. H., 1929, “Stress Produced in a Semi-infinite Solid by Pressure on Part of the Boundary,” *Philos. T. R. Soc. A*, **288**(377), pp. 54–59
- [17] Jakobsson, B., and Floberg, L., 1957, “The Finite Journal Bearing Considering Vaporization,” *Trans. Chalmers Univ. Technol.*, no. 190, Gothenburg, Sweden.
- [18] Olsson K., 1965, “Cavitation in Dynamically Loaded Bearings,” *Trans. Chalmers Univ. Technol.* no. 308, Gothenburg, Sweden.
- [19] Elrod, H. G., and Adams, M. L., 1974, “A Computer Program for Cavitation and Starvation Problems,” *Cavitation and Related Phenomena in Lubrication: Proc. 1st Leeds–Lyon Symp.*, D. Dowson et al., eds., Inst. Mech. Engrs. Publ., London, pp. 37–41.
- [20] Elrod, H. G., 1981, “A Cavitation Algorithm,” *ASME J. Lubr. Tech.* **103**(3), pp. 350–354.
- [21] Ausas, R. F., Jai, M., and Buscaglia, G. G., 2009, “A Mass-conserving Algorithm for Dynamical Lubrication Problems with Cavitation,” *J. Tribol.*, **131**(3), 031702.
- [22] Johnson, K. L., 2001, *Contact Mechanics*, Cambridge University Press, Cambridge, UK, pp. 244, 264, 329.
- [23] Dorsey, N. E., 1929, Viscosity of water, sulfuric acid, liquid carbon dioxide and certain organic liquids, in: *International Critical Tables of Numerical Data, Physics, Chemistry and Technology*, McGraw-Hill, New York.
- [24] Haines, D. J., and Ollerton, E., 1963, “Contact Stress Distribution on Elliptical Contact Surfaces Subjected to Radial and Tangential Forces,” *P. I. Mech. Eng.-J. Eng.*, **177**(4), pp. 95–114.
- [25] Kalker, J. J., 1967, “A Strip Theory for Rolling with Slip and Spin,” *K. Ned. Akad. Van Wet.-B.*, **70**(10), pp. 261–263.
- [26] Dyson, A., 1970, “Frictional Traction and Lubricant Rheology in Elastohydrodynamic Lubrication,” *Philos. T. R. Soc. Lond.-A*, **266**(1170), pp. 1–33.
- [27] Lewis, R., Lewis, S., Zhu, Y., Abbasi, S., and Olofsson, U., 2011, “The Modification of a Slip Resistance Meter for Measurement of Railhead Adhesion,” *IHHA 2011 Conference*, Calgary, AB, Canada.
- [28] White, R. C., Limbert, D. A., Hederick, J. K., and Cooperrider, N. K., 1978, *Guideway–Suspension Tradeoffs in Rail Vehicle Systems*, Report DOT-OS-50107, Washington, DC.
- [29] Shen, Z. Y., Hedrick, L., and Elkins, J. A., 1983, “A Comparison of Alternative Creep–Force Models for Rail Vehicle Dynamic Analysis,” *Proc. 8th IAVSD Symp. Dynamics of Vehicles on Roads and on Tracks*, Boston, MA, pp. 591–605.
- [30] Chen, H., Ban, T., Ishida, M., and Nakahara, T., 2008, “Experimental Investigation of Influential Factors on Adhesion between Wheel and Rail under Wet Conditions,” *Wear*, **265**(9–10), pp. 1504–1511.
- [31] Zhang, W., Chen, J., Wu, X., and Jin, X., 2002, “Wheel/rail Adhesion and Analysis by Using Full Scale Roller Rig,” *Wear*, **253**(1–2), pp. 82–88
- [32] Gallardo-Hernandez, E. A., and Lewis, R., 2008, “Twin Disc Assessment of Wheel/rail Adhesion,” *Wear*, **265**(9–10), pp. 1309–1316
- [33] Zhu, D., and Hu, Y., 2001, “A Computer Program Package for the Prediction of EHL and Mixed Lubrication Characteristics, Friction, Subsurface Stresses and Flash Temperatures based on Measured 3-D Surface Roughness,” *Tribol. T.*, **44**(3), pp. 383–390

- [34] Zhu, Y., Olofsson, U., and Persson, K., “Investigation of Influential Factors on Wheel–rail Adhesion Using Mini Traction Machine,” submitted to *Wear*.
- [35] Beagley, T. M., McEwen, I. J., and Pritchard, C., 1975, “Wheel/rail Adhesion: The Influence of Railhead Debris,” *Wear*, **33**(1), pp. 141–152.
- [36] Beagley, T. M., 1976, “The Rheological Properties of Solid Rail Contaminants and Their Effect on Wheel/rail Adhesion,” *P. I. Mech. Eng.-J. Eng.*, **190**(39), pp. 419–428.
- [37] Stolarski, T. A., and Tobe, S., 2000, *Rolling Contacts*, Professional Engineering Publishing Limited, Suffolk, UK, p. 245.

B

Investigation of factors influencing wheel–rail adhesion
using a mini traction machine

Y. Zhu, U. Olofsson, K. Persson

Submitted to *Wear*

Investigation of factors influencing wheel–rail adhesion using a mini traction machine

Yi Zhu^{a,*}, Ulf Olofsson^a, Karin Persson^b

^a Royal Institute of Technology, Department of Machine Design, SE100 44 Stockholm, Sweden

^b Institute for Surface Chemistry, Life Science and Chemical Industries Section, SE114 86 Stockholm, Sweden

ABSTRACT

Adhesion in the wheel–rail contact is a key factor determining stable running conditions and safety during train driving and braking. This paper presents an experiment performed in a mini traction machine to simulate the problems of low adhesion in the wheel–rail contact. Tests were conducted under dry conditions and using water or oil as lubricants to study the influence of surface roughness on the adhesion coefficient. The results indicate that the adhesion coefficient can be reduced to as low as 0.02 for smooth surfaces lubricated with water. For rougher contact surfaces, the water-lubricated tests indicate a higher adhesion coefficient than do oil-lubricated ones, but also a clear dependence on water temperature. The oil-lubricated tests indicate a very slight dependence of the adhesion coefficient on variation in rolling speed, temperature, and surface roughness.

Keywords: Wheel–rail, Adhesion, Surface roughness, Rolling–sliding contact

1. Introduction

In railway transport, the acceleration and deceleration ability of a vehicle is limited by the adhesion between wheel and rail. Because the wheel–rail contact is an open system, adhesion in the wheel–rail contact is affected by many environmental conditions. For example, under wet conditions from either drizzle or high humidity, the vehicle has insufficient acceleration or deceleration due to poor adhesion on the contact patches between wheel and rail. Poor adhesion during traction will cause performance problems, leading to delays and increasing operation costs. Furthermore, poor adhesion during braking is a safety issue as it extends braking distance [1].

Compared with friction in other well-studied components, such as bearings, the wheel–rail adhesion phenomenon is poorly understood. Pioneers in this research field were Beagley, Mcewen, and Pritchard [2–5], who used twin-disc, disc-on-cylinder, and disc-on-flat testing rigs to study the influence of water, oil, wear debris, and a water–iron oxide mixture on wheel–rail adhesion. In the past decade, studies have used a test train to investigate adhesion under dry and wet conditions [6], full-scale roller rigs in the National Traction Power Laboratory in China to study the effects of water, oil, load, and rolling speed [7], and a twin-disc rolling contact machine in Tokyo to study the effect of surface roughness, roughness orientation, and temperature [8]. Such tests can simulate real conditions, but are usually difficult to access and/or expensive to run. The wheel–rail contact can easily be simulated using scaled testing equipment, such as pin-on-disc [9], twin disc [10,11], and mini traction machines [12]. Because of their inherent limitations, these scaled machines can be run only in the low speed range, usually below 5 m/s. On the other hand, such scaled tests can be performed in the lab at relatively low cost and offer easily controlled

testing conditions using various contaminants. The use of field testing equipment, such as the hand-push tribometer and pendulum rigs, is also reported [13,14]; results obtained using both types of equipment display promising correlations with lab-scale results obtained using scaled testing equipment [9–12].

The present investigation examines the influence of surface roughness on the adhesion coefficient under dry, water-lubricated, and oil-lubricated testing conditions similar to those of the wheel–rail contact using a mini traction machine. In addition, the dependence of the adhesion coefficient on rolling speed, slide–roll ratio, lubricant temperature, and contact pressure was also studied.

2. Experimental

A mini traction machine (MTM) was used to measure the adhesion coefficient. Note that in some studies the term traction coefficient is used instead of adhesion coefficient, presumably because the research examined traction conditions, i.e., the wheels accelerating over the rail. Adhesion is defined as the friction that can be made available to transfer tangential forces (or traction force in the case of driving wheels) between a railway wheel and the rail [1]. The adhesion coefficient is limited by the friction coefficient and is defined as $\mu_{adhesion} = \frac{F_{tangential}}{F_{normal}} \leq \mu_{friction}$.

There is usually a velocity difference between wheel rolling speed and vehicle speed. The ratio between the velocity difference and the vehicle speed is defined as creep. Due to creep, the contact area can be divided into slip and stick regions, as shown in Fig. 1. When creep is zero, there is pure rolling motion and the stick region covers the whole contact area. When a tangential force starts to be transmitted, a slip region occurs in the contact patch. With increasing creep, the slip region increases and the stick region decreases in size, resulting in a rolling and sliding contact.

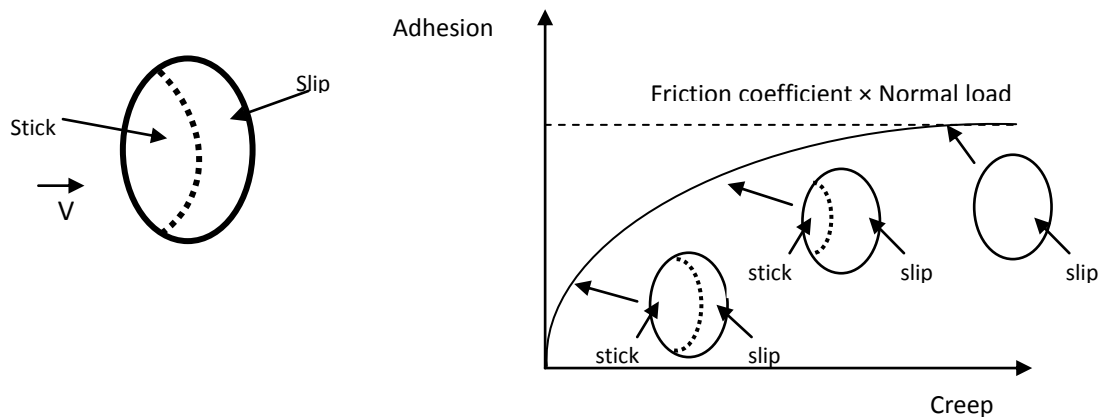


Fig. 1. Relationship between adhesion and creep.

The same situation can be identified in MTM tests. A velocity difference between the ball speed and disc speed will result in a rolling and sliding contact. Here, the slide roll ratio (SRR) is defined as the ratio between sliding speed and rolling speed: $SRR = |U_{disc} - U_{ball}| / ((U_{disc} + U_{ball}) / 2)$.

2.1. Test rig

The MTM uses a rotating steel ball in contact with a rotating steel disc (see Fig. 2). The ball is loaded against the face of the disc, and the ball and disc are driven independently to create a rolling and sliding contact. The disc is submerged in a lubricant bath that is temperature controlled to within $\pm 1^\circ\text{C}$ during testing. The ball-on-disc set-up is covered with a lid to maintain the temperature within a closed space. Using a computer, various testing parameters can be specified, such as ball and disc speed, slide roll ratio (SRR), temperature, and load. Adhesion is measured using a force transducer by taking the average value of friction forces from two measurements ($U_{\text{disc}} > U_{\text{ball}}$ and $U_{\text{disc}} < U_{\text{ball}}$) with the same specified SRR, which removes any offset errors in the friction measurements.

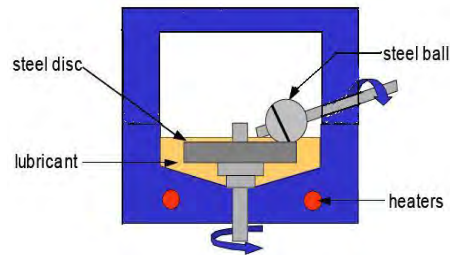


Fig. 2. Schematic of the MTM.

2.2. Test specimens

In this study, a $\frac{3}{4}$ " ball (approximately 19.05 mm in diameter) and a disc 46 mm in diameter were used to generate a contact pressure that approximates the real condition. The specimens consisted of AISI 52100, which is usually used as bearing steel. The material compositions of AISI 52100, wheel, and rail steel are presented in Table 1. The hardness of the discs was 300–320 HV, which is very close to that of rail steel. However, the ball was much harder (800 HV) than wheel or rail steel, due to manufacturing limitations. The discs have two kinds of surface topography. One is highly polished with centre-line average (CLA) $R_a = 0.01 \mu\text{m}$ (smooth) and the other is roughly finished with $R_a = 0.15 \mu\text{m}$ (rough). All the balls were manufactured using the same method with $R_a = 0.02 \mu\text{m}$. The smooth disc surfaces were much less rough than is typical of wheel–rail applications [9]. Fig. 3 (left) shows a real piece of rail that was cut from a commuter train track in Älvsjö, Stockholm [15]. On the rail surface, some parts were smoothed by mild wear, which was measured using a stylus machine. Two-dimensional measurements are shown in Fig. 3 (right). The R_a value is approximately $0.32 \mu\text{m}$.

Table 1
Material composition comparison.

Chemical composition (wt %)	C	Si	Mn	P	Ni	Cr
UIC60 900A rail	0.6–0.8	0.15–0.5	0.8–1.3			
R7 wheel	0.52	0.4	0.8	0.035	0.3	0.3
AISI 52100(standard)	0.98–1.1	0.15–0.3	0.25–0.45	≤ 0.025		1.3–1.6

Source: Wheel and rail material composition is from Lewis and Olofsson [16].

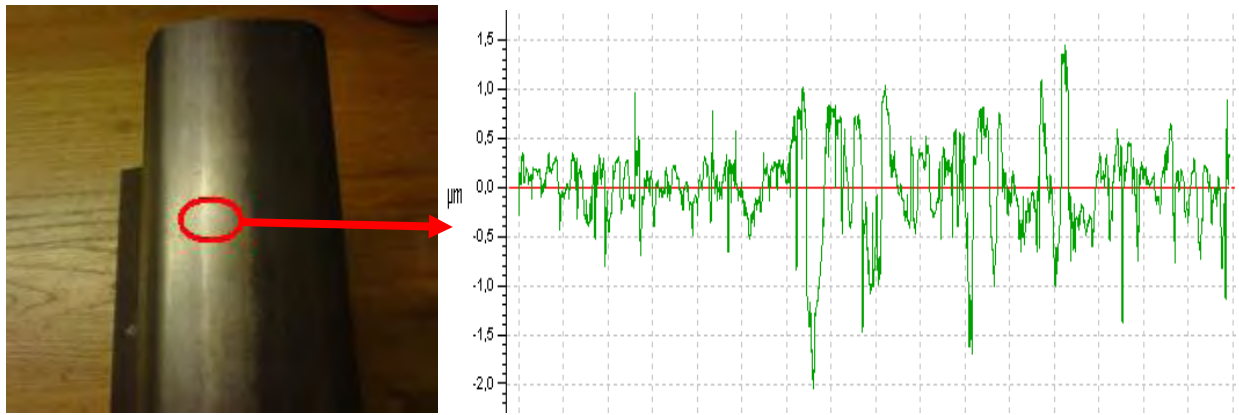


Fig. 3. A piece of rail cut from a commuter train track in Älvsjö, Stockholm (left) and the two-dimensional measurement of a smooth area on the rail head (right)

2.3. Test procedure

The MTM machine was used to simulate a rolling and sliding contact between wheel and rail. The test was run in a closed lib to control temperature and the disc was submerged in water or oil lubricant. The amount of lubricant used in the tests was far more than is found in practice. A synthetic ester oil rail lubricant was used in the tests (68cSt at 40°C, 12cSt at 100°C [17]). This oil is used as rail gauge corner lubricant by Storstockholms Lokaltrafik. Each test was performed using a pair of new surfaces, and before testing, all specimens were ultrasonically cleaned in toluene and then dried. In the adhesion curve test, the rolling speed was specified as 1500 mm/s. The SRR started at 0% and increased stepwise to 10% by 0.5% per step; from 10% to 100%, SRR increased by 5% per step. In the Stribeck curve test, SRR was kept constant at 50%. The rolling speed started at 10 mm/s and increased stepwise to 100 mm/s by 10 mm/s per step; from 100 mm/s to 1500 mm/s, rolling speed increased by 50 mm/s per step. Water and oil were used as the lubricants. The details of the tests are presented in Table 2.

Table 2
MTM test conditions.

Adhesion curve test		Stribeck curve test	
Hertz max. pressure	700 MPa	Hertz max. pressure	700 MPa, 900 MPa
Rolling speed	1500 mm/s	Speed range	10–1500 mm/s
SRR range	0–100%	SRR	50%
Lubricant	dry, water, oil	lubricant	water, oil
Temperature	20°C (except dry tests)	temperature	20°C; 5°C
Specimens	rough, smooth	specimens	rough, smooth

To minimize any running-in effects, all tests were pre-run for 3 min at a rolling speed of 1500 mm/s and a contact pressure of either 700 or 900 MPa under the intended lubricant conditions. Tests were repeated three times on the same sample. However, in the dry testing, tests were only run once or even stopped during the first repetition due to the high recorded frictional forces. The duration of the adhesion curve tests was approximately 20 min and of the Stribeck curve tests was approximately 12 min. Test

discs were measured using a stylus machine (Taylor Hobson PGI800) and examined using both optical microscope and atomic force microscopy (AFM).

2.4. Lubrication regime

To determine the lubrication regime associated with each set of test conditions, it is necessary to calculate the lambda value (i.e., film thickness parameter) under various test conditions. When $\Lambda < 1$, boundary lubrication prevails in which pressure build-up is negligible at low velocity and with thin film thickness (shown in Fig. 3). When $\Lambda > 3$, elastohydrodynamic lubrication prevails in which pressure in the film can separate the two surfaces, in which case the friction coefficient depends on the shear stress in the lubricant. The intermediate regime is mixed lubrication, in which friction decreases with increasing velocity [18]. Reducing the surface velocity will reduce the film thickness until the two surfaces come into contact. The minimum film thickness is the value of the film thickness before the asperities of the two surfaces come into contact. The film thickness parameter, Λ , is defined as

$$\Lambda = \frac{h_{\min}}{(R_{qa}^2 + R_{qb}^2)^{1/2}}$$

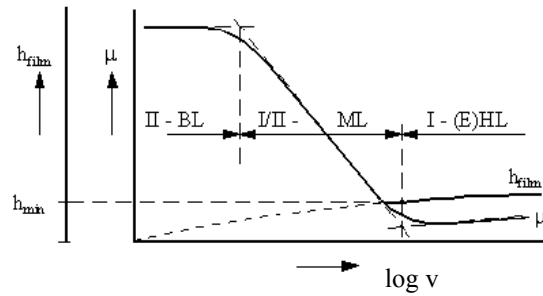


Fig. 3. Stribeck curve.

The equations to calculate lambda value are as follows:

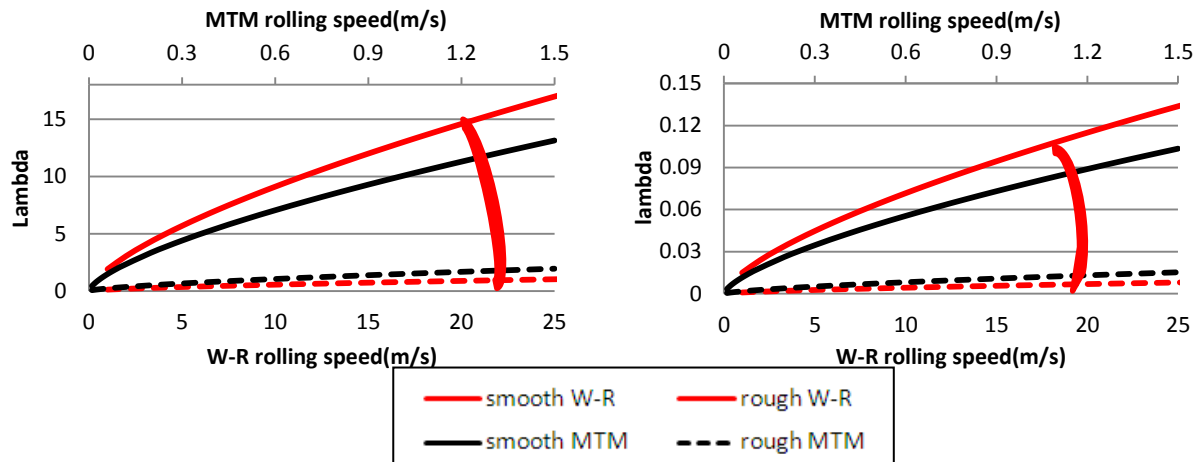
$$h_{\min} = 3.63R_x U^{0.68} G^{0.49} W^{-0.073} (1 - e^{-0.68k}); \text{ see [19]}$$

$$\text{where } R_x = \left(\frac{1}{r_{ax}} + \frac{1}{r_{bx}}\right)^{-1}; R_y = \left(\frac{1}{r_{ay}} + \frac{1}{r_{by}}\right)^{-1}; U = \frac{\eta_0 u}{E' R_x}; G = \xi E'; W = \frac{w_z}{E' R_x^2}; k = \left(\frac{R_y}{R_x}\right)^{2/\pi};$$

$$E' = 2 \times \left(\frac{1 - \nu_a^2}{E_a} + \frac{1 - \nu_b^2}{E_b}\right)^{-1}$$

Table 3
Inputs to the lambda value calculation.

Nomenclature	Values in wheel–rail contact	Values in MTM
r_{ax} r_{ay} r_{bx} r_{by} : radius of curvature in x,y direction of bodies a and b (mm)	$r_{ax}=500$; $r_{ay}=inf$; $r_{bx}=inf$; $r_{by}=300$;	$r_{ax}=inf$; $r_{ay}=inf$; $r_{bx}=9.525$; $r_{by}=9.525$;
E_a E_b : elastic modulus of bodies a and b (GPa)	$E_a = E_b = 210$	$E_a = E_b = 210$
ν_a ν_b : Poisson's ratio of bodies a and b	$\nu_a = \nu_b = 0.3$	$\nu_a = \nu_b = 0.3$
w_z : normal load (N)	42 kN	26.9 N
u : rolling speed (m/s)	1–25	0.01–1.5
R_{qa} R_{qb} : surface roughness of bodies a and b (μm)	Smooth pair: $R_{qa}=0.3$; $R_{qb}=0.3$; Rough pair; $R_{qa}=5$; $R_{qb}=5$;	Smooth pair: $R_{qa}=0.025$; $R_{qb}=0.012$; Rough pair; $R_{qa}=0.025$; $R_{qb}=0.2$;
	Values of water	Values of oil
ξ : pressure–viscosity coefficient (m^2 / N)	6.6×10^{-10}	2.2×10^{-8}
η_0 : absolute viscosity at $p = 0$ ($\text{Pa} \cdot \text{s}$)	0.001	0.2



Smooth W–R: smooth wheel–rail surfaces with root mean square average (R.M.S) $R_q = 0.3 \mu\text{m}$; rough W–R: rough wheel–rail surfaces with $R_q = 5 \mu\text{m}$.

Fig. 4. Lambda value of MTM tests and wheel–rail contacts of different roughnesses under oil-lubricated (left) and water-lubricated (right) conditions at 20°C .

Fig. 4 shows the lambda value of the wheel–rail contact and of the MTM tests under water- and oil-lubricated conditions at a contact pressure of 900 MPa and a temperature of 20°C . The rolling speed range is 1–25 m/s for the wheel–rail contact, which is the typical speed range for a commuter train in Stockholm. The area bordered by the two red curves is the range of the lambda value of wheel–rail contacts with surface roughnesses ranging from $0.3 \mu\text{m}$ to $5 \mu\text{m}$, i.e., from very smooth to rough [8, 9].

The red curves contain the two black curves, which indicates that MTM tests can simulate wheel–rail contact in terms of lubrication regime. The lubrication regime of the wheel–rail contact is either mixed or elastohydrodynamic lubrication under oil-lubricated conditions, but is entirely boundary lubrication under water-lubricated conditions.

3. Results

3.1. MTM results

Fig. 5 presents the adhesion curve results at a rolling speed of 1500 mm/s for dry tests (left) and oil- and water-lubricated tests (right). For the dry tests, when the SRR value is low, the adhesion coefficient increases almost linearly with increased SRR value. After that, the adhesion coefficient gradually decreases with increased SRR value. The first peak of the adhesion coefficient appears at SRR values of approximately 10%. The maximum adhesion coefficient is approximately 0.8 for rough surfaces and slightly higher for smooth surfaces. The test ends with an adhesion coefficient of 0.6–0.7. However, due to the limitation of the equipment and for safety reasons, the smooth surface test was run only once and the rough surface test was stopped at an SRR value of 75%.

For rough surfaces using water as a lubricant, the adhesion coefficient increases linearly when the SRR values are below 5%. Above that level, the adhesion coefficient increases gradually in the SRR value range of 5–50% until the adhesion coefficient becomes stable at approximately 0.15. For smooth surfaces in the water-lubricated test, the adhesion curve first increases to approximately 0.015 at low SRR values (5%). Above that level, the adhesion coefficient decreases gradually, ending up at approximately 0.01. For both surfaces in the oil-lubricated tests, the adhesion coefficient increases over the whole SRR range from 0% to 100%. The two curves are very close to each other. When the SRR value is high, the adhesion coefficient of the rough surfaces in the oil-lubricated case ranges from 0.03 to 0.04 while that of smooth surfaces is slightly lower.

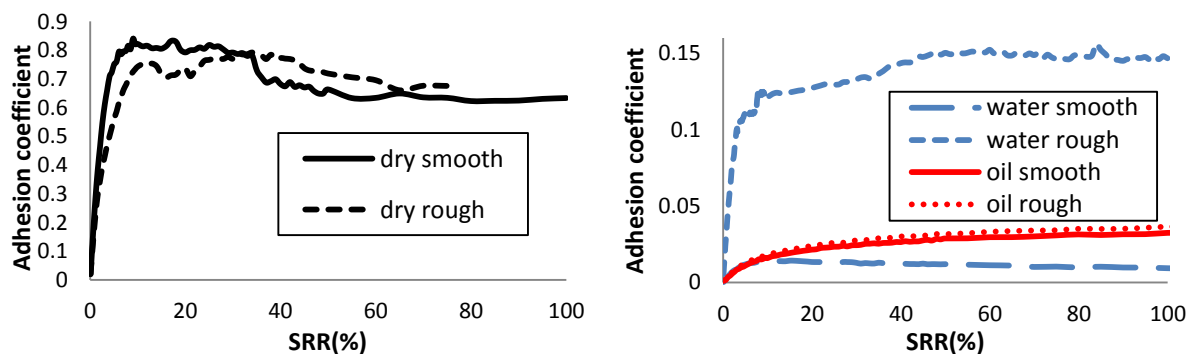


Fig. 5. Adhesion curve at a contact pressure of 700 MPa under dry test conditions (left) and under water- and oil-lubricated conditions (right).

Fig. 6 shows the Stribeck curve for water-lubricated tests at an SRR value of 50%. For the adhesion coefficient of the rough surfaces, the 900 MPa tests indicated higher adhesion coefficients than did the 700 MPa tests. The adhesion coefficient of the rough surfaces at 900 MPa reaches a steady value of 0.2,

while the steady value is approximately 0.15 at 700 MPa. For the smooth surfaces, the adhesion coefficient, which ranges from 0.05 to 0.02, decreases with increasing rolling speed at both pressures; here, the difference between the two curves is comparatively small.

Fig. 7 shows the Stribeck curve for the oil-lubricated tests at an SRR value of 50%. For both surfaces, the adhesion coefficient at the two contact pressures decreases with increasing rolling speed. Notably, in the low rolling speed range, the adhesion coefficient of rough surfaces is much higher than that of smooth ones. Ultimately, however, the adhesion coefficient becomes approximately the same in both the 900 MPa and 700 MPa tests. Over the complete rolling speed range, the adhesion coefficient is larger at 900 MPa (0.04) than at 700 MPa (0.03), though the difference is small.

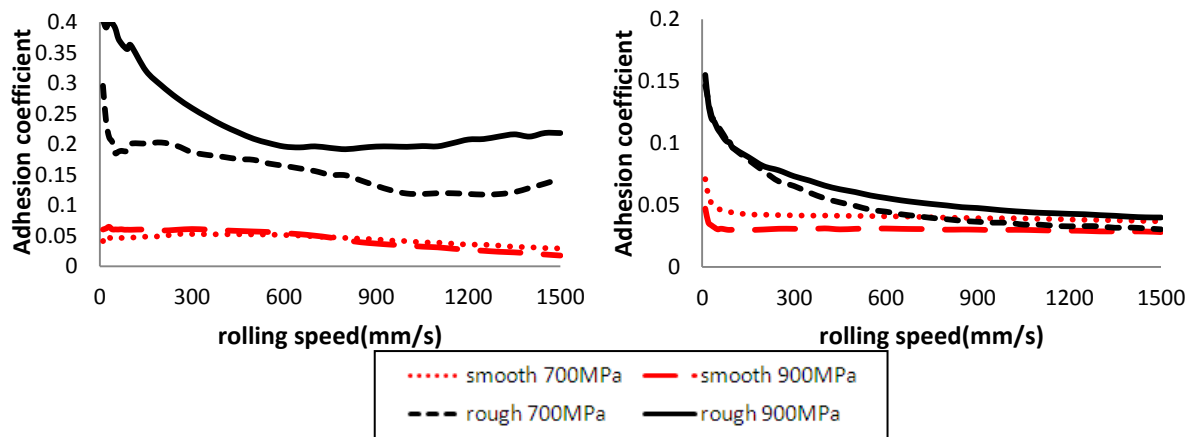


Fig. 6. Stribeck curve for water-lubricated tests.

Fig. 7. Stribeck curve for oil-lubricated tests.

Tests were conducted at 5°C for comparison with the results obtained at 20°C for both the water- and oil-lubricated cases, as shown in Figs. 8 and 9. In the oil-lubricated tests, the results obtained at 5°C are quite close to those at 20°C for both smooth and rough surfaces. In the water-lubricated tests, results for smooth surfaces display no notable differences. For rough surfaces, however, a significant difference is found: here, the adhesion coefficient varies from 0.1 to 0.15 at 5°C and is approximately 0.2 at 20°C.

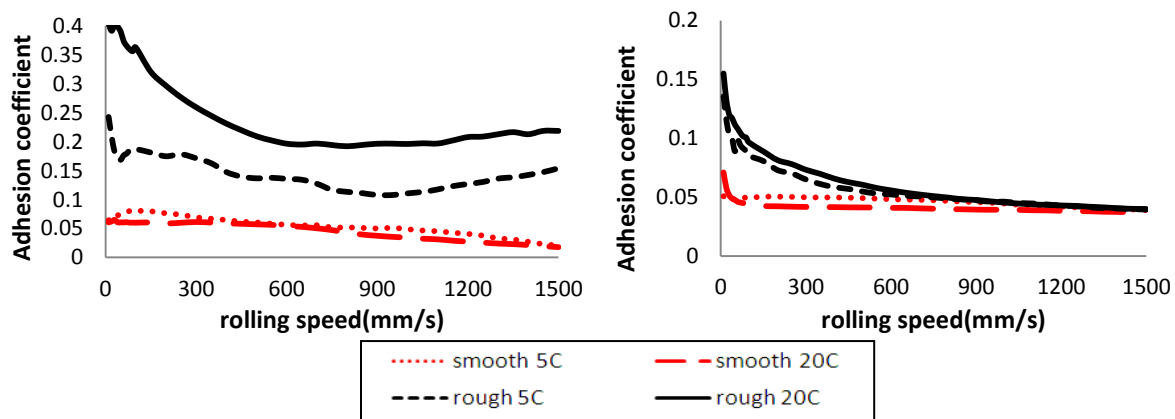


Fig. 8. Temperature effect of water-lubricated tests under 900 MPa.

Fig. 9. Temperature effect of oil-lubricated tests under 900 MPa.

3.2. Results of surface examination

To assess the surface damage, tests specimens from the 900 MPa Stribeck curve tests (i.e., unused, water-lubricated, and oil-lubricated specimens) were measured using a stylus machine. The measurement results are shown in Figs. 10–17.

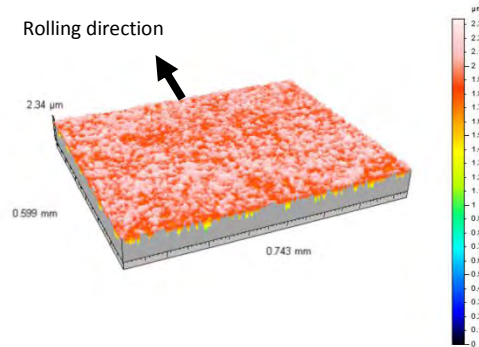


Fig. 10. Surface topography of a 900 MPa oil-lubricated rough disc.

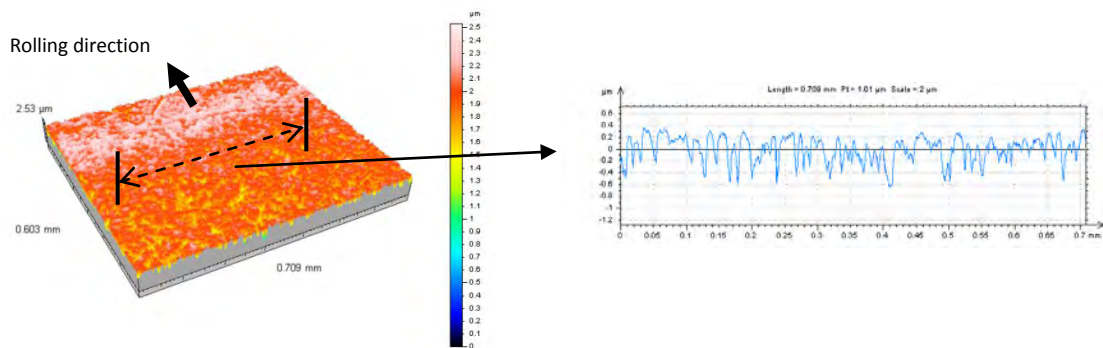


Fig. 11. Surface topography and two-dimensional measurements of an unused rough disc.

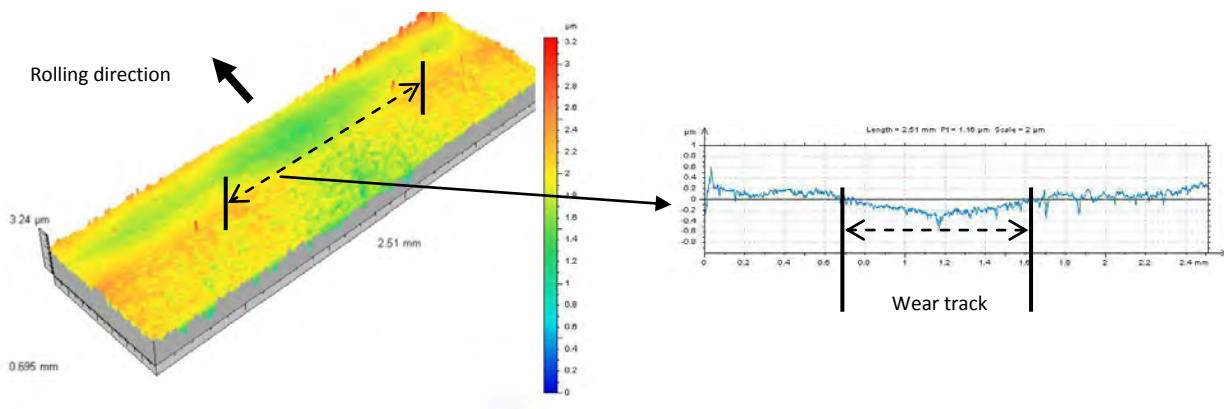


Fig. 12. Surface topography and two-dimensional measurements of a 900 MPa water-lubricated rough disc (below).

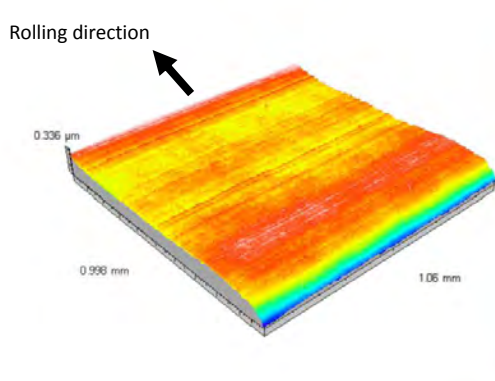


Fig. 13. Surface topography of an unused smooth disc.

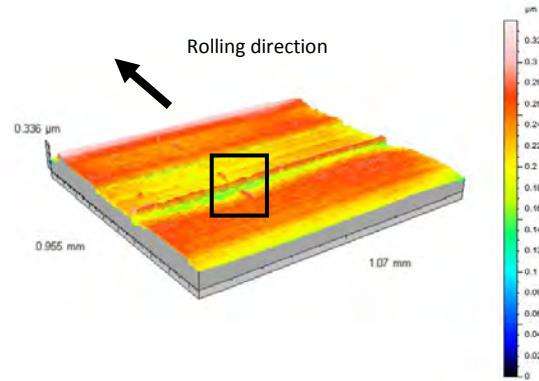


Fig. 14. Surface topography of a 900 MPa oil-tested smooth disc.

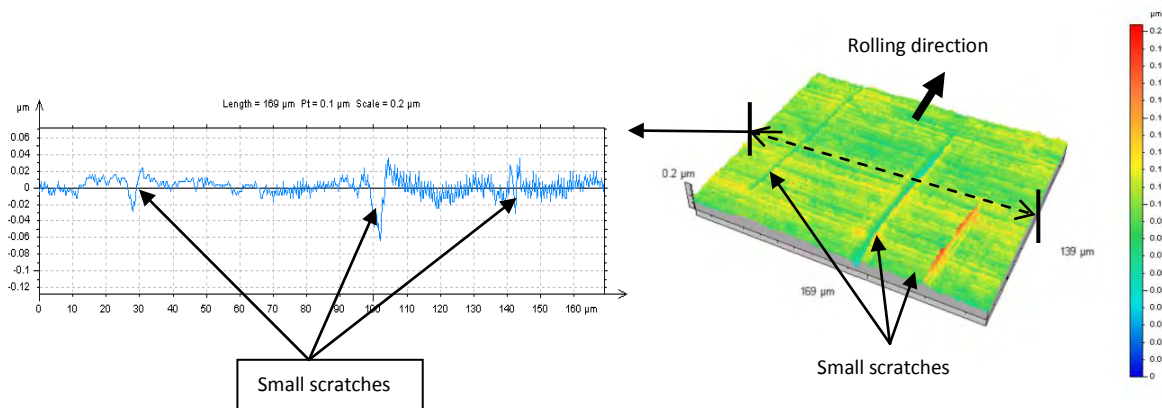


Fig. 15. Surface topography and two-dimensional measurements of a small area of a 900 MPa oil-lubricated smooth disc.

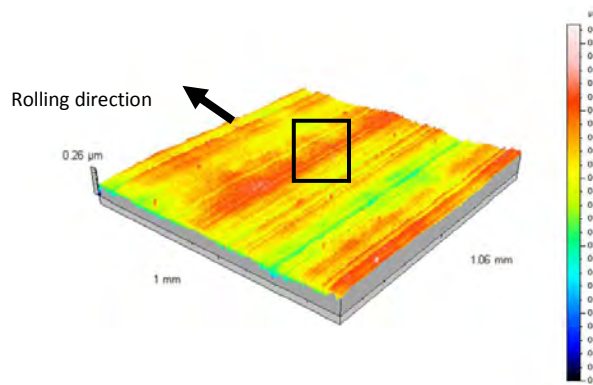


Fig. 16. Surface topography of a water-lubricated smooth disc

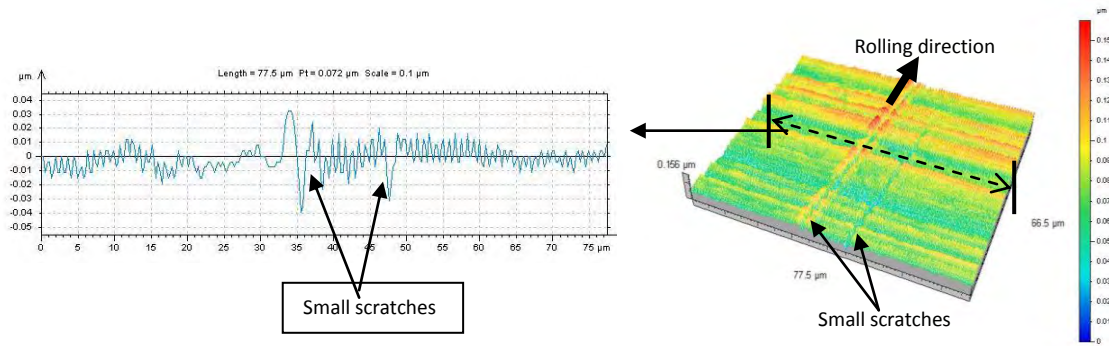


Fig. 17. Surface topography and two-dimensional measurements of a small area of a 900 MPa water-lubricated smooth disc.

The surface topographies and surface roughnesses of the oil-lubricated (Fig. 10) and unused (Fig. 11) rough discs were very similar. No visible wear track was found on the oil-lubricated rough disc. On the water-lubricated rough disc (Fig. 12), a wear track was clear, even to the naked eye, and the surface had become much rougher. From two-dimensional measurements, the width of the wear track was calculated to be approximately 1 mm. However, according to the two-dimensional measurements, the height of the asperities inside the contact area seemed comparable to that of asperities outside the contact area.

It was difficult to find any large-scale surface damage on the smooth discs (Figs. 13, 14, and 16); only surface textures in the axial direction, due to the polishing manufacturing process, were found. These textures remained almost the same after the tests. On both oil- and water-lubricated discs, some small-scale scratches were found in the rolling direction (Figs. 15 and 17); two-dimensional measurements also revealed these small scratches. Using optical microscopy, these small scratches were clearly visible on the disc surfaces (see Fig. 18); these long narrow scratches ran in the circumferential direction and differed greatly in size on the same disc. As well, there were far more scratches on the oil-lubricated than on the water-lubricated discs. To examine these small surface scratches more closely, some affected areas were visualized using AFM (Figs. 19 and 20), but it was impossible to find exactly the same scratches as had been found using three-dimensional measurements. However, most scratches on oil-lubricated discs are deeper than those on water-lubricated discs. According to the two-dimensional measurements of AFM photos, most scratches on oil-lubricated discs are approximately 300 nm deep, while most scratches on water-lubricated disc are under 100 nm deep.

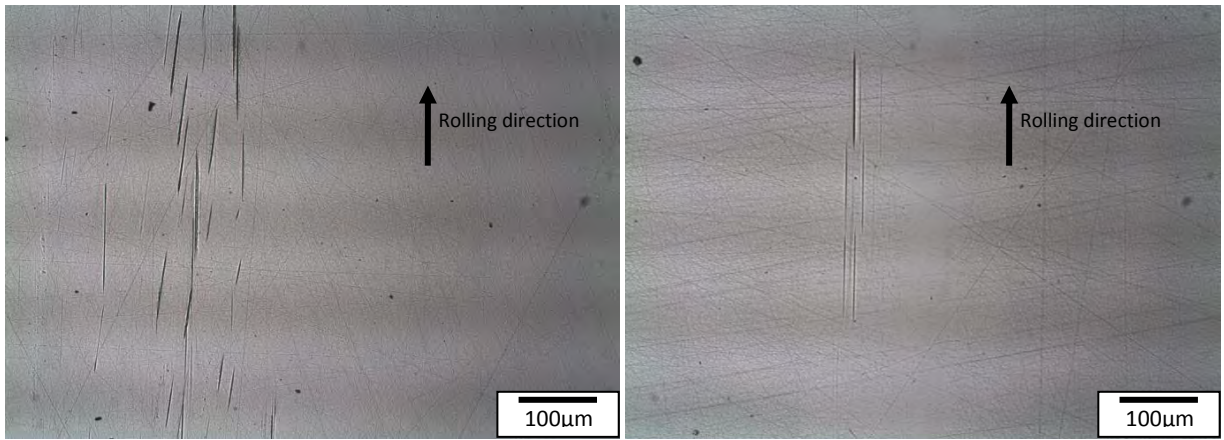


Fig. 18. Surface micro-photographs of discs after oil-lubricated (left) and water-lubricated (right) testing.

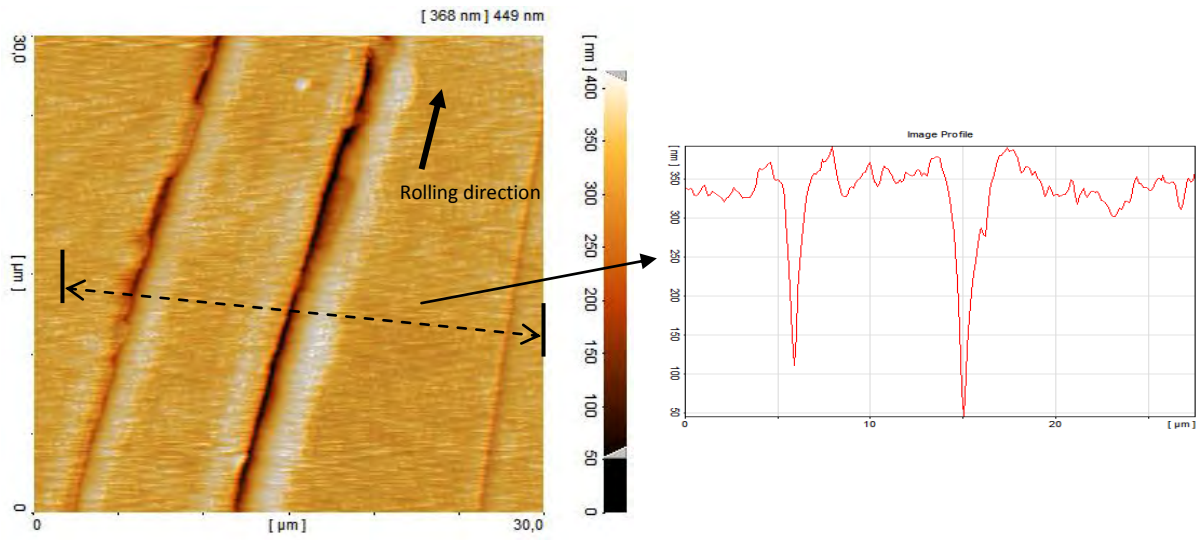


Fig. 19. AFM surface photographs of scratches on the oil-lubricated smooth disc.

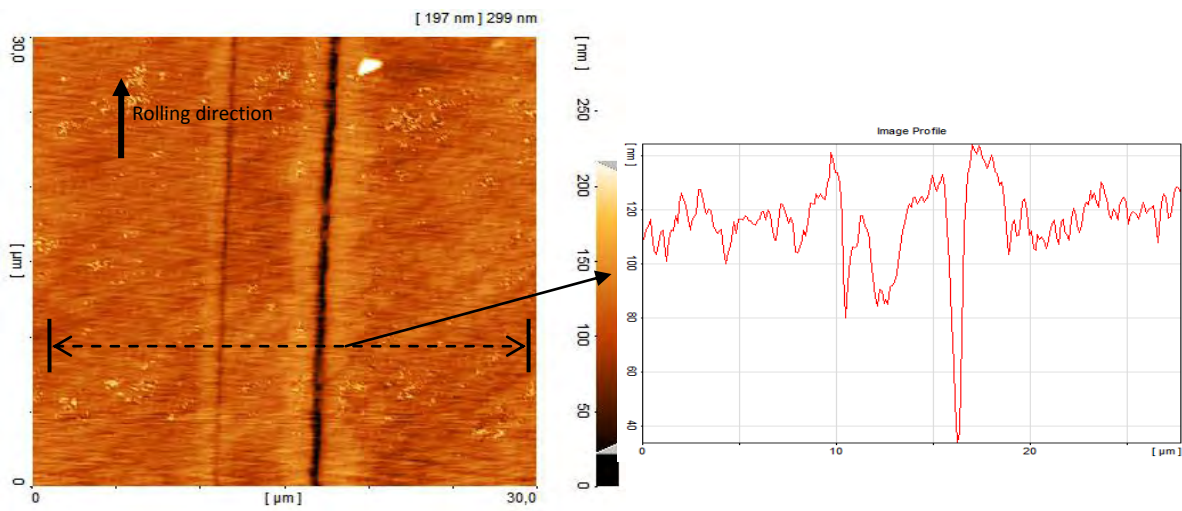


Fig. 20. AFM surface photographs of scratches on the water-lubricated smooth disc.

4. Discussion

This work is mainly interested in examining the influence of surface topography on adhesion under various operating conditions. The shapes of adhesion curves under dry conditions (Fig. 5, left) are very similar to those found in field tests [6] and using a full-scale test rig [7]. Furthermore, the saturated values are at the same level, i.e., 0.6–0.7, as those previously found in pin-on-disk tests [9] and in field tests using push tribometers [13] and pendulum rigs [14]. However, tests using full-scale test rigs [6] and creep curve studies using locomotives [7] have yielded lower values for the fully saturated adhesion coefficient. The reduction in the adhesion coefficient after it peaks may be due to temperature effects [20]. The adhesion coefficient displays no significant dependence on roughness in the dry contact, which is in line with previous results [20,21].

In the oil-lubricated case, variations in roughness and temperature exert no significant influence (Fig. 5, right). The Stribeck curve for oil-lubricated tests (Fig. 7) corresponds to classic tribological theory, the different surface topographies only affecting the adhesion coefficient when the rolling speed is low. The results for both rough and smooth surfaces are quite similar. The adhesion coefficient is typically approximately 0.04, in line with results obtained using other test rigs [7,11]. According to the three-dimensional measurements, there is no marked surface damage on the smooth discs, indicating that elastohydrodynamic lubrication is dominant. Lambda calculations indicate that the lubrication regime on smooth surfaces is mainly elastohydrodynamic, in which surfaces are separated and there is no asperity contact. Most scratches found on the surfaces might be caused by hard particle abrasion generated at low speeds when the surfaces were not fully separated. These scratches differ from the cracks created by rolling contact fatigue (RCF) [1] found in rails. RCF is initiated beneath the surface in the lateral direction then propagates to the surface. RCF usually occurs due to incremental deformation (i.e., by ratcheting) on the surface, caused by the traction applied by passing trains. However, the scratches found on the smooth discs are very small and oriented in the rolling direction. Moreover, the friction force is measured in an MTM by taking the average friction value at the same SRR but with the ball moving faster and slower, respectively, than the disc. The traction-induced deformation effect occurs in both directions and can be counteracted; this is different from RCF on rails, in which traction is usually exerted in only one direction, aggregating the deformation. On the other hand, lambda calculations indicate that mixed lubrication is the main regime occurring on rough surfaces on which asperity contact is still important. The adhesion curve also indicates that the adhesion coefficient decreases with increasing speed, in agreement with previous results [21]. However, no surface damage was found on the rough surface, which remained almost the same as that of the unused disc in terms of both surface topography and roughness. This might be because surface damage is negligible relative to the original surface roughness and because elastohydrodynamic lubrication starts to dominate as the speed increases.

In contrast, both roughness and temperature exert noticeable influence in the water-lubricated tests. In water-lubricated tests, the adhesion coefficient for smooth surfaces is approximately 0.02, versus 0.2 for rough surfaces; the former value is even lower than those obtained in oil-lubricated tests (see Fig. 6). According to surface measurements and microscopy photographs, only very small scratches 50–150 nm

in depth were found on the smooth discs. These scratches were fewer in number and shallower on water-lubricated than on oil-lubricated discs. This indicates less asperity contact in the water-lubricated than the oil-lubricated contacts, which is in agreement with the lower adhesion coefficient found in water-lubricated than oil-lubricated testing and suggests that elastohydrodynamic lubrication may be dominant, counter to what lambda calculations suggest. This could be because water can form a film between the smooth surfaces, separating them. Thus the adhesion coefficient is determined by the shear stress of water, which is lower than that of the oil. Another possibility is that the pre-oxide layer is not penetrated during the wear process [22], while the oxidized layer is a low-shear-stress layer that separates the two metal surfaces, preventing direct asperity contact [4,23]. On the rough surfaces, the adhesion coefficient is 0.15–0.2, comparable to values obtained by both full-scale [7,8] and scaled twin-disc testing [11]. Furthermore, the wear track is very obvious on the surface topography in Fig. 12, the contact width being approximately 1 mm. The two-dimensional measurements shown in Fig. 12 indicate that the wear mechanism is plastic deformation rather than asperity flattening, a previously reported phenomenon [24]. As a result, the lubrication regime is boundary lubrication. Asperities come into contact under water-lubricated conditions on rough surfaces, and the effect of water as a lubricant is very limited. Note that the roughness of the rough surfaces tested here is similar to that measured on typical rails in field studies. In addition, temperature also has a notable influence on the adhesion coefficient of rough surfaces. Low water temperature reduces the adhesion coefficient from 0.2 to 0.15 or even lower (this phenomenon has also been reported by Chen et al. [8]), which indicates that high water temperature can alleviate the adhesion loss problem.

According to J. Lundmark [25], wheel–rail surfaces run-in fairly rapidly: after just one and half day’s traffic, wheel and rail surfaces, initially differing in roughness, will run-in to almost the same lower roughness value. A regularly used railhead surface (without sand damage) is very smooth. So for an oil-lubricated railhead surface, this situation belongs to the elastohydrodynamic lubrication regime, in line with results of MTM tests and what lambda calculation indicates. However, under water-lubricated conditions, the variation of the adhesion coefficient is considerable. Zhang et al. [7] have reported that the adhesion coefficient was 0.13 at 120 km/h and 0.05 at 280 km/h, and similar results have been reported by Chen et al. [8]. From a tribological perspective, pure water is not a good lubricant because of its low viscosity, which is only one one-hundredth of that of a normal lubricant. However, an extremely low adhesion coefficient was found in the water-lubricated tests in the present work, and only very small scratches are seen on the water-lubricated disc surfaces. It turns out that, under wet conditions, surfaces can be separated, possibly due to the effect of wear debris, a water–oil mixture [3–5], or a third body layer [26,27]. Since the wheel–rail contact is an open system, it is sensitive to environmental conditions. There is usually a natural third body between wheel and rail surfaces that contains particles from the first bodies (i.e., wheel and rail), as well as screens, which are the natural layers of surface contaminants consisting of physisorbed, chemisorbed, or oxidized layers. The thickness of the third body can be up to 15 μm [26], which is enough to change the contact mechanics and the adhesion between wheel and rail. As a result, if the fluid (water) is not viscous enough to separate the first bodies (i.e., wheel and rail), the adhesion will be affected by the third body layer. The testing performed here, however, suggests that surface

topography may considerably affect the adhesion coefficient. A very smooth surface will generate extremely low adhesion or will promote the formation of an oxide layer that can prevent direct contact and hence lower the adhesion. The present testing found an adhesion coefficient of 0.02–0.05 for the smooth surfaces (Ra 0.01 μm) and of 0.15–0.2 for the rough surfaces (Ra 0.15 μm). Although the smooth surface is smoother than the surfaces tested previously, it has been determined, using a full test rig [8], that a smoother surface will have an adhesion coefficient of 0.05 while a rougher one will have a coefficient of 0.14 at a rolling speed of 100 km/h. After the testing, the authors [8] found that the contact regions of the wheel and rail discs had oxidized heavily. In high-speed railways, the rail surface may become extremely smooth (comparable to the smooth MTM disc), which can result in extremely low adhesion under wet conditions; unfortunately, we have found no surface data regarding the effects of high rolling speed on rail surfaces.

5. Conclusions

Ball-on-disc testing methods were used to evaluate the effects of various conditions on adhesion. Tests were conducted over a range of slide–roll ratios and rolling speeds using different contact pressures, surface roughness, and lubricant temperatures.

- (1) In oil-lubricated tests, rough surfaces had slightly higher adhesion coefficients than did smooth surfaces. The adhesion coefficients were similar to those found in previous studies. Surface topography changed little, except for some scratches found on smooth discs. Changing the temperature from 20°C to 5°C had little effect on the adhesion, but increasing the pressure increased the adhesion coefficient.
- (2) In water-lubricated tests, smooth surfaces had a very low adhesion coefficient of approximately 0.02, which was even lower than that found in the oil-lubricated tests. Only very small scratches were found on the water-lubricated surfaces, and there were fewer scratches than on the oil-lubricated surfaces. The adhesion coefficient of water-lubricated rough surfaces was comparable to that measured using other test rigs. High water temperature was able to alleviate the adhesion loss problem.
- (3) The influence of roughness and oil temperature on adhesion is slight under oil-lubricated conditions in which elastohydrodynamic lubrication dominates. However, both roughness and water temperature had a considerable impact on adhesion under water-lubricated conditions.

Acknowledgments

This research was performed under the auspices of the KTH Railway Group, with the support of Swedish Transport Administration and Stockholm Public Transport. The authors would like to thank Johan Andersson, from YKI (the Institute for Surface Chemistry), for his help with testing on the mini traction machine.

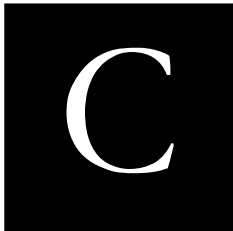
References

- [1] R. Lewis, U. Olofsson, Wheel–rail interface handbook, Woodhead Publishing Limited, Cambridge, UKs, 2009, pp. 284, 510, 514.
- [2] T.M. Beagley, I.J. McEwen, C. Pritchard, Wheel/rail adhesion: boundary lubrication by oily fluids, *Wear* 31 (1975) 77–88.
- [3] T.M. Beagley, I.J. McEwen, C. Pritchard, Wheel/rail adhesion: the influence of railhead debris, *Wear* 33 (1975) 141–152.
- [4] T.M. Beagley, C. Pritchard, Wheel/rail adhesion: the overriding influence of water, *Wear* 35 (1975) 299–313.
- [5] T.M. Beagley, The rheological properties of solid rail contaminants and their effect on wheel/rail adhesion, *Proc. Instn. Mech. Engrs.* 190 (39) (1976) 419–428.
- [6] O. Polach, Creep forces in simulations of traction vehicles running on adhesion limit, *Wear* 258 (2005), 992–1000.
- [7] W. Zhang, J. Chen, X. Wu, X. Jin, Wheel/rail adhesion and analysis by using full scale roller rig, *Wear* 253 (2002) 82–88.
- [8] H. Chen, T. Ban, M. Ishida, T. Nakahara, Experimental investigation of influential factors on adhesion between wheel and rail under wet condition, *Wear* 265 (2008) 1504–1511.
- [9] U. Olofsson, K. Sundvall, Influence of leaf, humidity and applied lubrication on friction in the wheel–rail contact: pin-on-disc experiments, *Proc. Instn. Mech. Engrs. Part F* 218 (3) (2004) 235–242.
- [10] Koan-Sok Baek, K. Kyogoku, T. Nakahara, An experimental study of transient traction characteristics between rail and wheel under low slip and low speed conditions, *Wear* 265 (2008) 1417–1424.
- [11] E.A. Gallardo-Hernandez, R. Lewis, Twin disc assessment of wheel/rail adhesion, *Wear* 265 (2008) 1309–1316.
- [12] P.M. Cann, The “leaves on the line” problem: a study of leaf residue film formation and lubricity under laboratory test conditions, *Tribol. Lett.* 24 (2) (2006) 152–158.
- [13] Lewis R., Lewis S., Zhu Y., Abbasi S., Olofsson U.: The modification of a slip resistance meter for measurement of railhead adhesion, *Proceedings of International Heavy Haul Association Conference 2011*, Calgary, Canada.
- [14] S.R. Lewis, R. Lewis, U. Olofsson, An alternative method for the assessment of railhead traction, *Wear*, in press.
- [15] U. Olofsson, T. Telliskivi, *Wear*, plastic deformation and friction of two rail steels: a full-scale test and a laboratory study, *Wear* 254 (2003) 80–93.
- [16] R. Lewis, U. Olofsson, Mapping rail wear regimes and transitions, *Wear* 257 (2004) 721–729.
- [17] J. Sundh, U. Olofsson, K. Sundvall, Seizure and wear rate testing of wheel–rail contacts under unlubricated conditions using pin-on-disc methodology, *Wear* 265 (2008) 1425–1430.
- [18] A. van Beek, *Advanced engineering design: lifetime performance and reliability*, T U Delft, 2009, pp. 275–276.
- [19] J. Hamrock, *Fundamentals of fluid film lubrication*, NASA reference publication, 1991, p. 473.
- [20] C. Tomberger, P. Dietmaier, W. Sextro, K. Six, Friction in wheel–rail contact: a model comprising interfacial fluids, surface roughness and temperature, 8th International Conference on Contact Mechanics and Wear of Rail/Wheel System (CM2009), Firenze, Italy, 15–18 Sept. 2009, pp. 121–132.
- [21] T. Ohyama, Tribological studies on adhesion phenomena between wheel and rail at high speeds, *Wear* 144 (1991) 263–275.

- [22] I.M. Hutchings, *Tribology*, Edward Arnold, London, 1992, pp. 95–98.
- [23] U. Olofsson, A multi-layer model of low adhesion between railway wheel and rail, *Proc. Instn. Mech. Engrs. Part F* 221 (3) (2007) 385–389.
- [24] U. Sellgren, S. Björklund, S. Andersson, A finite element-based model of normal contact between rough surfaces, *Wear* 254 (2003) 1180–1188.
- [25] J. Lundmark, E. Höglund, B. Prakash, Running-in behaviour of rail and wheel contacting surfaces, AITC-AIT 2006, International Conference on Tribology, Parma, Italy, 20–22 Sept. 2006.
- [26] Y. Berthier, S. Descartes, M. Busquet, E. Niccolini, C. Desrayaud, L. Baillet, M.C. Baietto-Dubourg, The role and effects of the third body in the wheel–rail interaction, *Fatigue Fract. Engng. Mater. Struct.* 27 (2004) 423–436.
- [27] E. Niccolini, Y. Berthier, Wheel–rail adhesion: laboratory study of “natural” third body role on locomotives wheel and rails, *Wear* 258 (2005) 1172–1178.

A field test study of leaf contamination on the rail head
surfaces

Y. Zhu, U. Olofsson, R. Nilsson



C

Submitted to *The first International conference on Railway Technology:*

Research, Development and Maintenance

Apr 18-20, 2012

Las Palmas de Gran Canaria, Spain

A field test study of leaf contamination on railhead surfaces

Y. Zhu¹, U. Olofsson¹, R. Nilsson²

¹Department of Machine Design, Royal institute of technology (KTH), Stockholm, Sweden

²Stockholm public transport AB, Stockholm, Sweden

yiz@kth.se

ABSTRACT

Leaves on train tracks affect adhesion between wheel and rail, especially in autumn. When crushed by wheels, leaves form a blackish, adhesion-lowering layer that sticks to the railhead surface and often requires mechanical removal. This problem has been simulated in scaled and full-scale laboratory tests. A Stockholm local traffic track with a long history of adhesion problems was subject to field tests of railhead contamination. Over a year, on five occasions under different conditions, the friction coefficient was measured using a hand-push tribometer and rail samples were taken. ESCA and GD-OES analyses were conducted to determine the composition of the top layer of rail contaminants and hardness was tested using nano-indentation. The blackish layer contains much higher contents of, for example, calcium, carbon, and nitrogen than do leaf residue layers and uncontaminated samples. These high element contents are generated from the leaf material, which chemically reacts with the bulk material. The hardness of the blackish layer is one fifth that of the non-blackish layer of the same running band. A chemical reaction occurs from the surface to a depth of several microns. The thickness of the friction-reducing oxide layer predicts the friction coefficient and leaf contamination extent.

Keywords: Leaf, Blackish layer, Wheel/rail, Field test, Surface analysis

1. Introduction

Railway vehicle traction is limited by the adhesion between wheel and rail. Low adhesion on the railhead affects railway operation in terms of performance and safety. In acceleration, low adhesion reduces the traction available, causing delay; in deceleration, low adhesion extends the braking distance, potentially causing accidents [1]. In addition, low adhesion can damage rails and wheels, increasing infrastructure costs. Low adhesion on the railhead is usually induced by contaminants, since the wheel–rail contact is an open system. The level of adhesion reduction depends greatly on the type of contaminant; water, oil or grease, and leaves are reportedly the most common contaminants negatively affecting railway operation [1]. Though water, oil, and grease contamination have been investigated in field tests [2], laboratory tests [3–6], and numerical modelling [7–10], the “leaves on the line” problem has attracted less attention. In the field, especially in autumn, many leaves fall onto railway lines to be swept onto the tracks by passing trains. The mechanism of leaf contaminant formation was discussed in a review [11], which found that the coefficient of friction declined to 0.1 with the presence of a black film (formed by leaves), and to 0.05 or less with the addition of a small amount of precipitation, based on tribometer train measurements (note that friction coefficient here refers to the maximum adhesion coefficient). Field

measurements in Sweden [12] produced similar results using both the hand-push tribometer and the pendulum rig. The Swedish national railroad administration estimated the costs associated with leaves on railway lines to be SEK 100 million annually [13], while the annual cost was reportedly GBP 50 million in the UK [14]. In the Netherlands, extremely low adhesion one day in autumn 2002 increased wheel defects by 20%, forcing the rail operator to halt service on most of the network [15].

The characteristics of railhead leaf contamination were studied by Delta Group and NewRail Group, which investigated the bonding mechanisms and properties of leaf film on the railhead [16]. In their study, they used a full-scale wheel-on-rail test rig to produce leaf film in the laboratory. The rail sample segments displayed leaf contamination (a black layer) on the running band down the centre of the railhead. The shear strength of the leaf contamination was inversely proportional to the moisture level. The average thickness of leaf films generated in the laboratory was 42.5 microns versus 44.5 microns in the field, implying that surface asperities would not have penetrated the leaf film to make actual contact. Scanning electron microscopy (SEM), energy dispersive X-ray (EDX), and Fourier transform infrared (FTIR) spectroscopy analyses indicated that three types of leaves produced similar results in terms of chemical composition, indicating that one specific type of leaf could be examined in studying the formation of railhead leaf contamination. The study also found that lignin (along with cellulose and pectin) was the main binding agent in the leaf film formation. Water which is absorbed by cellulosic material assists bonding the leaf film which is actually acted as a lubricant and resulting in low adhesion. In scaled lab testing, Olofsson and Sundvall [17] carried out pioneering work to simulate leaf contamination on the railhead. Their results indicated that, in the presence of leaves, the coefficient of friction declines significantly with high humidity. Olofsson [18] presented a multi-layer model of railhead leaf contamination in which crushed leaves formed a slippery layer coating an easily sheared, chemically reactive surface layer above the bulk rail. Like lubricating oil under boundary lubricated conditions, in which oil transports chemical substances that form an easily sheared layer, crushed leaves transport chemical substances to the wheel and rail surfaces. This model was validated by studying specimens made of actual wheel and rail material using glow discharge optical emission spectrometry (GD-OES) under the same conditions as previous tests [17]. The GD-OES analysis indicated that the leaf formed top layer contained substances such as phosphorus and calcium that were absent from tested specimens uncontaminated with leaves. Note that all visible signs of the coated slippery layer on the leaf-contaminated test specimens were removed. This phenomenon was observed in the field, i.e., that low adhesion also occurred on a hard, black, slippery layer without any visible sign. In addition, Gallardo-Hernandez and Lewis [6] and Arias-Cuevas [19] studied the problem of adhesion loss caused by leaf contamination, in a twin-disc experimental study using sanding as a removal method. Cann [20] simulated the leaf-caused adhesion loss problem on a mini traction machine (MTM). Examining the leaf residue lubricity, she suggested that pectin gel was highly viscous and generated an elasto-hydrodynamic lubrication film at high speeds, and found that dispersed cellulose was also present in the lubricating film as a solid boundary film. The blackish layer was created by a chemical reaction between pectin and rail steel to form iron pectate, rather than by the charring of organic material.

However, all these results were obtained from lab tests. Since we still do not know the actual reason for leaves cause low adhesion, it is necessary to investigate the actual situation, as it includes all possible factors. Accordingly, field tests were performed on actual tracks that had a long history of low adhesion caused by leaf contamination. Friction coefficient was measured in the field various times over the course of one year.

According to Bergseth et al. [21], the formation and composition of surface layers in the tribological contact depend strongly on the chemical composition of the lubricant and on the nature of the surface, for example, whether it is an oxide layer. If leaf film could be regarded as a lubricant between bulk materials, surface analysis to detect the chemical composition of the leaf-formed layer might be an efficient way to investigate the low adhesion problem and blackish layer formation caused by leaves. To this end, we cut rail section samples and examined their chemical composition in the laboratory using GD-OES and electron spectroscopy for chemical analysis (ESCA) techniques; the results of these analyses are presented here.

2. Test setup

2.1. Field tests

The test track is part of the Stockholm underground track system, operated and maintained by Stockholm Public Transport AB. The track is grade 900A steel, which is pearlitic in structure. Note that the wheel material is also pearlitic steel with a similar chemical composition (see Table 1 for the chemical composition of rail and wheel material). The chosen track section, a parallel straight section near the Brommaplan underground station, has a known history of adhesion problems. Over the course of one year, the friction coefficients of rail sections were measured using a hand-push tribometer in five periods, i.e., June 2008, September 2008, October 2008, November 2008, and March 2009. During these periods, rail section samples were cut and replaced. Fig. 1 shows photographs of the test track taken on four sampling occasions; no photograph from June 2008 is shown, as the conditions were similar to those of September 2008. In Fig. 2, images of three rail section samples show blackish, leaf residue, and uncontaminated layers.

Table 1

The chemical compositions of the wheel and rail materials [1,22].

Chemical composition (weight %)	C	Si	Mn	P	Ni	Cr	S
900A rail	0.6–0.8	0.15–0.5	0.8–1.3	max 0.04			max 0.04
Wheel	0.52	0.4	0.8	0.035	0.3	0.3	

2.2. Surface analysis

These rail section samples were further analysed in the lab using both ESCA and GD-OES. ESCA, which is also known as X-ray photoelectron spectroscopy (XPS), is a quantitative spectroscopic technique that measures the elemental composition and chemical state of elements in the analysed material. The spectra are obtained by irradiating a material with a beam of X-rays while simultaneously measuring the

kinetic energy and the number of electrons that escape from the top of the material. GD-OES is a quantitative elemental and depth profile analysis of the materials that works by measuring and analysing the photons emitted from the sputtered materials. According to Angeli et al. [23], the two techniques differ in their analytical and information depths. In the present study, ESCA or XPS was used to analyse the top 2–10 nm of the surface, while GD-OES was used for depths from 10 nm to several microns below the surface. Three rail section samples taken in October 2008, with uncontaminated, leaf residue, and blackish layers, along with uncontaminated samples from other periods were chosen for comparison using GD-OES analysis.



Fig. 1. Photographs of test tracks in four periods: upper left, Sept. 2008; upper right, Oct. 2008; lower left, Nov. 2008; lower right, Mar. 2008.



Fig. 2. Rail section samples, showing: left, blackish layer; middle, leaf residue layer; right, uncontaminated surface.

3. Results

3.1. Friction coefficient measurements

The testing conditions on the five occasions are shown in Table 2. The friction coefficients as measured using a hand-push tribometer on the five occasions are shown in Fig. 3. The friction coefficient from Oct 2008 was very low at approximately 0.15; the friction coefficients on the other occasions ranged from 0.45 to 0.7.

Table 2

Friction coefficient measurement conditions in the field.

Period	Rail temperature (°C)	Air temperature (°C)	Relative humidity (%)	Note
June 2008	13.7	12.1	69.7	No rain
Sept. 2008	13.2	10.1	83.7	No rain
Oct. 2008	8.1	7.6	91.9	Light rain
Nov. 2008	-3	-4	90.8	No rain
Mar. 2009	1	1.7	77	No rain

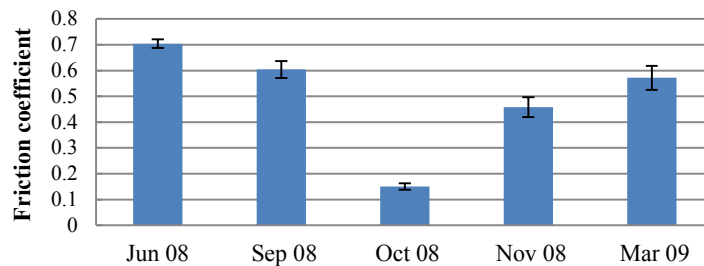


Fig. 3. Friction coefficient measurement results.

3.2. ESCA results

Three rail section samples, from September 2008, October 2008 (with a blackish layer), and November 2008, were subject to ESCA analysis. The elemental weight percent results are shown in Table 3. Compared with the two uncontaminated rail pieces (from Sept. 2008 and Nov. 2008), the blackish layer on the October 2008 sample contains an extremely high carbon content of approximately 48%. High amounts of nitrogen, sulphur, and calcium are also present on the outermost surface. A reduction of iron content is evident in the blackish layer. The results for functional groups of elements for samples taken in September 2008 and November 2008 are shown in Table 4. Due to a charging problem, measurements were unsuccessful for the October 2008 sample (not shown).

Table 3

Elemental weight percent results produced by ESCA analysis of rail samples taken in September (before adhesion problem), October (during adhesion problem), and November (after adhesion problem).

	C	O	Fe	N	Si	F	S	Na	Ca	Al	Mn
Sept. 08	14.0	27.3	50.7	0.5	3.2	0.2	0.2	-	1.3	2.2	0.5
Oct. 08	48.0	29.3	13.2	1.4	2.9	-	0.8	-	2.8	1.5	-
Nov. 08	11.4	26.8	54.6	0.6	2.3	0.9	0.3	0.2	1.1	1.3	0.5

- : below detection limit

Table 4

Functional groups of elements.

Sample	Iron (%)		Oxygen (%)		Carbon (%)				Nitrogen (%)	
	Fe1 707.0 eV	Fe2	O1 529–530 eV	O2 532–533 eV	C1 285.0 eV	C2 286.5 eV	C3 287.9– 288.1 eV	C4 288.9– 289.0 eV	N1 400– 401 eV	N2 402– 403 eV
Sept. 2008	1.3	98.7	40.1	59.9	70.8	15.2	5.3	8.7	100	-
Nov. 2008	0.7	99.3	48.8	51.2	74.4	12.4	5.0	8.2	100	-

Fe1: Fe metal; Fe2: FeO (709.4 eV), Fe₂O₃ (710.8–710.9 eV), Fe₃O₄ (708.2 eV, 710.4 eV), FeOOH (711.3–711.8 eV)

O1: FeO, Fe₂O₃, Fe₃O₄; O2: oxygen in organic compounds, but also FeOOH

C1: C-C, C=C, C-H; C2: C-O, C-O-C; C3: O-C-O, C=O; C4: O-C=O, C(=O)OH

N1: in amine/amide functional groups; N2: charged nitrogen peaks

3.3. GD-OES results

All samples taken on the five occasions were subject to GD-OES analysis. The three samples taken in October 2008 were an uncontaminated sample (“Oct”), a leaf residue sample (“Octleaf”), and blackish layer sample (“Octblackish”). The appearance of these samples is shown in Fig. 2. The GD-OES results for the elements calcium, carbon, nitrogen, phosphorus, aluminium, chromium, nickel, silicon, and manganese are shown in Figs. 4–12. The thickness of the friction-reducing oxide layer [24], which is the depth of the crossing point (D_0) of the oxygen and iron concentration curves depicted in Fig. 13, was measured based on GD-OES results and is shown in Fig. 14.

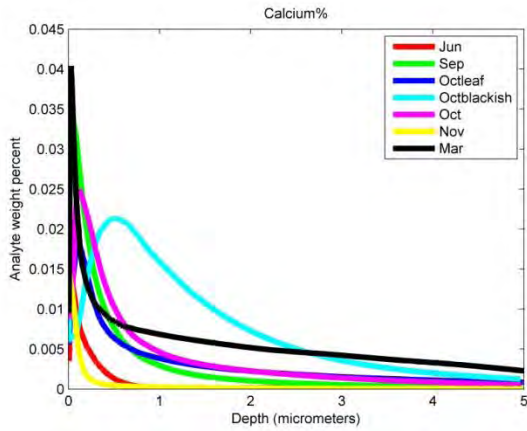


Fig. 4. GD-OES results for calcium content.

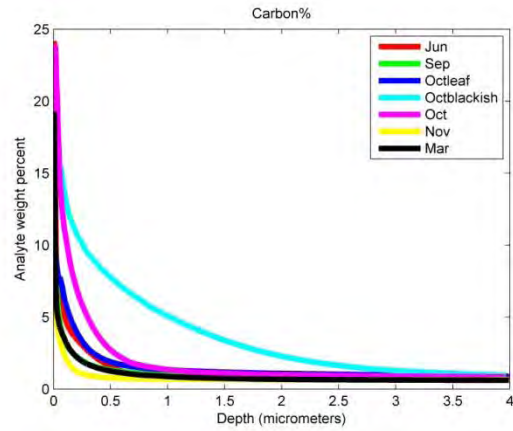


Fig. 5. GD-OES results for carbon content.

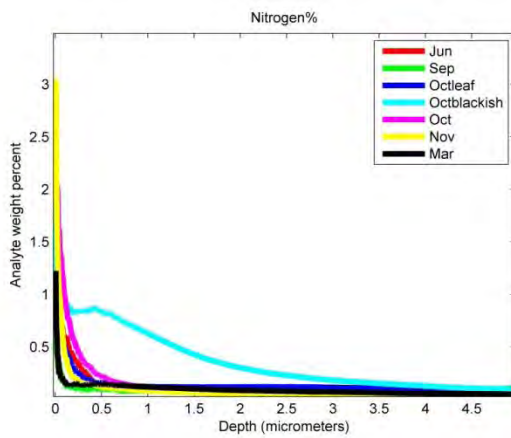


Fig. 6. GD-OES results for nitrogen content.

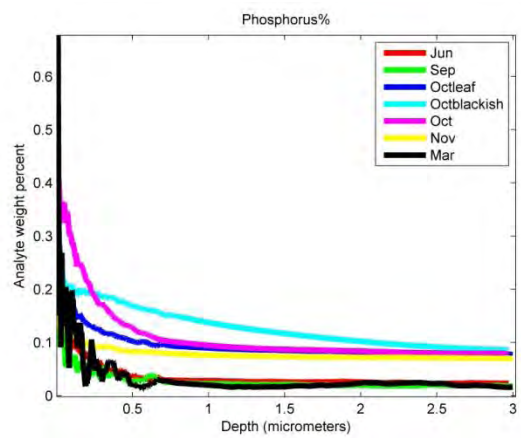


Fig. 7. GD-OES results for phosphorus content.

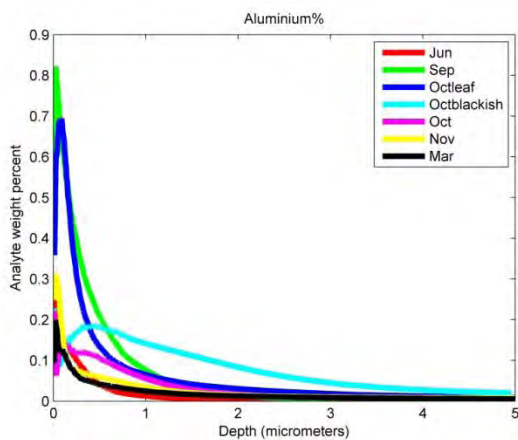


Fig. 8. GD-OES results for aluminium content.

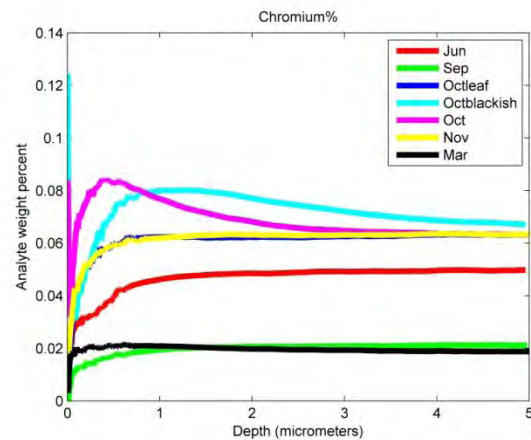


Fig. 9. GD-OES results for chromium content.

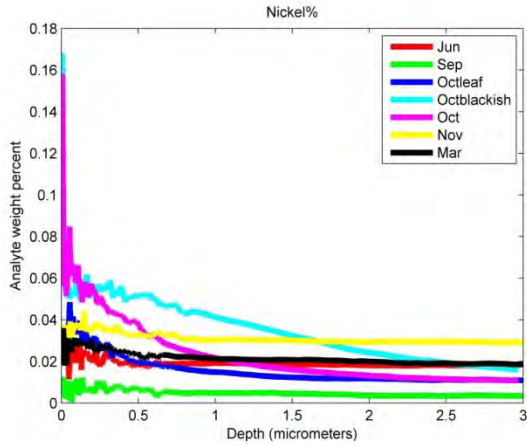


Fig. 10. GD-OES results for nickel content.

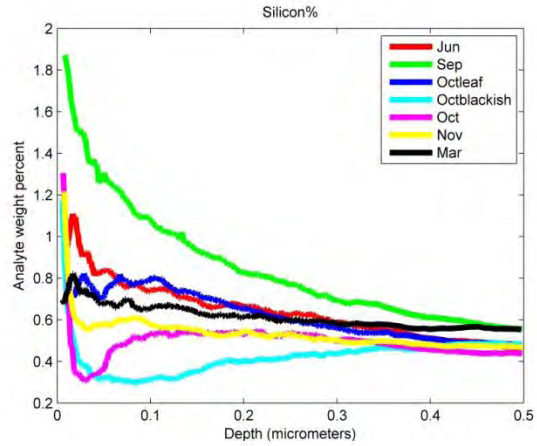


Fig. 11. GD-OES results for silicon content.

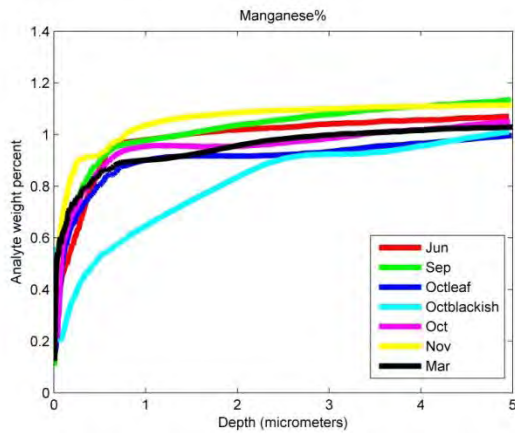


Fig. 12. GD-OES results for manganese content.

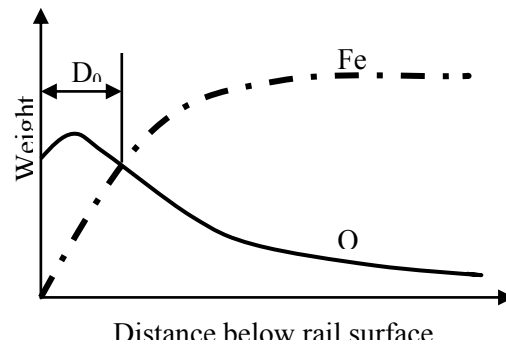


Fig. 13. Schematic depth profile. Crossing point (D_0) between the oxygen and iron contents is indicated.

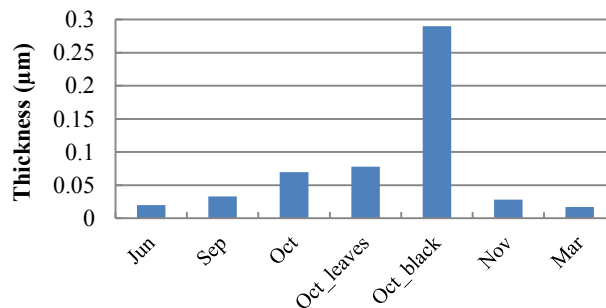


Fig. 14. Thickness of friction-reducing oxide layer.

The depth profile of the calcium content in the blackish layer of the “Octblackish” rail sample differs greatly from those of the other samples. The calcium content is higher in the “Octblackish” sample than in the others at depths ranging from approximately 0.3 μm to 2.5 μm, peaking at approximately 0.5 μm. The

carbon and nitrogen contents of the blackish layer of “Octblackish” are significantly higher than in the other samples at depths from approximately 0.3 μm to 4 or 5 μm below the surface. The contents of phosphorus, aluminium, chromium, and nickel in the blackish layer are also higher than in the other samples. The phosphorus content in the blackish layer of “Octblackish” decreases gradually with depth, approaching the phosphorus content of the other rail samples from October and November at a depth of 3 μm . The chromium content varies greatly between rail pieces. The contents of silicon and manganese, which are the original elements of the rail material, are lower in “Octblackish” than in the other samples.

In addition, nano-indentation was used to measure the hardness of the blackish and the uncontaminated layers. The indentation depth was approximately 100–150 nanometers. The hardness values of the blackish layer are 0.2–1.5 GPa with a mean value of 0.73 GPa, while those of the uncontaminated layer are 2.0–5.2 GPa with a mean value of 3.75 GPa.

4. Discussion

A living leaf contains approximately 80% by weight of water [25]. The rest of the leaf consists largely of cellulose plus a complex mixture of other compounds, including highly polymerized fatty acids as well as proteins, amino acids, saccharides, neutral fats, and resins, which contain elements such as nitrogen, calcium, phosphorus, magnesium, potassium, and manganese absorbed from the soil [26]. Fulford [11] analysed samples of the formed hard black film, finding that it comprised 60% metal, mainly ferrous debris from wheel and rail wear, and 40% plant-origin material originating from leaves. In the field, most of the trees along the test track are elms. In a previous pin-on-disc study [17, 18], elm leaves were collected from the field to create “natural lubricant” in the lab. According to Poole [16], SEM/EDX and FTIR analysis of three types of leaf residue indicated that they were similar in chemical composition: all leaf types contained the same set of elements and the FTIR spectra had the same valleys (indicating the same type of organic bonding). As a result, the results presented here are believed to be generalizable, since the influence of leaf type can be neglected.

The element weight percent results of ESCA analysis identified the presence of oxygen, calcium, and aluminium not from the original rail material. Moreover, the amounts of carbon, silicon, and sulphur on all three samples are significantly greater than those found in standard rail material. The oxygen detected is due to a natural oxide process. Large amounts of carbon, calcium, sulphur, and silicon were found using a twin-disc test rig under wet conditions [27], which is in line with our results for the September and November rail pieces without leaf contamination. On the “Octblackish” sample, increased calcium, sulphur, and nitrogen and a large amount of carbon were detected in the blackish layer, indicating that the leaves had chemically reacted with the bulk material and significantly changed the chemical composition of outermost surface (less than 10 nanometers from the surface).

GD-OES results indicated that the depth profile of the blackish layer of the “Octblackish” sample also differs greatly from those of other rail pieces. Of all elements, the contents of calcium, carbon, and nitrogen are significantly higher on the “Octblackish” sample than on the other samples, indicating these elements are highly reactive. Since the original rail material contains much less or none these elements,

the detected calcium, carbon, and nitrogen probably originate from leaves. A previous pin-on-disc study [17] and a full test rig study [11,16] also reported that leaf-formed black film contained a significant amount of calcium oxalate, in line with the present results. The carbon we found originated from organic molecules from the leaf structure, although a small amount (below 1%) of carbon is also found in the wheel and rail material. The detected carbon is mostly chemically combined as polysaccharides in cellulose and pectin; these substances were reported to make the main contribution to the low adhesion problem [20]. Cann [20] found C=O, C-O-C, and C-C vibrations in the surface film, generated from the pectin and cellulose of leaves. These vibrations were also found in the outermost surface of the rail sample from September 2008 and November 2008 in our ESCA study. Since these were uncontaminated samples, the presence of these vibrations may be due to previous leaf remnants or other contaminants. The rail sample from October 2008 contained a high carbon content, according to the ESCA and GD-OES study, and might display more C=O, C-O-C, and C-C vibrations than those from September 2008 and November 2008, though this result is uncertain due to charging problems. A study from Banverket [28] found a connection between the nitrogen content in the leaf contaminated layer and plant material. The study reported that plant material had become charred on the rail surface after the passage of a number of trains, and that the low friction was attributed to airborne nitrogen compounds. Nitrogen is one of the constituent elements of proteins and amino acids from leaves, and a high amount of nitrogen was detected in both the ESCA and GD-OES studies. In addition, all the nitrogen is present as amine/amino functional groups originating from the organic parts of leaves.

The contents of phosphorus, aluminium, chromium, and nickel in the blackish layer of the “Octblackish” sample are also higher than for the other samples. A clear difference in phosphorus content between surfaces with and without leaf contamination was found by Olofsson [18] in a previous pin-on-disc study simulating leaf contamination, though Brookes [29] reported a weak correlation between phosphorus and leaf contamination. According to the present GD-OES results, the phosphorus content increases below a depth of 0.25 μm in the blackish layer. This phosphorus could be from wheel material or wear debris; however, the phosphorus content found here is much higher than that in the wheel material, indicating leaves as the main source. Sulphur, a tribochemically active element in lubricated bearings [21,30], is not closely correlated with leaf contamination. Other elements such as silicon and manganese, which originate from rail material, were lower in amount in the blackish layer of the “Octblackish” sample than in the other samples, possibly because silicon and manganese are not reactive and were “occupied” by other foreign elements on the top surfaces. Nano-indentation results indicated that the blackish layer was softer than the uncontaminated layer, indicating that the blackish layer differs in properties from the bulk material. Gallardo-Hernandez and Lewis [6] and Arias-Cuevas [19] reported that the average hardness of the leaf-created layer was approximately 60 HV. Nano-indentation gave a mean hardness value of 730 MPa for the blackish layer, with quite large variations. This is because the indentation depth used here is less than in other studies and because the composition of the outermost leaf-contaminated layer varies considerably. The uncontaminated location gave an average hardness value of 3.75 GPa, which is harder than is typical for new rail material because of plastic deformation and work hardening of the material during operation [27]. The differences in chemical composition and hardness

indicate that chemical reactions took place in the blackish layer, from the outermost surface to a depth of several microns.

It is widely accepted that oxide layers have an essential impact on friction and wear, especially in boundary lubrication and unlubricated contacts. The ESCA binding energy results for the September 2008 and November 2008 rail pieces indicated that most of the iron oxides/oxyhydroxides are present as Fe (III), some being present as Fe (II). Nakahara et al. [27] also found Fe (III) and Fe (II, III) under both dry and wet conditions. As a result, the presence of iron oxide could not fully explain the low friction phenomenon. Fig. 14 shows the thickness of the friction-reducing oxide layer. The thickness of the blackish layer on the October 2008 rail sample was approximately 0.3 μm , significantly greater than on the other samples. The thicknesses of the friction-reducing oxide layer on the leaf residue and uncontaminated layers of the October 2008 rail samples are very similar; though they are less than that on the “Octblackish” sample, they are still much greater than on samples cut on other occasions. This result can clearly distinguish between rail samples taken during adhesion problem periods and during good adhesion periods. All three samples, uncontaminated (“to the naked eye”), with a leaf residue layer, and with a blackish layer, have thicker friction-reducing layers than do samples taken in other periods because of the effects of leaves. The layer that was uncontaminated “to the naked eye” was also thick, indicating that the layer had been contaminated but then cleaned by other solids, such as sand. Therefore, it is more accurate to call both the uncontaminated layer and leaf residue layer the “less contaminated” layer compared to the blackish layer. That the blackish layer is approximately four times thicker than the “less contaminated” layers is because the leaf debris reacted completely with the bulk material to form the blackish layers. The thickness of the friction-reducing oxide layer on the November sample decreases to less than 0.03 μm , which is close to the level of the September sample. This indicates that the leaf-contaminated layer on the November sample had recovered to the level found in September before the adhesion problem. ESCA functional group analysis of the September 2008 and November 2008 samples indicates that approximately 99% of the total iron signal represented various oxides; however, a very minor part, approximately 1% of the total iron signal, represented Fe metal. This result indicates that a thick oxide layer formed on the steel surface. Since a very weak metal peak was still detected, the oxide layer should be thinner than the analysis depth (10 nanometers). In this study, O-H vibrations were found in C1, C4, and O2 by ESCA analysis, indicating the presence of hydro-oxide. According to Nakahara et al.’s theory [27], the presence of hydro-oxide indicates a tribo-chemical reaction between the bulk material and water. The breakdown of the oxide film on the surface and the recovering with oxide and/or hydro-oxide would take place simultaneously. The measurements of the friction coefficient in different periods were highly correlated with the thickness of the friction-reducing oxide layer: the greater the thickness, the lower the friction coefficient. According to the twin-disc testing results [27], the oxide layer is a factor governing the traction reduction in the wheel–rail contact under both unlubricated and lubricated conditions. In a mini traction machine study, Zhu et al. [22] also found that, under water-lubricated conditions, an extremely low friction coefficient could be found on smooth surfaces, on which an oxide layer might contribute to forming an easily sheared oxide layer. However, the low friction coefficient of the track sample from October 2008 might also be attributable to the light shower

conditions during measurement. Unfortunately, the measuring length of the hand-push tribometer is at least 3 meters, making it difficult to localize the contamination section. An alternative method should be used with a more localized measuring area, such as the pendulum rig presented in Lewis et al. [12] and Lewis and Lewis [31].

5. Conclusions

- The contents of elements in the blackish layer, particularly those originate from leaves, differ from those in the leaf residue and uncontaminated layers on the same and other rail samples.
- Chemical reactions occur in the blackish layer, making the chemical composition of the blackish layer very different from that of other layers on other samples. The chemical reaction occurs on the outermost surface and extends to a depth of several micro meters below the surface.
- The thickness of the friction-reducing oxide layer is correlated with the friction coefficient results and can predict the extent of leaf contamination.

Acknowledgements

This research was performed under the auspices of the KTH Railway Group, with the support of Stockholm Public Transport and Swedish Transport Administration.

References

- [1] R. Lewis, U. Olofsson, *Wheel–Rail Interface Handbook*, Woodhead Publishing Limited, Cambridge, UK, 2009.
- [2] O. Polach, Creep forces in simulations of traction vehicles running on adhesion limit, *Wear* 258 (2005) 992–1000.
- [3] W. Zhang, J. Chen, X. Wu, X. Jin, Wheel/rail adhesion and analysis by using full scale roller rig, *Wear* 253 (2002) 82–88.
- [4] H. Chen, T. Ban, M. Ishida, T. Nakahara, Experimental investigation of influential factors on adhesion between wheel and rail under wet conditions, *Wear* 265 (2008) 1504–1511.
- [5] K.-S. Baek, K. Kyogoku, T. Nakahara, An experimental study of transient traction characteristics between rail and wheel under low slip and low speed conditions, *Wear* 265 (2008) 1417–1424.
- [6] E.A. Gallardo-Hernandez, R. Lewis, Twin disc assessment of wheel/rail adhesion, *Wear* 265 (2008) 1309–1316.
- [7] Y. Zhu, U. Olofsson, A. Söderberg, Adhesion modeling of wheel–rail contact under wet conditions using measured 3D surface, 22nd IAVSD Symposium , 14–19 Aug. 2011, Manchester, UK.
- [8] H. Chen, M. Ishida, T. Nakahara, Analysis of adhesion under wet conditions for three-dimensional contact considering surface roughness, *Wear* 258 (2005) 1209–1216.
- [9] C. Tomberger, P. Dietmaier, W. Sextro, K. Six, Friction in wheel–rail contact: a model comprising interfacial fluids, surface roughness and temperature, *8th International Conference on Contact Mechanics and Wear of Rail/Wheel System (CM2009)*, Firenze, Italy, 15–18 September 2009, pp. 121–132.

- [10] R.I. Popovici, Friction in wheel–rail contact, *Doctoral thesis*, University of Twente, Department of Engineering Technology, Enschede, Netherlands (2010).
- [11] C.R. Fulford, Review of Low Adhesion Research, Rail Safety and Standards Board, UK, 2004.
- [12] R. Lewis, S. Lewis, Y. Zhu, S. Abbasi, U. Olofsson, The modification of a slip resistance meter for measurement of railhead adhesion, *IHHA 2011*, Calgary, Canada.
- [13] L. Forslöv, wheel slip due to leaf contamination, Swedish National Rail Administration TM 1996 03 19, Borlänge, Sweden, 1996.
- [14] Managing low adhesion, Report published by the Adhesion Working Group, UK, (September 2001).
- [15] O.A. Cuevas, Low adhesion in the wheel–rail contact, *Doctoral thesis*, TUD, Delft, 2010.
- [16] W. Poole, Characteristics of railhead leaf contamination, summary report published by Rail Safety and Standards Board (May 2007).
- [17] U. Olofsson, K. Sundvall, Influence of leaf, humidity and applied lubrication on friction in the wheel–rail contact: pin-on-disc experiments, *P. I. Mech. Eng. F.-J. Rai.* 218 (2004) 235–242.
- [18] U. Olofsson, A multi-layer model of low adhesion between railway wheel and rail, *P. I. Mech. Eng. F.-J. Rai.* 221 (2007) 385–389.
- [19] O. Arias-Cuevas, Investigation some sanding parameters to improve the adhesion in leaf contaminated wheel–rail contacts. *P. I. Mech. Eng. F.-J. Rai.* 224 (2010) 139–157.
- [20] P.M. Cann, The “leaves on the line” problem: a study of leaf residue film formation and lubricity under laboratory test conditions, *Tribol. Lett.* 24 (2006) 151–158.
- [21] E. Bergseth, M. Torbacke, U. Olofsson, Wear in environmentally adapted lubricants with AW technology, *J. Synth. Lubric.* 25 (2008) 137–158.
- [22] Y. Zhu, U. Olofsson, and K. Persson, Investigation of influential factors on wheel–rail adhesion using mini traction machine, submitted to *Wear*.
- [23] J. Angeli, A. Bengtson, A. Bogaerts, V. Hoffmann, V.-D. Hodoroaba, E. Steers, Glow discharge optical emission spectrometry: moving towards reliable thin film analysis—a short review, *J. Anal. Atom. Spectrom.* 18 (2003) 670–679.
- [24] Y.W. Zhao, J.J. Liu, L.Q. Zheng, The oxide film and oxide coating on steels under boundary lubrication, in: *Proceedings of the 16th Leeds-Lyon Symposium on Tribology*, Lyon, France, 1989, pp. 305–311.
- [25] C. Pritchard, M.A. Tanvir, A basic study of wheel/rail adhesion 9: Further observations on leaves, BR research Report TM-TRIB-6, 1973.
- [26] T. Sariyildiz, J.M. Anderson, Variation in the chemical composition of green leaves and leaf litters from three deciduous tree species growing on different soil types, *Forest Ecol. Manag.* 210 (2005) 303–319.
- [27] T. Nakahara, K.-S. Baek, H. Chen, M. Ishida, Relationship between surface oxide layer and transient traction characteristics for two steel rollers under unlubricated and water lubricated conditions, *Wear* 271 (2011) 25–31.
- [28] Track adhesion southern Sweden, Banverket TASS 1996-04-10, 1996.
- [29] R. Brookes, Autumn 2003 Monitoring: Deep Dive Report, Draft 1, 25 Mar., Ove Arup & Partners Ltd., London, 2004.
- [30] U. Olofsson, S. Dizdar, Surface analysis of boundary-lubricated spherical roller thrust bearings, *Wear* 215 (1998) 156–164.

- [31] S.R. Lewis, R. Lewis, An alternative method for the assessment of railhead traction, in: Proceeding of the 8th International Conference on Contact Mechanics and Wear of Rail/Wheel System, Florence, Italy, 2009, pp. 219–227.

